University of Nevada, Reno

Nutrient Recovery from Biomass and Agricultural Wastes by Hydrothermal Carbonization Process

A dissertation submitted in partial fulfillment of the requirements for the degree of Doctor of Philosophy in Chemical Engineering

By

Saeed Vahed Qaramaleki

Dr. Charles J. Coronella / Dissertation Advisor

August 2022

THE GRADUATE SCHOOL

We recommend that the dissertation
prepared under our supervision by

SAEED VAHED QARAMAI

entitled

Nutrient Recovery from Biomass and Agricultural Wastes by Hydrothermal Carbonization Process

be accepted in partial fulfillment of the
requirements for the degree of

DOCTOR OF PHILOSOPHY

Charles J. Coronella, Ph.D.
Advisor

Sage R. Hiibel, Ph.D.
Committee Member

Victor R. Vasquez, Ph.D.
Committee Member

Jeffrey C. LaCombe, Ph.D.
Committee Member

S. Kent Hoekman, Ph.D.
Graduate School Representative

Markus Kemmelmeier, Ph.D., Dean
Graduate School

August, 2022

Abstract

Over the past few decades, livestock farming has undergone a significant transformation. Production has shifted from smaller family-owned farms to larger farms called confined animal feeding operations or CAFOs. While this kind of animal farming has many benefits in terms of efficiency, it has also caused many environmental issues. The most pressing issue associated with CAFOs stems from the sheer amount of manure they produce. For instance, some farms can overtake some US cities in waste generation. The numbers varied between 2800 to 1.6 million metric tons. Even though manure is valuable in farming, it becomes highly problematic when generated in such a tremendous amount. Because most of these CAFOs don't have their pasture land to apply the manure as fertilizer, instead, they buy animal feed from outside. In addition, the capacity of the cropland to absorb that amount of waste is limited. Thus, problems related to runoff and leaching nutrients into the ground water causing eutrophication, are common. Also, atmospheric emissions and foul odor from the manure handling and storage add to the extent of the manure issue.

In this dissertation, we tried to address these problems by developing a new manure management strategy that treats the farm's waste in a hydrothermal process. This process produces a solid product called hydrochar and a liquid stream containing nutrients such as nitrogen, phosphorous, and some soluble organic. The stream then undergoes crystallization to separate the recovered nutrients as solid fertilizer. The brine out of the crystallization step is partly recycled and mostly put into a membrane distillation process to generate sanitary water to be used back on the farm. This research mainly focuses on

hydrothermal carbonization, crystallization or separation of nutrients, and characterization of hydrothermal products. Hydrothermal carbonization (HTC), also known as "aqueous carbonization at elevated temperature and pressure," is a thermochemical process for treating wet organic compounds. It has a better carbon efficiency than other biomass conversion methods such as anaerobic digestion, Ficher-Tropch synthesis, fermentation, etc. Moreover, it allows pressing biomass without drying, which is a colossal advantage. In reality, HTC uses subcritical water or hot compressed water as the reaction media.

The research as part of this dissertation can be classified into several subprojects. In the first project, the main goal was extracting nutrients from biomass. In this project, a series of experiments were conducted to evaluate the effects of reaction time (5, 30, and 120 min), temperature (170, 200, and 230 °C), and the addition of acids (citric acid and HCl) at several concentrations (0.1, 0.3, and 0.5 M) on the solubilization of phosphate and organic nitrogen to the aqueous phase. Statistical analysis of the experimental results revealed a significant effect of reaction temperature, acid addition, and concentration on phosphate extraction. Within the range of conditions studied low HTC temperature and adding either citric acid or HCl resulted in enhanced phosphate recovery in the aqueous phase. The maximum P solubilization (98% of the total P) in the aqueous phase occurred at 170 °C with the addition of citric acid. On the other hand, the results indicate only a minor effect of the experimental conditions concerning N solubilization. The nitrogen mass balance showed that roughly 60% of the overall N was extracted into the aqueous phase.

The second project aimed at nutrient separation from the HTC process water with crystallization. The dissolution of nutrients (phosphorus and nitrogen) from cow manure

by the HTC process into the aqueous phase was demonstrated. Three organic acids (formic acid, oxalic acid, and citric acid) and sulfuric acid were evaluated as additives in HTC. The results indicated that more than 90% of the phosphorous content of cow manure could be leached to the process water as PO_4 at 170°C with all acids. Ammonia was extracted with relatively high efficiency in sulfuric and oxalic acids. Nutrients were recovered through reactive crystallization (precipitation) from process water by adjusting the molar concentration of the ionic species with pH = 9.5. Subsequently, nutrient-rich solids containing almost all (>95%) of the dissolved phosphorus in the sulfuric and formic acid-assisted runs were recovered and characterized for their elemental composition. Morphology and qualitative chemical analysis of the precipitates were determined.

In the third project, hydrothermal carbonization (HTC) of cow and pig manure under sulfuric and acetic acid as catalysts was done. The main goal was to characterize the different products of the HTC process. HTC experiments were carried out at 170°C for 10 min, and the concentration of acids was 0.3M. Based on our observation, acid catalysts increased the carbonization, thus energy densification for both types of manure, with sulfuric acid having the most significant impact. Both sulfuric and acetic acids increased the leaching of the inorganic minerals such as Ca, K, Mg, and Fe, albeit to varying degrees. Phosphorus leaching was increased with acid catalysts as well. The results confirmed above 90% conversion of total phosphorous to phosphate in hydrothermal conditions. The phosphorus contents of pig manure and its HTC liquid product were an order of magnitude above those of cow manure. Acetic acid barely affected nitrogen extraction and even caused a reduction in pig manure. On the other hand, sulfuric acid increased nitrogen's

hydrothermal leaching for both types of manure and enhanced the relative ammonia fraction.

Further analysis of the aqueous products signified the formation of acetic acid, furfural, and 3-aminopyrazine 1-oxide compounds for the sulfuric acid-catalyzed hydrothermal treatment of both types of manure. Analysis of the residual gas confirmed a trace amount of H_2S, NO_2, and SO_2 formation. The addition of sulfuric acid increased NO_2 significantly. Finally, detailed mass balances of the carbon and macronutrients (NPK) are presented.

Finally, the project running for the longest time was dedicated to the construction, commissioning, and test work of a continuous flow HTC reactor. A comparison of the batch and continuous reactor performance was made as a part of this project. In addition, the hydrochar obtained by HTC of glucose from the batch and continuous flow reactor were analyzed for their similarities and differences. The modification of the continuous reactor to improve the mixing and heat transfer was discussed and explained.

Acknowledgments

Words cannot express my gratitude to my professor and chair of the committee, Dr. Charles J. Coronella, for his invaluable patience, insightful feedback, and excellent mentoring. It would have been impossible for me to complete this work without his scientific and moral support. I feel fortunate to have the opportunity of working under his supervision, and what I have learned from him will continue to shine a light on my professional life.

I could not have undertaken this journey without my defense committee member Dr. Sage Hiibel, who generously provided knowledge and access to his lab equipment. Additionally, this endeavor would not have been possible without the support from the other committee members Dr. Victor Vasquez, Dr. Jeffery LaCombe, and Dr. Kent Hoekman.

I am also grateful to my groupmates and cohort members, Carlos Rocha Silva, Jose Cardenas, Cordel Bever, and Nick Silva, for their help and moral support.

Lastly, I would be remiss in not mentioning my family, especially my parents, Maryam and Akbar Vahed Qaramaleki. Their belief in me has kept my spirits and motivation high during this process.

Table of content

List of Tables

List of Figures

Chapter 1

Introduction

1.1 Background

Political, environmental, and economic regulations intensify the need to decouple human prosperity from non-renewable resources. Biomass is one of the most abundant renewable resources and has the advantage of storing $3*10^{21}$ J of sunlight energy in the chemical bonds; however, according to some estimates, only 3% of that biomass is currently being used for the production of fuel and chemicals. The latest Department of Energy (DOE) report [1] on advancing domestic resources for a thriving bio-economy (2016 billion-ton report) projected the potential for more than 1 billion dry tons of biomass per year to be potentially available by 2030. The report assumes market prices of $60 per dry ton at the farm gate or roadside (i.e., after harvest, ready for delivery to a processing facility). Waste resources amount to 123-155 million dry tons of overall available biomass from 2017 through 2040, and the trend is increasing. The utilization of waste biomass resources not only reduces the cost of bioenergy and biochemical production by eliminating the need for additional agronomic inputs such as land and fertilizer but also helps mitigate the environmental impact of dealing with these kinds of waste streams. The waste biomass included in the DOE report represents agricultural secondary wastes (sugarcane residues, soybean hulls, rice hulls, and field residues, grain dust and chaff, orchard and vineyard pruning, animal fats and yellow grease, cotton gin trash and field residues, animal manure), MSW (garbage fraction) and forestry and wood wastes.

Over the past few decades, animal farming operations have continuously moved towards fewer but more concentrated facilities known as concentrated animal feeding operations (CAFO); therefore, proper manure management problems have arisen. The typical situation is the lack of enough cropland and pasture to accommodate the massive influx of manure for distribution without posing a risk to water and human health. Additionally, there is a fundamental constraint on the ability of the adjacent land resources to absorb the nutrients supplied by the manure from these concentrated animal production facilities.

Multiple sources provide several estimates of the potentially available manure for utilization. For instance, USDA numbers indicate that 335 million dry tons of waste are available from all animal feed operations, including CAFOs. In addition, the American Gas Association's evaluation of usable manure generation shows 216-721 million wet tons, equivalent to 43 to 144 million dry tons given 20% dry matter content. Finally, the National Petroleum Council assessment estimates 156 million dry tons of animal manure, with 24 million dry tons considered a practical resource.

Land application in the form of spreading or spraying is the typical method of dealing with most animal manure and a large portion of selected municipal and industrial wastes, which also benefits agricultural lands. All these wastes can provide nutrients for crop production and improve soil properties due to their organic matter. Nonetheless, mismanagement of manure or other wastes can damage the soil, water, and air quality and threaten human and animal health.

Animal production is a significant economic sector in the US, with over $100 billion annual value. New technology and economy of scale benefits have caused substantial changes in

favor of large operations versus small farms. In such facilities, animals are grown in houses, feedlots, and other confinement units, called animal feeding operations. 40% of all animals produced in the US are from the top 2% of the large farms or CAFOs. Therefore, protecting the environment has become a significant challenge for animal farming from a policy and regulatory standpoint [2].

1.1.1 Nutrient Management:

The transformation of nutrients in the manure and other waste byproducts within the soil, water, and air can pose real environmental threats. The leakage of nutrients can be observed at different stages of the animal production operation, including at the production site, during storage, and after field application. Nitrogen and phosphorus, in particular, are believed to be responsible for algal blooms and the disastrous eutrophication of lakes and surface water streams [3][4][5][6]. Therefore, technology development for sustainable utilization of nutrients in animal waste is one of the critical aspects of this dissertation.

1.1.2 Atmospheric Emissions:

The main challenges of animal production and land application of generated manure from the perspective of atmospheric emissions are related to emissions of particular matter (PM), ammonia, volatile organic compounds (VOCs), odor and formation of tropospheric ozone, hydrogen sulfide (H_2S), methane, nitrogen oxides (NO_x) and pathogens [7][8][9]. For instance, Agricultural Research Service (ARS) study indicates that applying dairy slurries on the soil surface causes the highest ammonia emission by losing between 40% to 80% of the total ammonia within the first 24 to 48 hours. On the other hand, applying solid manures such as poultry litter had lower ammonia emission rates.

This work has focused on developing technology to resolve the problems associated with manure management. The fundamentals of the technique introduced in this project are based on the hydrothermal treatment of animal manure.

1.2 Hot compressed water as reaction media

The terminology used for subcritical water is not as rigorous as for supercritical water. However, hot compressed water (HCW) is the term with broad acceptance in the literature used for biomass processing. Herein it is defined as water at elevated temperature (>200˚C) and pressures. Understanding the chemistry of water under these conditions would help elucidate the chemical reactions of different components and predict potential products. Thus, it is crucial from not only a scientific point of view but also from an engineering standpoint. Studies of hot compressed water have investigated its properties on microscopic and macroscopic levels, even though some of these properties are highly intertwined, and a clear distinction is often difficult to make.

HCW exhibits unusual macroscopic properties in miscibility, dielectric constant, ionic product, and transport properties.

1.2.1 Miscibility (solvation characteristics)

Liquid water at standard conditions (T=25 ℃, P = 0.1MPa) can easily dissolve salts; however, it is rarely miscible with hydrocarbons and gases. At elevated temperatures, the solubility of organic materials increases as the water starts to behave more as a non-polar solvent. This behavior is mainly correlated with changes in the dielectric constant of HCW reflected in the diminished ability of water to shield charge. Even though the solubility of gases decreases by increasing temperature, in the critical region, non-condensable gases

and waster become completely miscible [10][11]. For example, at 250 bar, NaCl is very soluble (37 wt.%) at 25°C, but at 550°C, the solubility is only 120 ppm.

1.2.2 Dielectric constant

The dielectric constant of the solvent is a critical parameter in determining the pathway of chemical reactions. The reaction coordinate of most reactions passes through a transition state that may involve a more (or less) polar transition state depending on the chemistry of reactants. A reaction that produces a highly polar activation complex along the reaction coordinate would have a faster rate if the solution had a higher dielectric constant and vice versa. In transition state theory, the impact of temperature is embedded in activation energy, and the effect of pressure is described by the activation volume, which in fact, can be used to manipulate the dielectric constant of the solvent [12][13][14].

1.2.3 Ionic product

The ionic product of HCW is drastically higher than ambient water (some orders of magnitude). The high ionic porduct of HCW can be explained by the fact that the self-dissociation of water is endothermic; therefore, it is easier for water to dissociate at high temperatures. Under these conditions, water can act as an acidic or basic catalyst precursor by generating H_3O^+ and OH^- ions [15][16].

1.2.4 Transport properties

Water viscosity drops substantially at high temperatures, leading to a higher diffusion rate and eliminating mass transfer limitations. This, coupled with other properties mentioned above, makes HCW an excellent reaction media for a variety of reactions.

The properties of water at elevated temperatures from a microscopic point of view would be focused on collision frequency, hydrogen bonds, dipole moment, and caging effect of water molecules [17]. Many of the liquid water properties stem from the existence of hydrogen bonding among its molecules. However, hydrogen bond strength and persistence are markedly reduced in hydrothermal and supercritical conditions. Moreover, while the distribution of hydrogen bonds in ambient liquid water is highly uniform in hydrothermal and critical regions, the hydrogen bond network only exists in small clusters of hydrogen-bonded water molecules. Moreover, the size distribution of those clusters is state-dependent.

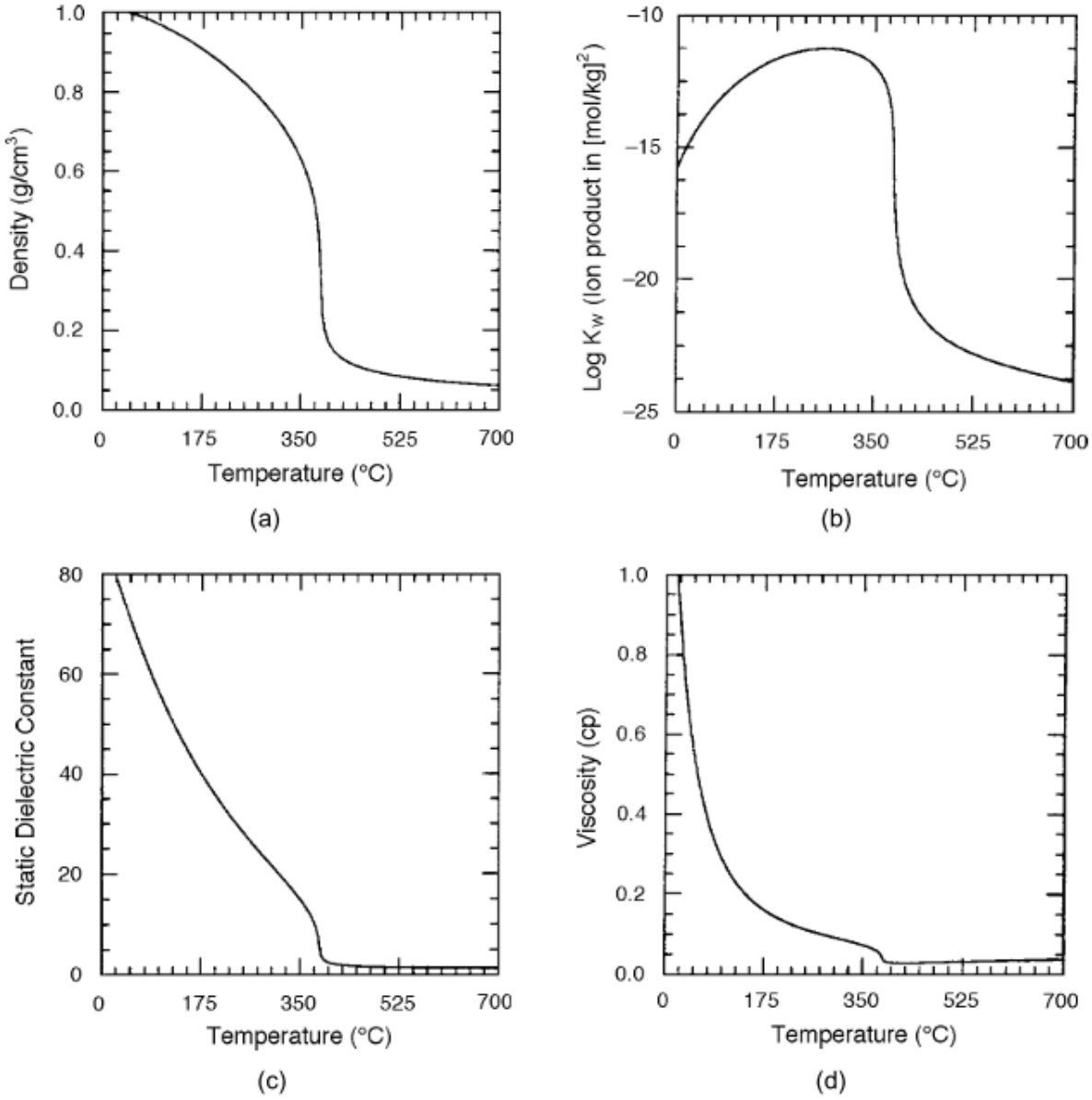

Figure 1.1 Hot compressed water (HCW) properties [18]

Water can affect the kinetics of chemical reactions in multiple ways. For instance, water can appear as a reactant or product of specific reactions, or water can be involved as a catalyst. On the other hand, water as reaction media can impact the reactions by energy transfer, diffusion, and solvent caging or its phase behavior [19][20].

1.2.5 Water as a Reactant/Product

The reactions in which water molecules are generated as a product or used as a reactant are hydrolysis, hydration, dehydration, hydrogen exchange, and free-radical oxidation.

1.2.5.1 Water in Hydrolysis and Hydration

Hydrolysis is a bond-opening reaction that breaks down large molecules and has been studied for its potential to recover valuable chemicals. While fully hydrocarbon materials are not reactive to a great extent in HCW without adding catalysts, compounds with a saturated carbon atom bonded to a heteroatom functional group are more likely to hydrolyze [21].

Autocatalysis by-products of some hydrolysis reactions are also possible in HCW. For example, hydrolysis of esters, aldehydes, and amines produces carboxylic acids, further catalyzing the reaction. In addition, hydrolysis of halogen- and nitrogen-containing compounds produces mineral acids, which also serve as catalysts. Similarly, ammonia produced by the hydrolysis of amines, amides, and nitriles can act as a base catalyst [22].

1.2.5.2 Water as a Hydrogen Source

There is experimental evidence indicating hydrogen supply from water for reactions in HCW. Due to this ability, water can be used to alter the distribution of products, especially from pyrolysis reactions. The presence of hydrogen in free radical chemistry causes a shift in selectivity towards lower from high molecular weight products due to chain-terminating reactions. Hydrogen donation by HCW occurs by many mechanisms. According to one proposed mechanism, hydrogen is produced during the conversion of alcohol to ketones.

Hydrogen could also be formed during hydrolysis reactions. The water-gas shift reaction is another potential pathway to generate hydrogen in HCW media [23].

$$CO + H_2O \rightarrow CO_2 + H_2$$

1.2.5.3 Water in Free-Radical Chemistry

Free-radical reactions are dominant in supercritical water (high temperature), whereas ionic reactions are the governing mechanism in subcritical regions. Free-radical reactions play a crucial role in supercritical water oxidation, biomass gasification, and other degradation reactions. However, free-radical reactions have a poor atom economy. Moreover, they are hard to control, and the products of these reactions are highly random, diverse, and gaseous [24][25].

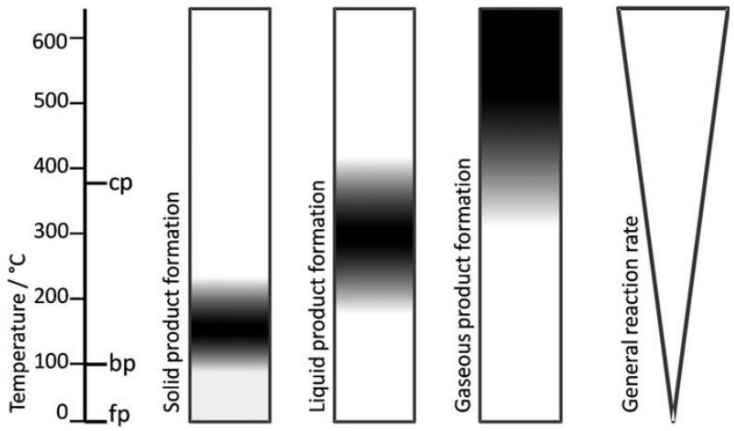

Figure 1.2 Simplified illustration of the temperature dependence of hydrothermal biomass transformation processes [26]

1.2.6 Water as a Catalyst

Acting as a source of acid/base catalyst or modifying and stabilizing the activated complex are two examples of the participation of water molecules in chemical reactions as a catalyst.

1.2.6.1 Water as Acid/Base Catalyst Precursor

HCW carries high concentrations of H^+ and OH^- due to the self-ionization of water at elevated temperatures, as evidenced by high ionic product. Therefore, many acids or base-catalyzed reactions that otherwise would need a much higher concentration of external mineral acid or base proceed efficiently. Some examples of these reactions are alcohol dehydration, hydrolysis, water addition to double bonds, rearrangement reactions, aldol condensation reactions, and the Cannizaro reaction. Temperature and density are essential factors in water dissociation, which control the availability of H^+ and OH^- ions. Thus the kinetics of these reactions are highly dependent upon those two parameters [27][28].

1.2.6.2 Water as Catalyst in the Transition State

Another way of water catalyzing a reaction is by getting involved in the activated complex and reducing its energy level. In particular, reactions that require intramolecular hydrogen transfer benefit from this unique ability of HCW. Water molecules surrounding the activated complex provide a less geometrically strained environment suitable for the reaction to proceed [29]. For example, computational chemical calculations indicate that the presence of water molecules reduces the activation barrier of the isomerization reaction of nitromethane by 27 kcal/mol compared to the activation barrier for neat isomerization [22].

1.3 Scale-Up and Commercialization Efforts in Hydrothermal Carbonization

Any commercial and real-world application of hydrothermal carbonization requires (HTC) to process large amounts of biomass feedstock. Therefore, a proper scale-up procedure must be done. Increasing the processing capacity is a conventional way to reduce the cost of production and treatment, as increasing the volume or size of unit operations does not lead to increased capital expenses by the same factor. This practice inevitably leads to a sizeable concentrated process plant. Regarding HTC scale-up, the high water content of typical feedstock should be considered to avoid hefty transportation costs. Therefore, having a modular design is preferred because it enables on-site treatment of the generated biomass. Process scale-up is effortful, and although scaling rules have been established that incorporate critical dimensionless numbers, in reality, matching similarity among processes is hard to achieve. This makes modular process design even more appealing, where production increase can be achieved only by adding modules.

Another challenge needed to be overcome regarding feeding the biomass into the HTC reactor. This becomes even more difficult when there is a continuous operation and a higher solid load percentage. That being said, feeding particles is generally more accessible at a larger scale. In addition, the batch operation has the advantage of a more straightforward feeding system since there is no pressure to go against in batch operation.

As it becomes clear from the above discussion choosing the right type of reactor is not straightforward. Furthermore, using each batch, flow, or mixed reactor has its advantages and drawbacks; here, we attempt to discuss those by giving real-world examples.

Batch operation is the easiest to handle, which can even be filled manually or by elementary systems such as bucket elevators. However, in batch operation, filling and emptying the reactor is time-consuming. Probably the most significant complication of batch operation is heat recovery and management. The heat recovery efficiency for batch systems is pretty low, and designing and operating a proper heat exchanger is challenging. Moreover, providing the reactor with heat becomes problematic from the outside as the reactor wall thickness increases by increasing the reactor volume. An example of a batch reactor on the industrial scale is constructed by a German company called HTCycle (former AVA-CO_2).

The application of flow reactors for hydrothermal carbonization has rarely been reported. Feeding this type of reactor requires a pump that can handle solids, provide very high pressures and operate at low flow rates, which is necessary for long residence times typically used in HTC. The solid load of the feed is also critical when choosing flow reactors, as for some biomass slurries, it becomes impossible to pump with more than a

certain solid mass content. For the flow reactor, the heat transfer from the outside is more efficient compared to a batch reactor due to a higher surface-to-volume ratio.

Mixed reactors for HTC have the advantage of better heat transfer, given that sufficient mixing is provided. Mixing reactors, however, are not known for their narrow residence time distribution, which means that some particles spend a very short time in the reactor and therefore do not undergo a chemical reaction. Still, some particles stay in the reactor for a long time. In addition, feeding this type of reactor needs a proper pump that can work against the very high pressure of the reactor.

The literature for the continuous flow HTC reactor is so limited, whereas reports of process simulation studies of continuous HTC are more common in the literature [30][31][32]. Recently Heidari *et al.* published a study on semi-continuous feeding for HTC of sawdust [33]. A hydrolytic system was used to push the biomass slurry into the reactor. The flow rate of 0.22L/h was provided to reach a reaction time of 60 minutes. The feeding system was designed to utilize the high pressure of reactor effluent to offset the enormous pressure difference between the feed hopper and the reactor itself. No cooling mechanism for the effluent slurry was mentioned in the study. By operating the same setup in batch mode, they could produce the hydochar to be compared with the semi-continuous operation product. They concluded that at temperatures below 240 °C, the degree of carbonization is slightly lower in semi-continuous operation; however, above that temperature, the carbon content of the hydrochar from the semi-continuous process was significantly higher. Such behavior was ascribed to the temperature gradient experienced by the biomass entering the

reactor in semi-continuous mode, resulting in the domination of the primary carbonization at the expense of the secondary carbonization pathway.

Hoekman *et al.* designed and constructed a process development unit (PDU) for hydrothermal carbonization of lignocellulosic biomass in semi-batch mode. They then compared its performance and products with a laboratory scale, 2-liter stirred Parr reactors [34]. The difficulty of feeding biomass slurry continuously into a high-pressure reactor was attempted to resolve by using a V-shaped tubular reactor system in which two conveyer augurs are used in an inclined configuration to move the slurry in and out of the reactor. The reacting zone containing the hot compressed water was at the bottom of the V shape configuration where two augurs met. The heating was provided externally using band heaters. The hydrochars produced by the continuous reactor showed overlapping results regarding energy densification and gaseous product yield with the batch reactor. Chemical analysis of the obtained liquid samples also showed good agreement with batch reactor tests.

In another study on the continuous HTC process published by Hoekman *et al.*, the idea of using a twin-screw extrusion system was described [35]. The system was designed to produce hydrochar from loblolly pine in fast hydrothermal carbonization. The reactor was equipped with co-rotating screws with reversed screw segments to create a high-pressure reaction zone where the HTC process takes place. The operational temperature, residence time, and flow rate were 230-250°C, 20-30 sec., and 9.4-6.5 kg/h, respectively. Analysis of the produced chars indicated lower energy densification compared to batch operation.

The chemical composition of the obtained products was different as well. The observed difference was ascribed to the short reaction time within the system.

1.4 Organization of Dissertation

This dissertation thoroughly investigates nutrient recovery and solid hydrocar production utilizing hydrothermal treatment of animal waste. The extraction and solubilization of nutrients under different hydrothermal treatment conditions are reported in Chapter 2. Reaction temperature, reaction time, acid addition, and the concentration of the added acids were scrutinized for their impact on the extraction of phosphorus and nitrogen content of cow manure into the process water. Moreover, a mass balance of total nitrogen and phosphorus is reported. Using the optimum experimental condition identified in Chapter 2 for nutrient extraction, we extended the recovery of nutrients further in Chapter 3. Where the precipitation of extracted nutrients is inspected, the effect of organic matter in the precipitation process and the nutrient removal efficiency have been explored under various experimental conditions. The elemental composition of the precipitates is reported, and the X-ray diffraction technique presents the crystalline structure of the solids.

Chapter 4 describes the hydrothermal treatment of pig and cow manure and compares the properties of hydrochar produced from the two different feedstocks. The fractionation of total nitrogen and phosphorus into organic nitrogen, nitrate, and ammonia is investigated in depth. The difference between total phosphorus and phosphate in the process water is presented as well. The fuel properties of produced hydrochars, such as their high heating values, are reported and compared under different experimental conditions. The hydrochar yield of several inorganic minerals is calculated and compared. Finally, a complete mass

balance of carbon, nitrogen, and phosphorus is carried out to understand the partitioning of those elements among the process products.

In the end, a set of conclusions are drawn in Chapter 5 to summarize the results and discuss their implications on nutrient recycling technology developments. Several features uncovered during this dissertation can help understand hydrothermal carbonization's benefits and limitations, while some predictions may guide future investigations.

1.5 References

[1] B. M. H. J. Langholtz, L. M. Stokes, and Eaton, “2016 billion-ton report advancing domestic resources for a thriving bioeconomy,” 2016.

[2] D. N. and M. E., “FY-2005 Annual Report Manure and Byproduct Utilization,” 2005.

[3] S. R. Carpenter, N. F. Caraco, D. L. Correll, R. W. Howarth, A. N. Sharpley, and V. H. Smith, “Nonpoint pollution of surface waters with phosphorus and nitrogen,” *Ecol. Appl.*, vol. 8, no. 3, pp. 559–568, 1998.

[4] O. Oenema, D. Oudendag, and G. L. Velthof, “Nutrient losses from manure management in the European Union,” *Livest. Sci.*, vol. 112, no. 3, pp. 261–272, Dec. 2007.

[5] D. Chadwick, J. Wei, T. Yan’an, Y. Guanghui, S. Qirong, and C. Qing, “Improving manure nutrient management towards sustainable agricultural intensification in China,” *Agric. Ecosyst. Environ.*, vol. 209, pp. 34–46, Nov. 2015.

[6] E. Feinerman, D. J. Bosch, and J. W. Pease, “Manure applications and nutrient standards,” *Am. J. Agric. Econ.*, vol. 86, no. 1, pp. 14–25, 2004.

[7] J. Webb, R. E. Thorman, M. Fernanda-Aller, and D. R. Jackson, “Emission factors for ammonia and nitrous oxide emissions following immediate manure incorporation on two contrasting soil types,” *Atmos. Environ.*, vol. 82, pp. 280–

287, Jan. 2014.

[8] S. G. Sommer and N. J. Hutchings, “Ammonia emission from field applied manure and its reduction - Invited paper,” *European Journal of Agronomy*, vol. 15, no. 1. Elsevier, pp. 1–15, 01-Sep-2001.

[9] N. T. Phan, K. H. Kim, D. Parker, E. C. Jeon, J. H. Sa, and C. S. Cho, “Effect of beef cattle manure application rate on CH4 and CO2 emissions,” *Atmos. Environ.*, vol. 63, pp. 327–336, Dec. 2012.

[10] P. E. Savage, S. Gopalan, T. I. Mizan, C. J. Martino, and E. E. Brock, “Reactions at supercritical conditions: Applications and fundamentals,” *AIChE J.*, vol. 41, no. 7, pp. 1723–1778, 1995.

[11] T. M. Pawlowski and C. F. Poole, “Solvation characteristics of pressurized hot water and its use in chromatography,” *Anal. Commun.*, vol. 36, no. 3, pp. 71–75, Jan. 1999.

[12] H. Weingärtner and E. U. Franck, “Supercritical water as a solvent,” *Angewandte Chemie - International Edition*, vol. 44, no. 18. John Wiley & Sons, Ltd, pp. 2672–2692, 29-Apr-2005.

[13] M. Plaza and C. Turner, “Pressurized hot water extraction of bioactives,” *TrAC Trends Anal. Chem.*, vol. 71, pp. 39–54, Sep. 2015.

[14] N. Galamba, A. Paiva, S. Barreiros, and P. Simões, “Solubility of Polar and Nonpolar Aromatic Molecules in Subcritical Water: The Role of the Dielectric

Constant," *J. Chem. Theory Comput.*, vol. 15, no. 11, pp. 6277–6293, Nov. 2019.

[15] W. L. Marshall and E. U. Franck, "Ion product of water substance, 0–1000 °C, 1–10,000 bars New International Formulation and its background," *J. Phys. Chem. Ref. Data*, vol. 10, no. 2, p. 295, Oct. 2009.

[16] Y. Cheng, F. Xue, S. Yu, S. Du, and Y. Yang, "Subcritical water extraction of natural products," *Molecules*, vol. 26, no. 13, Jul. 2021.

[17] P. Karásek, B. Hohnová, J. Planeta, L. Št'avíková, and M. Roth, "Solubilities of selected organic electronic materials in pressurized hot water and estimations of aqueous solubilities at 298.15 K," *Chemosphere*, vol. 90, no. 6, pp. 2035–2040, Feb. 2013.

[18] J. W. Tester and J. A. Cline, "Hydrolysis and oxidation in subcritical and supercritical water: Connecting process engineering science to molecular interactions," *Corrosion*, vol. 55, no. 11, pp. 1088–1100, 1999.

[19] D. R. Lide, "SteamTab: Thermodynamic and Transport Properties of Steam," *J. Chem. Inf. Comput. Sci.*, vol. 36, no. 6, pp. 1228–1228, Jan. 1996.

[20] A. Kruse and E. Dinjus, "Hot compressed water as reaction medium and reactant. Properties and synthesis reactions," *J. Supercrit. Fluids*, vol. 39, no. 3, pp. 362–380, Jan. 2007.

[21] M. Akizuki, T. Fujii, R. Hayashi, and Y. Oshima, "Effects of water on reactions for waste treatment, organic synthesis, and bio-refinery in sub- and supercritical

water," *J. Biosci. Bioeng.*, vol. 117, no. 1, pp. 10–18, Jan. 2014.

[22] N. Akiya and P. E. Savage, "Roles of water for chemical reactions in high-temperature water," *Chem. Rev.*, vol. 102, no. 8, pp. 2725–2750, 2002.

[23] O. M. Ogunsola, "Decomposition of isoquinoline and quinoline by supercritical water," *J. Hazard. Mater.*, vol. 74, no. 3, pp. 187–195, Jun. 2000.

[24] J. Feng, S. N. V. K. Aki, J. E. Chateauneuf, and J. F. Brennecke, "Hydroxyl radical reactivity with nitrobenzene in subcritical and supercritical water," *J. Am. Chem. Soc.*, vol. 124, no. 22, pp. 6304–6311, Jun. 2002.

[25] A. Yousefifar, S. Baroutian, M. M. Farid, D. J. Gapes, and B. R. Young, "Fundamental mechanisms and reactions in non-catalytic subcritical hydrothermal processes: A review," *Water Res.*, vol. 123, pp. 607–622, Oct. 2017.

[26] M. Möller, P. Nilges, F. Harnisch, and U. Schröder, "Subcritical water as reaction environment: Fundamentals of hydrothermal biomass transformation," *ChemSusChem*, vol. 4, no. 5, pp. 566–579, May 2011.

[27] N. Akiya and P. E. Savage, "Kinetics and mechanism of cyclohexanol dehydration in high-temperature water," *Ind. Eng. Chem. Res.*, vol. 40, no. 8, pp. 1822–1831, Apr. 2001.

[28] N. Simsek Kus, "Organic reactions in subcritical and supercritical water," *Tetrahedron*, vol. 68, no. 4. Pergamon, pp. 949–958, 28-Jan-2012.

[29] Y. Jung and R. A. Marcus, "On the theory of organic catalysis 'on water,'" *J. Am.*

Chem. Soc., vol. 129, no. 17, pp. 5492–5502, May 2007.

[30] G. Ischia and L. Fiori, "Hydrothermal Carbonization of Organic Waste and Biomass: A Review on Process, Reactor, and Plant Modeling," *Waste and Biomass Valorization*, vol. 1. Springer Science and Business Media B.V., p. 3, 06-Oct-2020.

[31] J. Gómez, G. Corsi, E. Pino-Cortés, L. A. Díaz-Robles, V. Campos, F. Cubillos, S. K. Pelz, S. Paczkowski, S. Carrasco, J. Silva, M. Lapuerta, A. Pazo, and E. Monedero, "Modeling and simulation of a continuous biomass hydrothermal carbonization process," *Chem. Eng. Commun.*, vol. 207, no. 6, pp. 751–768, 2020.

[32] B. Erlach, B. Harder, and G. Tsatsaronis, "Combined hydrothermal carbonization and gasification of biomass with carbon capture," *Energy*, vol. 45, no. 1, pp. 329–338, Sep. 2012.

[33] M. Heidari, O. Norouzi, K. MacDermid-Watts, B. Acharya, Y. Zhang, and A. Dutta, "Product evaluation of hydrothermal carbonization of biomass: semi-continuous vs. batch feeding," *Biomass Convers. Biorefinery*, vol. 12, no. 1, pp. 15–25, Jan. 2022.

[34] S. K. Hoekman, A. Broch, C. Robbins, R. Purcell, B. Zielinska, L. Felix, and J. Irvin, "Process Development Unit (PDU) for Hydrothermal Carbonization (HTC) of Lignocellulosic Biomass," *Waste and Biomass Valorization*, vol. 5, no. 4, pp. 669–678, Aug. 2014.

[35] S. K. Hoekman, A. Broch, L. Felix, and W. Farthing, “Hydrothermal carbonization (HTC) of loblolly pine using a continuous, reactive twin-screw extruder,” *Energy Convers. Manag.*, vol. 134, pp. 247–259, Feb. 2017.

Chapter 2

Factors Affecting Solubilization of Phosphorus and Nitrogen Through Hydrothermal Carbonization of Animal Manure

2.1 Introduction

The damaging impacts of using fossil resources as the primary energy source and chemicals on Earth's climate are scientifically precise [1]. On the other hand, the scarcity of such resources adds to the pressure of finding feasible and sustainable alternatives. As there is no single ultimate solution to the problem, the approach to mitigate the environmental effects of petroleum use has prompted the rationale to develop new production chains. Using biomass as a sustainable source of energy carriers and producing material products is a proposed alternative that has led to the emergence of the biorefinery concept [2]. The biomass feedstock can be processed in a biorefinery to produce bio-derived chemicals and biofuels by applying different conversion technologies. The development of these technologies has been the main focus of much academic research. This paper, in particular, will discuss the potential application of hydrothermal carbonization (HTC) in producing value-added biochemicals from biomass. As of 2017, around 709 million dry tons of agricultural residue, energy crops, and waste resources are available in the US, and this number is expected to reach 1.5 billion tons by 2040 [3]. In addition, the availability of high moisture biomass such as animal manure, food waste, and sludge is also significantly increased in the US. For example, livestock and poultry in the U.S. produced over 1.1 billion tons (wet weight) of manure [4]. Given the sheer amount of waste biomass

continuously generated worldwide, finding feasible ways to utilize this enormous untapped potential is highly alluring.

The ever-increasing production of animal manure from large confined animal feeding operations (CAFOs) has raised concerns over the environmental impacts of surplus manure. The expansion in the number and size of CAFOs stemming from the need to meet the rising demand for meat of an increasing world population and from changing diets has resulted in the amount of manure production far beyond what the local cropland may use as fertilizer [5]. The environmental burden of such an excessive amount of manure via the emission of greenhouse gases (methane and N_2O) is documented [6][7]. Ammonia emission can deteriorate the local air, soil, and water quality [8][9]. On the other hand, since animal manure contains nutrients such as nitrogen and phosphorus, the pollution of ground and surface water through runoff and leaching of these nutrients (eutrophication) is highly likely [7].

Phosphorus is an essential structural element of cell membranes for all living organisms and a necessary agricultural fertilizer considered a nonrenewable resource with a finite supply [10]. Reported values for cow manure's phosphorus (P) and nitrogen (N) content show a wide variation primarily due to the animals' diet. For example, the total P content of dairy manure can vary in the range of 2.8-18.3 g/kg. Generally, the P content of the manure can be classified as organic and inorganic, where the latter is the more significant portion of the total P content. The most biologically available form is water-soluble P, which makes it susceptible to runoff in surface water. The second most available P is labile P, which is any sort of bicarbonate extractable form of inorganic and organic P. Sorbed P

is the following available form identified by its solubility in sodium hydroxide solution. The most refractory form of manure P is acid-extractible phosphorus, which occurs as a stable residual form in the soil when applied to the cropland [11][12]. The dominant P species in dairy manure is orthophosphate (PO_4^{3-}), classified as inorganic P. Phosphorus can also be in the form of phytate (mainly phytic acid and α-glycerophosphate), which is identified as organic phosphorus [13]. For nitrogen, the primary source of manure N comes from nitrogenous compounds such as amino acids, constituents of undigested proteins in animal diet, amino sugars, nucleic acids, and urine. Several sources have reported that almost 70-80% of the nitrogen, 60-85% of the phosphorus, and 80-90% of the potassium in animal diet end up in its manure [14][15].

Hydrothermal carbonization (HTC) is one of the many technologies developed to convert biomass [16]. The HTC process includes heating biomass in a water medium at subcritical temperatures (180-240˚C) and autogenous pressures. By ensuring that the pressure consistently exceeds the water vapor pressure, liquid water is kept present as the reaction medium. One of the main advantages of hydrothermal processing is its compatibility with treating high moisture (wet) feedstocks such as animal waste. While some technologies, such as thermal pyrolysis, require dry biomass substrate to process, HTC has the inherent advantage of avoiding the energy needed for drying by promoting reactions in an aqueous medium. As a thermochemical conversion method, HTC exploits the properties of subcritical water to facilitate a network of reactions, including dehydration, decarboxylation, hydrolysis, polymerization, and aromatization [16][17]. HTC reactions produce a carbon-rich solid product known as hydrochar and an aqueous solution

containing various organic compounds. In addition, depending on the reaction temperature, a gas phase, mainly CO_2, is generated with increasing temperature. Subcritical water undergoes a dramatic change in dielectric constant and ionic product [18][19]. Biomass in this hydrothermal environment reacts in an overall exothermic process [20]. Although the exact reaction mechanisms are mainly unknown, some simple reaction models have been proposed. It is believed that hydrolysis is the first reaction initiated at temperatures above 180 °C that leads to the breakup of ester and ether bonds of the bio-macromolecules present in the biomass [21]. Various organic acids are created as intermediate compounds during the HTC reaction, reducing the reaction medium's pH and further catalyzing the HTC reactions. The production of solid hydrochar is attributed mainly to condensation and polymerization reactions. Temperature is an essential factor in the HTC process due to its dominant effect on the properties of subcritical water, prominently characterized by high ionic activity. Aside from the change in the ionic activity of water at elevated temperatures, the alteration in bulk properties of water, such as viscosity, promotes more effortless mass transfer from and into porous media, thus further degrading the biomass [16][17].

Furthermore, its decreased dielectric constant results in substantially different solubilization behavior more commonly associated with nonpolar solvents. Although the effects of HTC reaction temperature on the properties of the solid product (hydrochar) have been studied extensively, the same cannot be claimed concerning HTC aqueous products. In general, hydrochar produced at increased temperatures also has a higher energy value due to the reduction in O/C and H/C atomic ratios [22]. In addition, temperature has a

preeminent effect on the distribution of HTC products. Higher reaction temperatures result in lower hydrochar yield and increased gas production [23] [24].

Thus far, the HTC process research has mainly focused on two applications [25]. The first one uses the HTC process as an alternative method for waste disposal, competing with techniques such as anaerobic digestion. The second application produces solid fuel from different kinds of biomass. However, relatively few efforts have been put towards understating its potential to produce chemicals and extract nutrients from waste manure. Recently, Ghanim *et al.* [26] have studied the effects of the initial pH of the reaction mixture on the yield and chemical properties of hydrochar from hydrothermal carbonization of poultry litter. They found that using sulfuric acid and acetic acid increases the carbon content and HHV of the resulting hydrochar. In terms of solid yield, the results reported the importance of the acid strength is more pronounced than the initial pH. Furthermore, sulfuric acid as an additive obtained a fifty percent increase in the hydrochar yield. They assigned this to the catalytic effect of sulfuric acid, which accelerates the formation of humins [26]. However, Reza *et al.* [27] observed an opposite trend in the HTC treatment of wheat straw at 200 and 260 ℃ by using acetic acid and potassium hydroxide (KOH) to provide a pH range of 2-12 for the HTC reaction. According to their study, at both 200 ˚C and 260 ˚C, the hydrochar yield decreased by increasing the pH of the feedwater. The proposed explanation was the enhancement of hydrogen bond cleavage at lower pH, especially at low temperatures, resulting in maximum hemicellulose degradation in biomass. That being said, the effect of reaction temperature on the solid yield of hydrochar was more dominant than feedwater pH's effect [27].

Heilman *et al.* [28] have investigated the application of HTC to capture and recycle phosphate from poultry, swine, and cow manure. The hydrothermal reaction conducted at the temperature range of 240-260 ^{o}C resulted in more than 90% of the total phosphorus in all three feedstocks occurring as phosphate salt in the solid hydrochar. The proposed mechanism of phosphorus capture in hydrochar involves the formation of insoluble phosphates that can arise in colloidal form or electrostatically bond to the protein existing in the animal manure. These phosphates can be trapped within or precipitated onto the growing hydrochar. The main factor behind the formation of insoluble phosphate salts was the presence of multivalent metal cations, including aluminum, magnesium, calcium, potassium, and iron. It was shown that the relative concentration of phosphorus to multivalent cations was correlated with the extent of phosphorus capture in the solid hydrochar [28]. The influence of different acidic and basic additives on the extraction of nitrogen and phosphorus in the aqueous phase of hydrothermal treatment of swine manure has been studied by Ekpo *et al.* [29]. They reported that acid addition favors phosphorus extraction into the aqueous phase. Moreover, the effect of reaction temperature on phosphorus extraction was shown to be negative. The results showed that neither acid nor base added impacted nitrogen extraction substantially. The highest level of phosphorus recovery was achieved by using sulfuric acid at 170 ^{o}C, where 94% of the overall phosphorus was extracted to the aqueous phase [29]. Kruse *et al.* [30] studied nitrogen's fate during hydrothermal carbonization using three different biomass types, including carrot green, the algae *Chlorella pyrenoidosa,* and straw. The partition of nitrogen was highly dependent on the nature of the biomass, and the total removal of the nitrogen from feedstock was not observed. It was concluded that the chemical nature of nitrogen in the

feedstock plays an important role. The high protein content can result in a high amount of ammonium in the liquid phase.

On the other hand, when the protein content of the biomass is low, for example, in the case of carrot green and straw, the amount of nitrate is much higher concerning ammonium [30]. Reza *et al*. investigated the distribution of carbon and nutrients (NPK) during the hydrothermal treatment of cow manure in the range of 180-260 °C for 5 and 30 min. The results indicated that large portions of the phosphorus and other minerals were retained in the solid hydrochar. Concerning nitrogen and potassium, they reported roughly 50% solubilization of nitrogen and almost total solubilization of potassium [31]. The present work aims to study the effect of HTC operational conditions (reaction time, temperature, acid addition, and acid concentration) on nutrient (N and P) recovery in the liquid phase through the HTC of cow manure. No previously published works have conducted a rigorous study to consider the effects of time, temperature, and acid (organic and inorganic) on nutrient recovery from cow manure. The results presented in this chapter have been published as a peer-reviewed paper in the *ACS Sustainable Chemistry & Engineering* journal (ACS Sustainable Chem. Eng. 2020, 8, 33, 12462–12470).

2.2 Material and Methods

2.2.1 Feedstock preparation

Raw manure was obtained from the University of Nevada, Reno (UNR) Main Station Farm (Reno, NV). The farm is keeping about 100 beef steers for various research purposes, with the current animal age of 2 years. The steers are fed a standard alfalfa diet with a composition of 91.8% dry matter, 40.5% natural detergent fiber (NDF), 29.1% acid

detergent fiber (ADF), and 18.7% crude protein (dry base). In comparison, 60.5% of the protein is digestible. A typical manure collection procedure involved scooping manure into plastic bags from a pile of fresh manure in the steer pen. After collection, the manure was dried under open air conditions for several days before being ground in a hammer mill to reduce its particle size to 0.5-3 mm. The manure is then stored in Ziploc bags before HTC experiments. Dried manure was digested, and its composition of selected cations was measured by ICP-OES. In addition, CHNS composition was measured by LECO elemental analyzer. Table 2.1 summarizes the elemental composition of the manure used as the feedstock in this study.

Table 2.1 Characterization of the starting cow manure (composition in weight percent, dry basis).

[a]: calculated value

Element	Wt.%
C	37.40
H	5.00
N	1.80
S	0.50
O[a]	28.30
Al	0.16
Ca	1.44
Fe	0.17
K	0.41
Mg	0.43
Na	0.69
P	0.38
Ash	27.00

2.2.2 HTC experimental procedure

HTC experiments were conducted in a 1.8 L Parr reactor with a 4545 temperature controller. The reactor was filled with 80 g of dried manure and 1 liter of solution (deionized water or acid solution) to maintain a 1:12 biomass-to-water ratio. After carefully sealing the reactor lid, trapped oxygen inside the reactor was purged by a steady flow of nitrogen gas for 10 min at 5 bar. A PID controller supplied by Parr Instrument Company with an accuracy of ±5 ^{o}C controlled the reactor temperature. The heating ramp for all experiments was identical at around 5 ^{o}C/min. The reactor was mixed with two turbine-type impellers mounted on a stirring shaft, while the stirring speed of the mixer was fixed at 140 rpm for all experiments. One of the impellers was positioned closer to the bottom of the vessel to keep solids in suspension. The other was located near the vortex's base to pull solids down from the surface and minimize mass transfer resistance. The reactor's pressure was measured and monitored throughout the reaction. After finishing the experiment, the pressure was recorded at room temperature to estimate gas production. The liquid samples were withdrawn during the reaction using a sample collection vessel (10 mL) provided by Parr Instrument Company. This mechanism allowed for the collection of liquid samples at elevated temperatures and pressures. The arrangement for this sampling mechanism included a cooling sleeve to cool the sample while removing it. Liquid samples were filtered with a Whatman 6 (3 µm pore size) filter paper, and the pH was measured and recorded. The samples were transferred into 50 mL centrifuge tubes and stored in a refrigerator prior to further chemical analysis. At the end of the experimental run, the

reactor was cooled by immersing the reactor body inside an ice water bath to reach a maximum cooling rate of 10 ^{o}C/min. After reaching room temperature, the reactor was depressurized under the fume hood. The reactor and the glass liner were rinsed with DI water to capture all the solids. Vacuum filtration with Whatman 6 filter paper was used to collect the hydrochar. Filtered hydrochar was dried at 105 ^{o}C overnight inside a heating oven and stored inside Ziploc bags for future chemical analysis.

2.2.3 Chemical Analysis of liquid samples

The liquid samples were analyzed for the total Kjeldahl nitrogen (TKN), nitrite (NO_2^-), nitrate (NO_3^-), total nitrogen (TN), and total phosphorus (TP). A spectrophotometric method was applied to measure the samples' nitrogen and phosphorus content, which were digested at 100 ˚C for 1 hr in a HACH DRB200 digester. After cooling the samples, measurements were made with a HACH DR1900 spectrophotometer. In TP analysis, all phosphorus content of the sample is converted into orthophosphate ions (PO_4^{3-}) in the digestion stage. Then phosphate ions react with molybdate and antimony ions in an acidic solution to form an antimonyl phosphormolybdate complex that is reduced by ascorbic acid to phosphormolybdenum with blue color. In the TKN method, inorganic and organic nitrogen (TN) are first oxidized to nitrate by digestion with peroxodisulfate. The nitrate ions react with 2,6-dimethylphenol in a sulfuric and phosphoric acid solution to form a nitrophenol, and the TN is subsequently measured. Oxidized forms of nitrogen (NO_2^- and NO_3^-) in the original sample are determined in the second test vial and then subtracted from the TN, which results in TKN.

2.2.4 Chemical analysis of solid samples

The elemental composition (C, N, S, and H) of each solid sample was determined by a CHNS analyzer (LECO CHNS-932). Each analysis was performed in triplicates with a standard deviation of less than 5% in all cases. The quantification of metal content was obtained by ICP atomic emission spectroscopy using a model Elan 6000 Sciex Perkin Elmer apparatus. Before analysis, the samples were digested for 15 min in a microwave oven, using a mixture of hydrogen peroxide and nitric acid at 250 °C. This analysis was performed in duplicate.

2.2.5 Design of experiment

One strong inorganic acid (HCl) and one organic acid (citric acid) were selected to study the effect of acid addition on nutrient solubilization. An experiment was conducted for each temperature (170, 200, and 230 °C). During each experiment, liquid samples were collected after 5, 30, and 120 minutes of reaction time. A low and a high value (0.1 and 0.5) were used for both additive concentration and temperature, and a center point was used to detect any potential curvature in corresponding responses. As for additive concentration, 0.1 M was used for the low and 0.5 M for the high concentration. The center point for this experimental design was specified as 200°C and 0.3 M for temperature and additive concentration, respectively. The center point experiments were carried out in duplicate.

2.2.6 Statistical analysis

To understand the different effects of each factor (time, temperature, additive type, and additive concentration), collected samples were categorized into three groups (low, center, and high) based on the operational conditions. While the factor in question was constant

within each group, the other factors varied over all the experimental conditions. These factors, when averaged, would converge at the center point and would not change, moving from one group to the other. Therefore, the only parameter distinguishing the groups would be the single factor being investigated. For example, three groups were defined when studying the effect of time (5 min, 30 min, and 120 min), and the data from the samples collected at each of the mentioned reaction times above were included. Within each group (e.g., 5 min), data at all reaction temperatures and all acid additions were taken. For each group, the mean concentration of TP, TKN, and inorganic nitrogen (NO_2^-/NO_3^-) and the standard errors were calculated. An ANOVA test was used to determine if there was a significant difference between the group means. Moreover, a rigorous Tukey's HSD test was followed to identify statistically meaningful reaction conditions and trends. This statistical approach would rigorously allow for the study of primary factors' effects. However, this approach is limited to only evaluating the primary factors' impact. It does not allow for the evaluation of interactions between the factors, and it does not allow the assessment of higher-order effects.

2.3 Results and discussion

2.3.1 Solid yield and hydrochar properties

The solid yield and the elemental composition of the hydrochar produced in various experimental conditions are reported in Table A4. The obtained data indicate an increase in the carbon content of the hydrochars when high temperatures and high acidity were applied during the hydrothermal processing. The impact of high acidity on the carbon composition of the hydrochar is even more significant compared to high temperatures. The

solid yield of the hydrochar production is also substantially affected by HTC process conditions. Experiments carried out at higher temperatures generally resulted in lower hydrochar yields. The application of acidic additives decreased the yield of hydrochar as well. Accordingly, the HCl experiments created less hydrochar than citric acid. The lowest hydrochar yield was observed with HCl at 230 °C, and the highest solid yield was obtained with deionized water at 170 °C.

2.3.2 Time effect

The effect of reaction time on phosphorus and nitrogen recovery is represented in Figure 2.1. Figure 2.1(a) shows the concentration of PO_4^{3-} in HTC process liquid as a function of reaction time. While there is an apparent decrease in the amount of phosphate in the aqueous phase as the reaction proceeds, this trend is not significant at a 95% confidence level. The p-value obtained from ANOVA was 0.59. Therefore, it appears that reaction time's effect on the phosphorus's solubilization is without substantial importance, at least over the time studied in this research. The results suggest relatively quick phosphorus solubilization in HTC process liquid, in agreement with other studies investigating the reclamation of manure phosphorus for soil amendment applications [32]. For instance, in one study, around 90% of the total phosphorus content of pig manure was successfully recovered by a process called quick wash, where phosphorus was extracted by adding citric acid and HCl at ambient temperature [32].

The time effect on extracting organic and inorganic nitrogen in HTC process liquid is reflected in Figure 2.1(b) and 2.1(c), respectively. Although a trend of increasing TKN with reaction time can be seen, a statistical analysis shows no significant impact of time at

a 95% confidence level. In this case, ANOVA resulted in a p-value of 0.46. Although phosphorus extraction is relatively fast (Figure 2.1(a)), total nitrogen solubilization does not show the same behavior. Nitrogen recovery is less efficient in HTC conditions stemming from the nature of nitrogen species present in cow manure. Most nitrogen content comes from the breakdown of proteins, which starts by hydrolysis of large protein molecules into smaller amino acids. According to Ekpo *et al*. [33], further deamination of these amino acids occurs at elevated temperatures around 500 ˚C, well above the HTC temperature range.

The recovery of nitrogen oxide ions (NO_2^-/NO_3^-) is shown in Figure 2.1(c). As can be seen, the amount of inorganic nitrogen (NO_2^-/NO_3^-) is substantially less than that of organic nitrogen, resulting in an organic-to-inorganic nitrogen ratio of 4-5. The recovery of nitrogen oxide ions is approximately constant with reaction time (p-value 0.67). The time effect on inorganic nitrogen extraction in the liquid phase is negligible, as seen in the cases of phosphate and organic nitrogen (TKN).

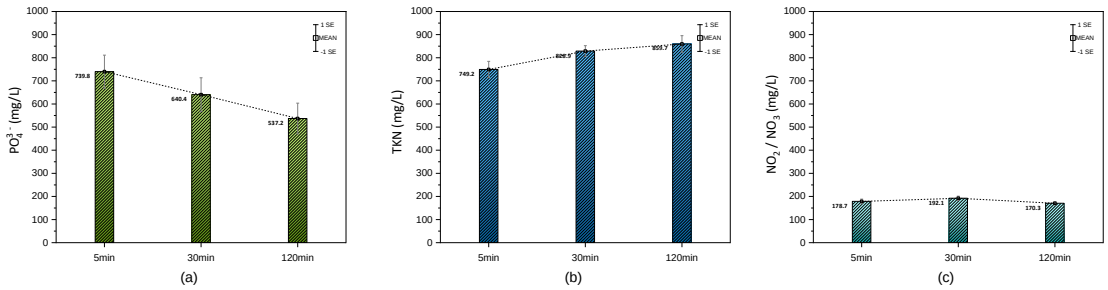

Figure 2.1 Phosphate (a), TKN(b), and NO_2^-/NO_3^- (c) recovery at different reaction times.

The error bars represent the standard error of all collected data at each reaction time. The average reaction temperature and acid concentration for each group are 200°C and 0.3M, respectively.

2.3.3 Temperature effect

The effect of temperature on the solubilization of nutrients is studied by arranging the collected data with the same methodology shown while looking at the effect of time. Figure 2.2(a) indicates the impact of temperature on phosphate recovery in the aqueous phase. Increased HTC reaction temperature bears a remarkably negative effect on the phosphate recovery, as seen from the steep slope of Figure 2.2(a). The statistical analysis (ANOVA) of these data confirms the significance of the trend with a p-value of 0.002. this observation agrees well with what has been reported in the literature [29]. The maximum amount of phosphate (847 mg/L) was recovered in the aqueous phase at 170 °C.

The effect of reaction temperature on organic and oxidized nitrogen recovery is shown in Figure 2.2(b) and 2.2(c). The organic nitrogen (TKN) content of the HTC liquid seems to increase by increasing the reaction temperature. There is a slight peak in TKN

concentration (857 mg/L) at 200°C. ANOVA test of these data reveals that the difference among the reported TKN values is not significant (p-value 0.44); therefore, the actual effect of reaction temperature on the organic nitrogen solubilization is highly doubtful within the range of reaction conditions studied. Conversely, the same statistical analysis (ANOVA) for the inorganic nitrogen (NO_2^-/NO_3^-) indicates that the values of NO_2^-/NO_3^- recorded at three reaction temperatures are statistically distinct (p-value 0.021), indicating a rather complex trend in oxidized nitrogen with a maximum concentration at 200 °C. Similar observations have been reported by Zhuang *et al.* [34] for hydrothermal treatment of sewage sludge at 150°C-300 °C.

The origin of TKN nitrogen in the liquid phase of the HTC process can be traced to the decomposition of protein-based nitrogen present in the feedstock, which is a pretty complex reaction mechanism. At first, the protein undergoes a hydrolysis reaction resulting in the cleavage of peptide bonds that link amino acids together, forming labile and stable (cyclic) amides. Then, under hydrothermal conditions (below 340 °C), the labile amides undergo a deamination reaction to generate ammoniacal nitrogen that contributes to the TKN amount of the HTC liquid [35]. On the other hand, further release of ammoniacal nitrogen is bound to the ring opening reaction that does not occur until the reaction condition becomes severe enough (above 380 °C) [34].

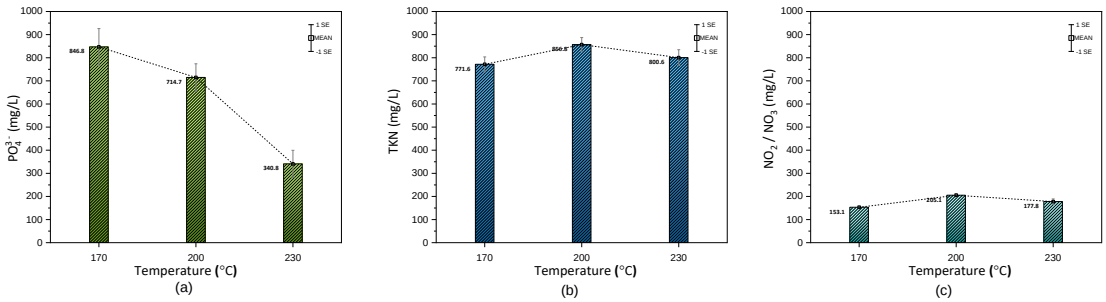

Figure 2.2 Phosphate, TKN, and NO_2^-/NO_3^- recovery at different reaction temperatures.

The error bars represent the standard error of all collected data at each reaction temperature. The average reaction time and acid concentration for each group are 52 min and 0.3M, respectively.

2.3.4 Effect of acid addition

Figure 2.3 shows the effect of acid addition on the solubilization of phosphorus and organic and inorganic nitrogen. As shown in Figure 2.3(a), the positive impact of using acidic additives on improving phosphate recovery is evident (p-value of 0.003). The maximum solubilization of phosphate occurred with citric acid at 895 mg/L. The addition of HCl was nearly as effective, with an average phosphate concentration of 742 mg/L. The lowest phosphate concentration in HTC liquid was observed after processing with deionized water and no acid addition. Previous studies have shown the favorable effect of acid addition on the extraction of phosphate [29]. Any possible explanation for the observed behavior of the phosphorus must include two aspects of the phenomena. First, the stripping of phosphorus from feedstock to the reaction mixture must be addressed. Second, phosphorus speciation (i.e., complexation and mineral forms) in the reaction mixture after extraction must be accounted for. Regarding the first process, while the exact mechanism of the phosphate

release remains to be fully understood, it seems that a high concentration of H^+ cations in the HTC reaction environment has catalyzed the reactions involved, i.e. (dehydration, deoxygenation, decarboxylation) in the extraction of phosphate from the feedstock [16]. Numerous studies have suggested that hydrothermal processing of biomass feedstock transforms all the phosphorus species into orthophosphates [36][37][38].

Regarding the second process, high amounts of Ca and Fe content in cow manure can induce the complexation process (i.e., formation of Ca- and Fe-associated P mineral) of orthophosphate anions [36]. As a result, insoluble minerals may be formed that precipitate during the HTC reaction alongside the hydrochar. Thus, a fraction of the overall P content of the feedstock is retained in the solid phase of the HTC process (hydrochar). For instance, the recovery of P in hydrochar for animal manure and sludge (high in Ca, Mg, Fe, and Al) is generally above 80% [28]. In contrast, it is virtually zero for the wasted agricultural biomass and algae that are low in the metals mentioned above [39][40]. However, reducing the pH of the reaction mixture by adding acidic additives hampers the complexation of P by altering the solubility of Ca- and Fe-associated P minerals resulting in increased phosphorus in the aqueous phase.

Figure 2.3(b) and 2.3(c) show the performance of citric acid and hydrochloric acid in generating TKN and NOx compared to deionized water. The results suggest similar amounts of TKN extraction with or without adding HCl, with mean values of 896 and 801 mg/L, respectively. However, a slightly smaller quantity of TKN (mean value of 737 mg/L) was observed with the addition of citric acid. Instead, the results of oxidized nitrogen in Figure 2.3(c) show that using citric acid leads to producing more oxidized nitrogen than

HCl and deionized water. ANOVA test of these results indicates that while TKN has not been affected by acid addition (p-value 0.10), the same cannot be claimed about NO_2^-/NO_3^- (p-value 0.00006); according to Tukey's test, citric acid is contributing the most to this difference. Nonetheless, since the concentration of NO_2^-/NO_3^- is low compared to TKN, total nitrogen concentration is not substantially affected to translate into a meaningful impact of used acidic additives on the solubilizing nitrogen content of the feedstock into the aqueous phase of the HTC process. In their study of applying different pH levels, including both acidic and basic pHs, in hydrothermal treatment of swine manure, Ekpo *et al.* also concluded that nitrogen extraction was not significantly influenced by pH [29].

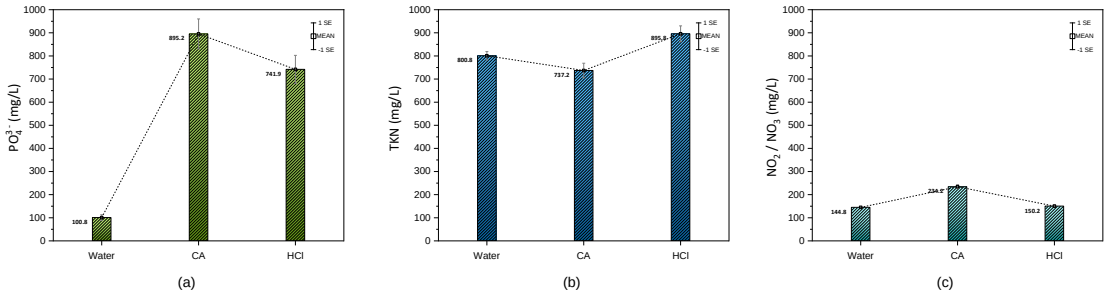

Figure 2.3 Phosphate, TKN, and NO_2^-/NO_3^- recovery with different acidic additives.

The error bars represent the standard error of all collected data at each reaction condition. The average reaction temperature, time, and acid concentration for each group are 200 °C, 52 min, and 0.3M, respectively.

2.3.5 Additive concentration effect

Table 2.2 summarizes the recorded pH values of the aqueous solutions obtained under each experimental condition. In general, pH varied between 0.92 and 7.56, with acid addition of HCl corresponding to the lowest pH. Interestingly, the pH increased within the first 5 min for all experiments except for one, a trend most apparent with the addition of either HCl or citric acid. The exception was the experiment done in DI water at 230 °C. The evolution of pH during the HTC reactions without acid addition shows increasing acidity, most probably due to the production of organic acids. The variation of pH during the experimental scenarios involving the addition of HCl and citric acid generally indicates a rising trend. This might be due to the destructive oxidation of the organic acids released by the HTC process, which leads to the formation of excessive gaseous byproducts such as CO and CO_2. Destructive oxidation of acids in solution reduces the acidity, hence causing the increase in the solution pH [41].

Table ٢.2 Recorded pH and solid yield

experiment	Solid yield (%)	pH			
		initial	5 min	30 min	120 min
DI water 170°C	60.35	6.70	7.56	6.53	6.21
DI water 200°C	54.88	6.70	7.47	6.47	5.91
DI water 230°C	43.50	6.69	5.87	5.60	5.51
HCl 0.1M 170°C	57.38	1.28	5.49	5.37	5.00
HCl 0.1M 230°C	45.50	1.28	4.48	4.50	4.46
HCl 0.3M 200°C	38.51	0.89	1.42	1.51	1.56
HCl 0.5M 170°C	38.88	0.68	0.92	0.96	0.99
HCl 0.5M 230°C	33.63	0.68	1.04	1.05	1.09
CA 0.1M 170°C	59.87	2.09	3.94	4.00	4.13
CA 0.1M 230°C	47.30	2.09	4.65	4.89	4.93
CA 0.3M 200°C	48.00	1.81	3.13	3.33	3.67
CA 0.5M 170°C	56.38	1.69	2.62	2.71	2.69
CA 0.5M 230°C	46.32	1.69	3.05	3.36	3.88

The acid concentration in the HTC process played an essential role in solubilizing phosphorus in the produced liquid phase (p-value of 0.001). Figure 2.4(a) displays the effect of acid concentration on the phosphate concentration in the liquid phase of the HTC process. Experiments with deionized water (no acid addition) resulted in the lowest phosphate concentration in the liquid phase (101 mg/L). The amount of phosphate increased dramatically from 339 to 1018 mg/L when the concentration of acid increased from 0.1 to 0.3 M. However further increase in additive concentration from 0.3 M to 0.5 M shows a minor change in the amount of phosphate in the aqueous phase. As discussed previously, acid addition has little effect on TKN solubilization, results that are confirmed in Figure 2.4(b) and Figure 2.4(c). The effect of acid concentration on NO_2^-/NO_3^- extraction is complex; we can see that 0.3 M is a critical concentration where NO_2^-/NO_3^- extraction increases. The corresponding amount of NO_2^-/NO_3^- for zero (no acid additive) and 0.1M acid concentration are 145 mg/L and 147 mg/L, respectively. However, by increasing the acid concentration to 0.3M, the amounts of NO_2^-/NO_3^- in the aqueous phase increase to 235 mg/L. Further increase beyond 0.3M in the acid concentration had no impact on the NO_2^-/NO_3^- concentration.

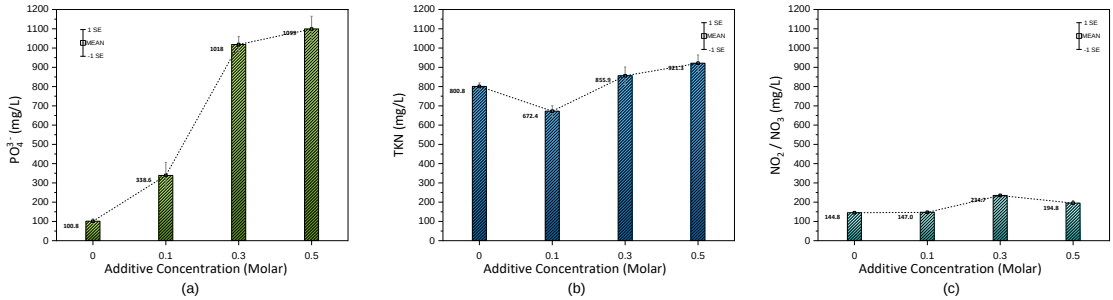

Figure 2.4 Phosphate, TKN, NO_2^-/NO_3^- concentration for different acidic concentrations.

The error bars represent the standard error of all collected data at each acid concentration. The average reaction temperature and time for each group are 200 ℃ and 52 min, respectively.

2.3.6 Mass balance of nitrogen and phosphorus

Here we report on mass balances for both N and P, comparing the contents of each in manure to that recovered in the reaction products. The data were normalized based on the mean mass balance of each element for all experiments. For each experimental condition, the fraction of P and N in the solid hydrochar and aqueous phase was divided by the total P and N fractions and multiplied by the mean mass balance of P and N obtained from all experiments. The mean mass balance of P for all experiments was 99.4%, with a standard error of 5.3%. For N, the mean mass balance was calculated as 102% with a 3.1% standard error.

Figure ٢.5(a) presents phosphorus mass balance during the HTC process at different temperatures. Note that it is not possible to determine a mass balance for reaction times less than 120 min since no solids were recovered for shorter reaction times. At 170 °C, the

majority (around 70 %) of phosphorus in the feedstock ends up in the liquid phase. However, by increasing reaction temperature, phosphorus partitioning between liquid and solid phases starts to change. At 200 °C, phosphorus is almost equally (45-50%) distributed between the solid phase hydrochar and the liquid phase. By further increasing the HTC reaction temperature to 230 °C, phosphorus in the hydrochar constitutes a large part of the overall phosphorus content present in the feedstock.

Figure 2.5(b) presents the partitioning of the phosphorus content of the feedstock between the solid and liquid phases during the experiments done with acid addition. Without an acidic additive, around 94% of the original manure phosphorus is retained in the hydrochar. The addition of acid has a significant effect on phosphorus distribution. The maximum phosphorus recovery in the aqueous phase occurs in the experiments conducted in HCl solutions. Citric acid also solubilizes phosphorus, with around 54% extraction of phosphorus. Due to the corrosive nature of HCl for the devices and equipment, its industrial application has severe constraints. Therefore, any future attempt to commercialize or scale up the HTC process aimed at nutrient recovery should consider the application of citric acid instead.

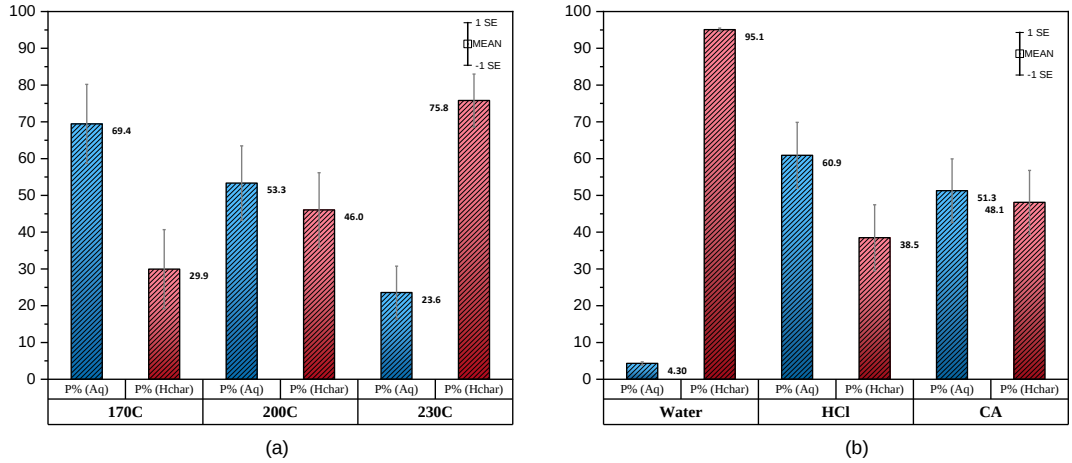

Figure 2.5. Phosphorus mass balance at different (a) reaction temperatures and (b) acidic additives. Liquid recovery is shown in blue (Aq), while solid recovery is shown in red (Hchar).

The mass balance closure for the nitrogen is shown in Figure 2.6. Regardless of the reaction temperature, approximately 60% of the total nitrogen is transferred to the liquid phase. At the same time, around 40% is retained in the hydrochar. The data indicate that changing temperature in the range studied does not significantly alter the distribution of nitrogen between the two phases. However, the maximum nitrogen solubilization occurs at 200 °C, with 63.4% of the nitrogen extracted into the aqueous phase. Nitrogen mass balances for the experiments performed with acid addition are represented in

Figure 2.6(b). The addition of HCl and citric acid shifted the partitioning of nitrogen to the aqueous phase. HCl increased nitrogen recovery in the liquid phase from 54% to 66% compared to trials done with deionized water, and this result is valid at a 95% confidence level. However, citric acid, on the other hand, only improved the recovery by around 6%,

which is within the margins of error and is not statistically distinct from the mass balance shown in deionized water. Taking a look at the individual data points might be insightful. The maximum phosphorus recovery in the liquid phase occurred in the trial with 0.5M citric acid at 170 °C after 30 min. The phosphate concentration in this sample was 1500 mg/L, accounting for 98% of the total phosphorus content of the feedstock. The second most effective trial in phosphorus solubilization was the experiment conducted with 0.5M HCl at 170 °C for 120 min, where the sample had a phosphate concentration of 1470 mg/L. For nitrogen, the most effective run could solubilize 78% of overall nitrogen with the experimental condition of 0.5M HCl at 230 °C after 120 min.

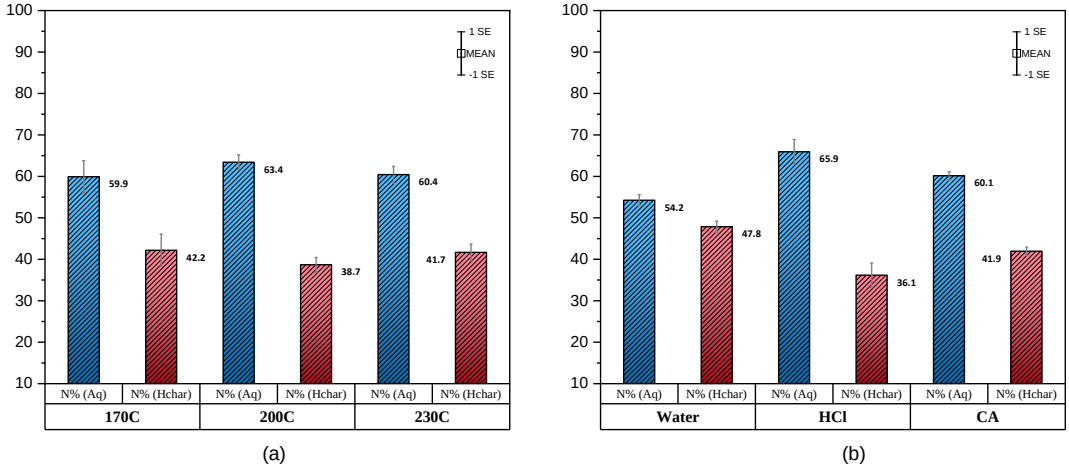

Figure 2.6. Nitrogen mass balance at different (a) reaction temperatures and (b) acidic additives.

2.4 Conclusion

This study investigated the influences of different operational conditions, including reaction time, temperature, the addition of acids, and their concentration, on the hydrothermal solubilization of nutrients in cow manure. Solubilization of phosphorus by hydrothermal carbonization is highly temperature dependent. Using low temperatures and low pH resulted in increased phosphorus recovery in the liquid phase. The impact of reaction time was negligible for nitrogen and phosphorus recovery in the 5 – 120 min range. Therefore, based on these results, the optimal operating condition for maximum recovery of phosphorus would be 170 °C for the reaction temperature and 5 min for the reaction time, using 0.3M citric acid as an acidic additive. Solubilization of TKN nitrogen was not affected significantly by altering reaction conditions. Nonetheless, solubilization of inorganic nitrogen (NO_2^-/NO_3^-) is impacted by the temperature and addition of citric acid, an effect attenuated by the observation that the generation of aqueous inorganic nitrogen is substantially smaller than the production of organic nitrogen under all conditions studied.

2.5 Supporting Information

The raw data was obtained from liquid and solid analyses for all experiments to produce figures for the primary manuscript (Appendix A).

2.6 Acknowledgement

The authors gratefully acknowledge the financial support from the US National Science Foundation (NSF #CBET-1856009), Spain's MINECO (PID2019-108445RB-I00), and Madrid Regional Government (S2018/EMT-511 4344). The authors thank Dr. Sage R. Hiibel and Nicholas Silva for their assistance with chemical analyses.

2.7 References

[1] S. Solomon, D. Qin, M. Manning, M. Marquis, and K. Averyt, *Climate Change 2007: The Physical Science Basis*. Cambridge: Cambridge University Press, 2007.

[2] F. Cherubini, "The biorefinery concept: Using biomass instead of oil for producing energy and chemicals," *Energy Convers. Manag.*, vol. 51, no. 7, pp. 1412–1421, Jul. 2010.

[3] B. M. H. J. Langholtz, L. M. Stokes, and Eaton, "2016 billion-ton report advancing domestic resources for a thriving bioeconomy," 2016.

[4] USEPA, "Literature Review of Contaminants in Livestock and Poultry Manure and Implications for Water Quality," 2013.

[5] H. Zhang and J. Schroder, "Animal manure production and utilization in the US," in *Applied Manure and Nutrient Chemistry for Sustainable Agriculture and Environment*, vol. 9789401788, Dordrecht: Springer Netherlands, 2014, pp. 1–21.

[6] A. B. Leytem, R. S. Dungan, D. L. Bjorneberg, and A. C. Koehn, "Emissions of ammonia, methane, carbon dioxide, and nitrous oxide from dairy cattle housing and manure management systems," *J. Environ. Qual.*, vol. 40, no. 5, pp. 1383–1394, 2011.

[7] P. H. Pagliari and C. A. M. Laboski, "Investigation of the inorganic and organic phosphorus forms in animal manure," *J. Environ. Qual.*, vol. 41, no. 3, pp. 901–

910, 2012.

[8] P. S. Hooda, A. C. Edwards, H. A. Anderson, and A. Miller, “A review of water quality concerns in livestock farming areas,” *Sci. Total Environ.*, vol. 250, no. 1–3, pp. 143–167, 2000.

[9] A. W. Jongbloed and N. P. Lenis, “Environmental Concerns about Animal Manure 1,” *J. Anim. Sci.*, vol. 76, no. 10, pp. 2641–2648, 1998.

[10] S. J. Van Kauwenbergh, M. Stewart, R. Mikkelsen, and others, “World reserves of phosphate rock… a dynamic and unfolding story,” *Better Crop.*, vol. 97, no. 3, pp. 18–20, 2013.

[11] Z. He, B. J. Cade-Menun, G. S. Toor, A.-M. Fortuna, C. W. Honeycutt, and J. T. Sims, “Comparison of Phosphorus Forms in Wet and Dried Animal Manures by Solution Phosphorus-31 Nuclear Magnetic Resonance Spectroscopy and Enzymatic Hydrolysis,” *J. Environ. Qual.*, vol. 36, no. 4, pp. 1086–1895, 2007.

[12] Z. He and C. W. Honeycutt, “Enzymatic Characterization of Organic Phosphorus in Animal Manure,” *J. Environ. Qual.*, vol. 30, no. 5, p. 1685, 2010.

[13] G. Li, H. Li, P. A. Leffelaar, J. Shen, and F. Zhang, “Characterization of phosphorus in animal manures collected from three (dairy, swine, and broiler) farms in China,” *PLoS One*, vol. 9, no. 7, p. e102698, 2014.

[14] J. A. Moore and M. J. Gamroth, “Calculating the fertilizer value of manure from livestock operations,” *Rehabilitation*, pp. 1–8, 1993.

[15] University of Massachusetts Amherst, “Crops, Dairy, Livestock and Equine: Sampling Dairy Manure | UMass Center for Agriculture, Food and the Environment,” 2019. [Online]. Available: https://ag.umass.edu/crops-dairy-livestock-equine/fact-sheets/plant-nutrients-from-manure. [Accessed: 12-Jan-2020].

[16] A. Funke and F. Ziegler, “Hydrothermal carbonization of biomass: A summary and discussion of chemical mechanisms for process engineering,” *Biofuels, Bioprod. Biorefining*, vol. 4, no. 2, pp. 160–177, Mar. 2010.

[17] M. Möller, P. Nilges, F. Harnisch, and U. Schröder, “Subcritical water as reaction environment: Fundamentals of hydrothermal biomass transformation,” *ChemSusChem*, vol. 4, no. 5, pp. 566–579, May 2011.

[18] Bröll, Kaul, Krämer, Krammer, Richter, Jung, Vogel, and Zehner, “Chemistry in Supercritical Water.,” *Angew. Chem. Int. Ed. Engl.*, vol. 38, no. 20, pp. 2998–3014, Oct. 1999.

[19] A. Kruse and E. Dinjus, “Hot compressed water as reaction medium and reactant. Properties and synthesis reactions,” *J. Supercrit. Fluids*, vol. 39, no. 3, pp. 362–380, Jan. 2007.

[20] A. Kruse and A. Gawlik, “Biomass conversion in water at 330-410 °C and 30-50 MPa. Identification of key compounds for indicating different chemical reaction pathways,” *Ind. Eng. Chem. Res.*, vol. 42, no. 2, pp. 267–279, 2003.

[21] A. A. Peterson, F. Vogel, R. P. Lachance, M. Fröling, M. J. Antal, and J. W. Tester, "Thermochemical biofuel production in hydrothermal media: A review of sub- and supercritical water technologies," *Energy Environ. Sci.*, vol. 1, no. 1, pp. 32–65, Jul. 2008.

[22] Y. Gao, X. H. Wang, H. P. Yang, and H. P. Chen, "Characterization of products from hydrothermal treatments of cellulose," *Energy*, vol. 42, no. 1, pp. 457–465, 2012.

[23] W. Yan, T. C. Acharjee, C. J. Coronella, and V. R. Vásquez, "Thermal pretreatment of lignocellulosic biomass," *Environ. Prog. Sustain. Energy*, vol. 28, no. 3, pp. 435–440, Oct. 2009.

[24] S. Román, B. Ledesma, A. Álvarez, C. Coronella, and S. V. Qaramaleki, "Suitability of hydrothermal carbonization to convert water hyacinth to added-value products," *Renew. Energy*, vol. 146, pp. 1649–1658, Feb. 2020.

[25] T. Wang, Y. Zhai, Y. Zhu, C. Li, and G. Zeng, "A review of the hydrothermal carbonization of biomass waste for hydrochar formation: Process conditions, fundamentals, and physicochemical properties," *Renew. Sustain. Energy Rev.*, pp. 223–247, Jul. 2018.

[26] B. M. Ghanim, W. Kwapinski, and J. J. Leahy, "Hydrothermal carbonisation of poultry litter: Effects of initial pH on yields and chemical properties of hydrochars," *Bioresour. Technol.*, vol. 238, pp. 78–85, 2017.

[27] M. T. Reza, E. Rottler, L. Herklotz, and B. Wirth, “Hydrothermal carbonization (HTC) of wheat straw: Influence of feedwater pH prepared by acetic acid and potassium hydroxide,” *Bioresour. Technol.*, vol. 182, pp. 336–344, Apr. 2015.

[28] S. M. Heilmann, J. S. Molde, J. G. Timler, B. M. Wood, A. L. Mikula, G. V Vozhdayev, E. C. Colosky, K. A. Spokas, and K. J. Valentas, “Phosphorus reclamation through hydrothermal carbonization of animal manures,” *Environ. Sci. Technol.*, vol. 48, no. 17, pp. 10323–10329, 2014.

[29] U. Ekpo, A. B. Ross, M. A. Camargo-Valero, and L. A. Fletcher, “Influence of pH on hydrothermal treatment of swine manure: Impact on extraction of nitrogen and phosphorus in process water,” *Bioresour. Technol.*, vol. 214, pp. 637–644, 2016.

[30] A. Kruse, F. Koch, K. Stelzl, D. Wüst, and M. Zeller, “Fate of Nitrogen during Hydrothermal Carbonization,” *Energy and Fuels*, vol. 30, no. 10, pp. 8037–8042, 2016.

[31] M. Toufiq Reza, A. Freitas, X. Yang, S. Hiibel, H. Lin, and C. J. Coronella, “Hydrothermal carbonization (HTC) of cow manure: Carbon and nitrogen distributions in HTC products,” *Environ. Prog. Sustain. Energy*, vol. 35, no. 4, pp. 1002–1011, Jul. 2016.

[32] A. A. Szögi, M. B. Vanotti, and P. G. Hunt, “Phosphorus recovery from pig manure solids prior to land application,” *J. Environ. Manage.*, vol. 157, pp. 1–7, 2015.

[33] U. Ekpo, A. B. Ross, M. A. Camargo-Valero, and P. T. Williams, “A comparison of product yields and inorganic content in process streams following thermal hydrolysis and hydrothermal processing of microalgae, manure and digestate,” *Bioresour. Technol.*, vol. 200, pp. 951–960, Jan. 2016.

[34] X. Zhuang, Y. Huang, Y. Song, H. Zhan, X. Yin, and C. Wu, “The transformation pathways of nitrogen in sewage sludge during hydrothermal treatment,” *Bioresour. Technol.*, vol. 245, pp. 463–470, 2017.

[35] C. He, K. Wang, Y. Yang, P. N. Amaniampong, and J. Y. Wang, “Effective nitrogen removal and recovery from dewatered sewage sludge using a novel integrated system of accelerated hydrothermal deamination and air stripping,” *Environ. Sci. Technol.*, vol. 49, no. 11, pp. 6872–6880, Jun. 2015.

[36] R. Huang and Y. Tang, “Evolution of phosphorus complexation and mineralogy during (hydro)thermal treatments of activated and anaerobically digested sludge: Insights from sequential extraction and P K-edge XANES,” *Water Res.*, vol. 100, pp. 439–447, 2016.

[37] L. Dai, F. Tan, B. Wu, M. He, W. Wang, X. Tang, Q. Hu, and M. Zhang, “Immobilization of phosphorus in cow manure during hydrothermal carbonization,” *J. Environ. Manage.*, vol. 157, pp. 49–53, Jul. 2015.

[38] W. Zhu, Z. R. Xu, L. Li, and C. He, “The behavior of phosphorus in sub- and super-critical water gasification of sewage sludge,” *Chem. Eng. J.*, vol. 171, no. 1, pp. 190–196, 2011.

[39] S. M. Heilmann, L. R. Jader, M. J. Sadowsky, F. J. Schendel, M. G. von Keitz, and K. J. Valentas, “Hydrothermal carbonization of distiller’s grains,” *Biomass and Bioenergy*, vol. 35, no. 7, pp. 2526–2533, Jul. 2011.

[40] S. M. Heilmann, L. R. Jader, L. A. Harned, M. J. Sadowsky, F. J. Schendel, P. A. Lefebvre, M. G. von Keitz, and K. J. Valentas, “Hydrothermal carbonization of microalgae II. Fatty acid, char, and algal nutrient products,” *Appl. Energy*, vol. 88, no. 10, pp. 3286–3290, 2011.

[41] S. Reiche, N. Kowalew, and R. Schlögl, “Influence of Synthesis pH and Oxidative Strength of the Catalyzing Acid on the Morphology and Chemical Structure of Hydrothermal Carbon,” *ChemPhysChem*, vol. 16, no. 3, pp. 579–587, Feb. 2015.

Chapter 3

Phosphorus Recovery from Aqueous Product of Hydrothermal Carbonization of Cow Manure

3.1 Introduction

Phosphorus is a finite resource with a world reserve of 69 billion metric tons [1]. Based on some estimations, its production is expected to peak between 2030 and 2040, after which supply will fall short of the rising demand [2]. Even though there is disagreement among the scientific community concerning phosphorus scarcity, there is a common agreement regarding the unsustainable state of the situation [3]. In recent years, there have been many efforts to develop new methods for recovering phosphorus from diverse waste streams. In addition to preserving a non-renewable resource, phosphorus recovery has a critical environmental protection aspect. Phosphorous pollution pervasive impacts aquatic ecosystems in rivers and ponds through eutrophication. Worldwide, excess phosphorus lost from agriculture is estimated to be around 8 million tons yearly. Most phosphorus and nitrogen inputs to cropland are attributed to synthetic fertilizers. However, due to the localized production of manure, the associated effect of excess nutrient supply is more problematic near large-scale animal farms [4]. According to a United States Department of Agriculture Economic Research Service (USDA ERS) report, 60%-70% of nitrogen and phosphorus from manure cannot be absorbed by the farmland on which it was generated or in adjacent and nearby fields [5].

Hydrothermal carbonization (HTC) has been used to carbonize diverse biomass feedstocks [6]. Nonetheless, the potential of using this technique to extract nutrients is relatively overlooked. The recovery of nutrients can be achieved either by solubilizing them into the aqueous phase or concentrating them in the solid phase [7]. Heilmann *et al.* explored the latter method to recover phosphorus from different kinds of animal manure by HTC and achieved a 90% phosphate recovery yield [8]. Sarrion *et al.* used HCl with HTC of food waste at 170 °C to increase the extraction of N and P as NH_4-N and PO_4-P into the process water [9]. The fate of nutrients during the hydrothermal treatment of various feedstocks has been investigated as well [10][11][12]. Alhnidi *et al.* studied the distribution of carbon and nutrient elements (NPK) among the products of hydrothermal carbonization of three model compounds representing biogas residues from silage and cattle manure. They found that most of the PO_4-P and K stayed in the process water during HTC [13]. Similarly, Dima *et al.* discovered that most potassium, sodium, and calcium in biogenic municipal waste were transferred to the liquid phase and less impacted by HTC conditions [10]. Idowu *et al.* investigated the impact of reaction time and temperature on the carbonization of food wastes and concluded that the phosphorous content of the hydrochar increases with reaction temperature. According to the results from this work, nitrogen, calcium, and magnesium were mainly sequestrated within the hydrochar during high-temperature HTC. At the same time, potassium and sodium were transferred into the process liquid [12]. In another study, Motavaf *et al.* investigated the possibility of nutrient recovery from simulated food waste by hydrothermal carbonization. They reported around 38% nitrogen and above 50% phosphorus transformation into the process water [14]. In their study of hydrothermal carbonization combined with anaerobic digestion of dairy manure, Belete *et*

al. found that using single-stage HTC with whey as the reaction media would enhance the nutrient concentration in the aqueous phase product. And improve the prospect of using it as liquid fertilizer [15]. The combination of hydrothermal carbonization and a nutrient recycling strategy via precipitation has been investigated by Becker *et al.* for phosphorus reclamation from sewage sludge. Because of the low phosphorus content in the HTC process waster, an additional acid leaching step was introduced to remove the phosphorus from hydrochar [16].

So far, the technologies developed to recycle phosphorus mainly focus on phosphorus recovery from industrial and municipal wastewater. However, phosphorus recovery is only feasible in waste streams with a minimum PO_4-P concentration of 50-60 mg/L [17], and with concentrations exceeding that threshold, recovery of phosphorus from livestock manure shows excellent potential.

The methods used for phosphorous removal and recovery from waste streams can be divided into biological, chemical, and physical processes. Although biological methods are pretty effective at removing almost 100% of P, they can be inconsistent or unreliable. For example, they can lead to starvation of the microorganism when the concentration of P in the influent is low. In addition, biological treatments require complex aeration control systems and are often land- and energy-intensive [18].

Physical methods used for phosphorus recovery include reverse osmosis, membrane bioreactors, and electrodialysis. Membrane bioreactors can achieve very low P discharge concentrations and have a lower ecological impact; however, membrane fouling is a

significant challenge in their application, making the whole process expensive and difficult to scale up [19][20].

Physical adsorption is another technique with high P removal efficiency and a fast rate, especially at low P concentrations. However, solution pH and the characteristics of the adsorbent can negatively and substantially influence the adsorption of phosphorus. Another disadvantage of this method is the need for sorbent regeneration, which makes the P recovery process a two-staged process. Finding the optimal and suitable absorbent is another challenge [21][22].

Chemical methods mainly focus on crystallizing P-containing minerals as recyclable products, such as magnesium ammonium phosphate (struvite, $MgNHPO_4 \cdot H_2O$). It contains a significant amount of phosphate, nitrogen, and magnesium. Therefore, it can be the basis of a slow-release organic fertilizer with a low heavy metal content compared to phosphate rock [23]. Factors impacting the formation of struvite, such as pH, supersaturation, etc., have been investigated previously [24][25]. In addition, other phosphorus-bearing minerals have been precipitated from wastewater, for example, hydroxyapatite ($Ca_5(PO_4)_3(OH)$) [26], which has many applications in agriculture and industry [27]. It has been reported that above neutral pH and Ca^{2+} concentration are the main contributors to the effectiveness of phosphorus recovery via HAP crystallization [28].

In addition to struvite and HAP, other phosphorus-containing minerals can be obtained from wastewater with the precipitation method as well; minerals such as monocalcium phosphate ($Ca\text{-}(H_2PO_4)2 \cdot H_2O$) and dicalcium phosphate ($CaHPO_4 \cdot 2H_2O$) that have comparable fertilization ability with struvite [29]. These materials can be produced at a

lower cost than struvite [26]. Moreover, industrial fertilizer production has no specific preference for raw materials. Therefore, struvite doesn't have any particular advantage over other materials if the feedstock's appropriate content of P_2O_5 is present [26]. The phosphorus recovery from livestock manure presented in this paper involves the dissolution of the bound phosphorus and separating phosphorus by precipitation processes.

Previously, we showed that HTC treatment of manure in an acidic environment and at the lower temperature limits of hydrothermal carbonization remarkably improves the dissolution of phosphorus from cow manure. The premise of the present study is to introduce a nutrient recycling strategy via coupling of hydrothermal carbonization and precipitation of phosphorus-incorporated solids from the aqueous phase of hydrothermal treatment of cow manure carried out with different acids. The results presented in this chapter have been submitted in a manuscript to the *Waste Management* journal on April 13, 2022.

3.2 Materials and Methods

3.2.1 Feedstock

The manure used throughout the experiments was freshly collected from the University of Nevada, Reno Main Station Farm. The manure had no additional water, with a minimal amount of bedding and straws. The manure was then dried in open air condition for a few days until its moisture content dropped below 5%. The dry solids were ground in a hammer mill down to the maximum size of 1 mm to homogenize the biomass. The fine solids were stored in plastic bags before analysis and used as feedstock for the hydrothermal carbonization reactions. CHNS/O compositions of the solids were obtained using a Thermo

Scientific FlashSmart elemental analyzer, including direct oxygen measurement. A detailed analysis of the manure used in this work is presented in Table 3.1. After digestion in an acidic environment, the total P content and other cations of the manure were measured by ICP-AES (Agilent 4200 MP-AES). The digestion was done in Anton Paar, Multiwave GO Microwave Digestion System. The samples were dissolved in a mixture of nitric acid, hydrochloric acid, and hydrogen peroxide, then moved into a pressure vessel and sealed properly. The vessel was heated up to 180°C and kept at that temperature for 10 minutes before being cooled. The numbers reported in Table 3.1 are the triplicate measurements average for ultimate analysis (CHNS/O) and elemental analysis (ICP-AES).

Table 3.1 Elemental analysis of raw manure, dry basis

Element	[mg/g]
P	4.38±0.05
Zn	0.14±0.01
Ca	25.37±0.11
Fe	3.24±0.01
Cu	ND
Pb	ND
Li	ND
K	10.42±0.02
Mg	7.40±0.03
Mn	0.14±0.02
Al	2.98±0.01
N	22±0.15
C	408±2.0
H	52.5±0.55
S	3.1±0.55
O	271.5±4.6

3.2.2 Hydrothermal reaction

Hydrothermal carbonization of dried solid wastes was carried out in a 1.8 L stainless steel closed vessel (Parr Instrument Company, IL), heated by a Calrod-Type sheathed element heater. For each HTC experiment, 80 gr of dried manure was mixed with 1 L of the solution to achieve a liquid to biomass ratio of 12 to 1. Four acids, citric acid, formic acid, oxalic acid, and sulfuric acid, each at 0.3M, were used to acidify the HTC reaction medium. According to our previous results, 170 °C yielded the highest phosphorus solubilization. Therefore, all HTC experiments were conducted at that temperature. Before heating, oxygen was purged from the reactor with a nitrogen flow. On average, the time needed for the reactor to reach 170 °C was 40 minutes (heating rate of 4 °C/min).

Reaction time was set at 10 min for all experiments [30]. That is, the reactor was held at 170 °C for 10 minutes starting at the time that the reactor first reached that temperature. A thermocouple and PID controller were used to control the temperature during the reaction. An impeller provided the mixing at a speed of 140 rpm. At the end of the experiment, the reactor was quickly cooled by removing the heater and immersing the sealed reactor in iced water. No gas or solid samples were collected from the reactor in these experiments. Instead, the liquid was separated using Whatman 6 (3 μm pore size) filter paper and refrigerated for further processing and analysis. For each liquid sample, phosphate and ammonia concentrations were measured by spectrophotometry. The concentration of other elements, such as Mg and Ca, was determined by ICP analysis.

3.2.3 Precipitation process

Precipitation of phosphate from hydrothermal carbonization aqueous product was carried out at three different Mg:P molar ratios (1.0, 1.5, 2.0). Ammonia was added to each solution to increase phosphorus recovery from the solution, as shown in other studies [31]. The amount of added ammonia was adjusted to achieve a molar ammonia to phosphate ratio of 2.0. All the precipitation experiments were conducted at room temperature and pH 9.5 with the addition of 10 N sodium hydroxide. The time for precipitation was held constant at 2 hr, and throughout this period, the solution was mixed using a shaker at 110 RPM. The precipitated solids were collected by filtration using Whatman 6 (3 μm pore size) filter paper, washed with deionized water, and dried at 105 ˚C overnight.

3.2.4 Analysis of solid waste (manure) and precipitants

CHNS/O composition of the solid samples was obtained in a Thermo Scientific FlashSmart elemental analyzer. The analysis was performed three times for each sample, and the average value was reported. Other cations were quantified by ICP-AES following digestion, as described above in the section on feedstock. The analysis for each sample was done in triplicate. And the average value was reported along with the standard error.

For their crystalline phase determination, solid precipitants were further characterized by X-ray diffraction (XRD). Finally, the solids were characterized by scanning electron microscopy / energy-dispersive X-ray spectroscopy (SEM/EDX) analysis to understand the morphology and qualitative elemental composition.

3.2.5 Analysis of hydrothermal aqueous product and supernatant

The spectrophotometry method measured the phosphate (PO4) and ammonia (NH4) content of liquids obtained from hydrothermal carbonization. The details of this can be found elsewhere [30]. Supernatant samples remaining after precipitation were likewise analyzed. ICP-AES measured the concentration of other elements following the procedure described in the previous section for the solids.

The efficiency of the precipitation for phosphate and ammonia was calculated according to the following formula:

$$\text{Efficiency} = \frac{C_i - C_f}{C_i} \times 100$$

Where C_i is the molar concentration before precipitation and C_f represents the concentration of the same species after precipitation. Note that the calculation of ammonia precipitation efficiency is based on total ammonia concentration, including ammonia added to raise the molar ratio of NH_4:P to 2.0, as described above.

Table 3.2 Analysis of hydrothermal aqueous products with different acids. All entries are given in mg/L, but N:P is calculated as a molar ratio.

	Citric Acid	Formic Acid	Oxalic Acid	Sulfuric Acid
pH	2.7	2.9	1.7	1.3
NH_4 [mg/L]	152	153	257	274
PO_4 [mg/L]	971	956	1010	1070
Zn [mg/L]	19.4 ± 0.14	21.8 ± 0.38	9.7 ± 0.28	16.9 ± 0.53
Ca [mg/L]	1849.7 ± 6.8	3132.8 ± 17	24.2 ± 0.06	1551.9 ± 6.4
Fe [mg/L]	84.7 ± 0.18	116.2 ± 0.78	4.8 ± 0.04	503.6 ± 2.8
K [mg/L]	774.7 ± 13	1840.0 ± 11	825.6 ± 5.8	874.0 ± 3.6
Mg [mg/L]	912.7 ± 7.7	1721.4 ± 5.7	581.1 ± 5.1	958.7 ± 5.3
Mn [mg/L]	14.5 ± 0.05	24.2 ± 0.11	7.3 ± 0.04	21.8 ± 0.16
Al [mg/L]	89.6 ± 0.74	29.1 ± 0.04	113.8 ± 1.0	138.0 ± 0.37
NH_4-N: PO_4-P (Molar Basis)	0.82	0.84	1.34	1.35

3.3 Results and Discussion

3.3.1 Analysis of the hydrothermal aqueous product

The concentration of phosphate in liquid products of acidic HTC experiments is presented in Table 3.2. The concentration of phosphorous found here was similar to the results we found previously when evaluating the effects of various acids [30]. Sulfuric acid and oxalic acid appeared to fare best in terms of phosphate solubilization performance by producing a liquid product with a phosphate concentration of more than 1000 mg/L. The phosphate concentration decreased slightly with the use of formic acid and citric acid, but in all cases, the phosphate concentration was within 7% of 1000 mg/L. The differences were not extremely large; hence, it is reasonable to assume a comparable phosphate extraction for each of the four acids. Moreover, the results indicated that above 90% of phosphorus from manure had been dissolved into the liquid phase. This percentage is calculated based on 80 grams of manure with 4.38 mg/g of phosphorus diluted in 1 liter of total liquid.

Table 3.2 also shows the concentration of ammonia in every liquid product of the HTC experiment for different acids. Clearly, the addition of sulfuric acid resulted in the highest concentration of ammonia, among other acids, similar to what was observed for phosphate. However, the similarities between ammonia and phosphate results end here. Looking at these data, we see that acids can be divided into two groups: sulfuric acid and oxalic acid in one group and citric acid and formic acid in another. With 152 mg/L and 153 mg/L of ammonia for liquids produced in citric acid and formic acid assays, respectively, the ability of those two acids to instigate ammonia release was almost identical. However, the other two acids, oxalic acid, and sulfuric acid increased the ammonia formation by 74% on

average. The disparity in the ammonia and phosphate concentrations can be observed by comparing their corresponding molar values. The molar ratio of N:P presented in Table 3.2 for all obtained hydrothermal aqueous products indicates that solutions generated by formic and citric acids had a ratio of N:P close to 0.8. On the other hand, for the solutions obtained by sulfuric and oxalic acids, the ratio was approximately 1.3. In general, sulfuric and oxalic acids showed higher extraction of ammonia and phosphate from the manure. In all cases, the proportion of N:P was below 2.0, necessitating the addition of NH_4 before precipitation, as described above.

3.3.2 Thermodynamic modeling of precipitation

The potential of any solids to precipitate out of a solution can be determined based on its saturation index (SI) at any given solution condition. SI of each solid phase depends on the thermodynamic equilibrium of the species present in the solution. Any solid with a SI of greater than zero could be a potential candidate for precipitation; however, this doesn't guarantee the formation of that specific solid. The reason is hidden in the complex nature of crystallization, which is often driven by the kinetics of nucleation, crystal growth, and agglomeration instead of mere thermodynamic equilibrium. Nonetheless, thermodynamic models would help us identify any possible precipitating products. In the present study, the SI of the various minerals was calculated using the geochemical software PHREEQC® developed by the US Geological Survey (USGS). SI of each mineral can be calculated by dividing the ionic activity product (IAP) of its forming ions in the solution by its equilibrium solubility product or K_{sp}. IAP is a product of the concentration and ionic activity of each species which can be obtained by modification of the Debye–Hückel

equation [32][33][34]. It is important to mention the PHREEQC program is solely used to account for well-established equilibrium conditions for inorganic complexes, excluding reactions involving dissolved organic matter. The reason is the difficulty quantifying macromolecular organic acid's dissociation and metal complexation reactions [35]. There are other advanced models beyond PHREEQC, such as WHAM and NICA-Donnan [36], which can be applied to simulate real systems more accurately; however, this topic is beyond the scope of the present study.

Table 3.2 shows concentrations of various ions. Looking at this data, one can easily recognize the complexity of the obtained mixture at the end of hydrothermal treatment of manure in terms of the diversity of chemical species. The existence of these ions, along with the other organic matter generated during HTC, further complicates the chemistry and thermodynamics of the precipitation process. We have tried to characterize the produced liquids to the extent that would enable us to explain our observations later in the precipitation stage. Using this data as an input for thermodynamic equilibrium calculations would help us predict certain solid precipitants' formation. The data in Table 3.2 were input to PHREEQC to calculate SI for each potential precipitating solid. SI values were calculated at pH = 9.5 and 25°C, and several phosphate-containing minerals become supersaturated (SI>0) and have good potential for precipitation. Detailed results of the PHREEQC output can be found in the supporting material. Several phosphate-containing minerals, alongside other solids, can be identified as potential precipitants, including amorphous calcium phosphate, bobierrite, hydroxyapatite, monetite, newberyite, struvite,

etc. It seems that the thermodynamics of this system precludes precipitation of a pure compound, e.g., struvite.

3.3.3 P and N recovery efficiency from hydrothermal aqueous product

Previous studies have investigated the impact of the N:P ratio on the crystallization of struvite and phosphate recovery from mostly wastewater effluent streams. It is now well established that having an excess amount of ammonia has a positive effect on phosphorus reclamation [37][38][39]. Therefore, as described above, excess ammonia was added to the HTC liquid before precipitation to raise the molar ratio of NH_4:P to 2.0.

The efficiency of phosphorus precipitation (defined above) is shown in Figure 3.1. Remember that this shows the percentage of phosphorus dissolved in the solution after HTC, with a slightly different basis for each acid, as shown in Table 3.2. The precipitation efficiency differed substantially depending on the acid used during HTC. These results indicate that phosphorus dissolved during HTC with oxalic acid or citric acid was mainly retained in the liquid phase instead of transferring into the solid precipitate. On the other hand, sulfuric acid and formic acid produced liquids that readily precipitated nearly all the phosphorus. Especially the sample with sulfuric acid can be singled out from which close to 99% efficiency of phosphorus precipitation was achieved. The liquid sample produced with citric acid had the lowest efficiency, followed by the sample from oxalic acid. The divergence in the results can be attributed to the interaction between inorganic content and organic matter present in the liquid samples produced during HTC. Previous studies on the role of organic matter during the precipitation of phosphorus-containing solids from various liquid waste streams might help elucidate the chemical principles of our

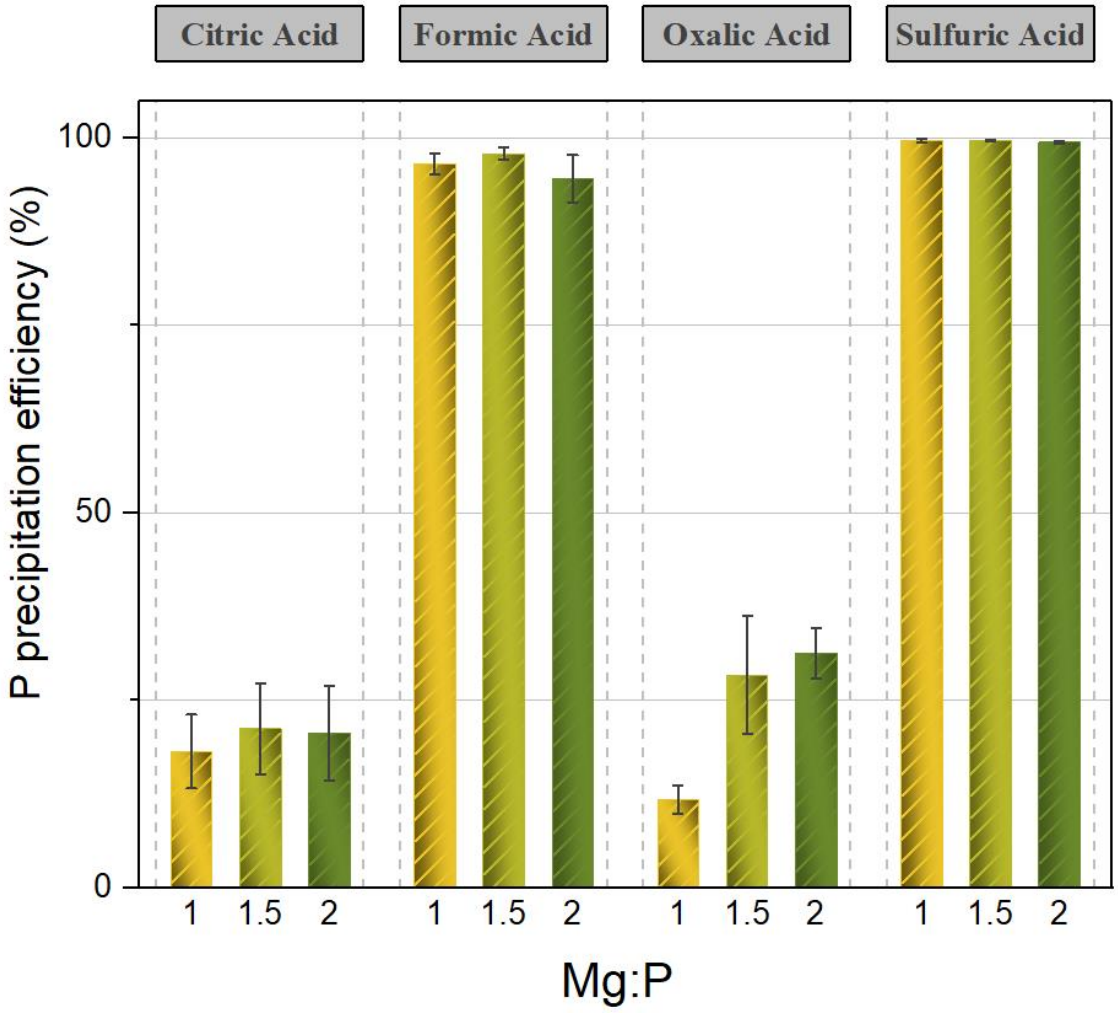

Figure 3.1 P recovery percentage in the precipitant for different acids and Mg:P molar ratios. The error bars represent the standard error of triplicate trials.

observation [40][41][42]. The presence of organic matter inhibited the crystallization of struvite and other P-containing solids. For instance, citrate with three and acetate with one carboxylate functional groups have been studied as small molecular weight organic ligands [42]. Similar results were obtained with succinic acid and acetic acid on phosphorus recovery from synthetic swine wastewater [41]. Nonetheless, the impact of organic matter on the crystallization/precipitation of solids in P recovery methods is not unilateral. As

shown by Capdevielle *et al.*, even though the presence of organic matter, especially colloidal particles, hampered the kinetics of crystallization, that same presence increased crystal size [40]. Larger crystals are easier to harvest and handle and are, therefore, desirable. The inhibition of crystallization by organic matter might happen through two different mechanisms. Organic ligands can form stable complexes with cations such as Mg^{2+} and NH_4^+ in the solution to form more stable compounds, which reduces the availability of those cations in the solution to bind with phosphate. Consequently, the ionic activity of the solution is decreased, and the solution moves away from the supersaturation. On the other hand, the organic matter can bind to the newly formed nuclei and inhibit its growth or block the nucleation altogether.

Figure 3.1 also illustrates the impact of the Mg:P molar ratio on the recovery of PO_4 from HTC liquid products. For three out of four acids (citric acid, formic acid, and sulfuric acid), the loss of phosphate by precipitation was essentially independent of the ratio Mg:P in the range studied. The exception was PO_4 recovery from liquid samples produced by oxalic acid, which indicated increased phosphate recovery by increasing Mg:P ratio. However, conducting ANOVA analysis among all results suggested no significant trend in data concerning Mg:P ratio across all four acids. Contradictory results about Mg:P impact could be found in the literature. Studies have shown the positive influence of Mg addition on P recovery from different waste streams [43][44]. Nonetheless, an optimum Mg:P has not been established, mainly due to the variation of the chemical composition of the supernatant used [45][46][47]. Regardless of the chemical composition of the solution,

Mg:P of over one is always required to increase the possibility of the formation of solids containing phosphate anion by turning it into the limiting reactant [48].

The removal of ammonia from the solutions obtained by hydrothermal carbonization of manure is illustrated in Figure 3.2. The results presented in this figure were calculated based on the total concentration of ammonia, including the extra ammonia supplied to achieve an N:P ratio of 2. Ammonia may leave the aqueous phase by either precipitation to a solid or evaporation to the gas phase. The removal of NH_4 from the solutions obtained with formic acid, citric acid, and oxalic acid were quite similar, with the average efficiency for each of these acids at approximately 23%. In comparison, ammonia loss from the solution acquired with sulfuric acid was 11.7%.

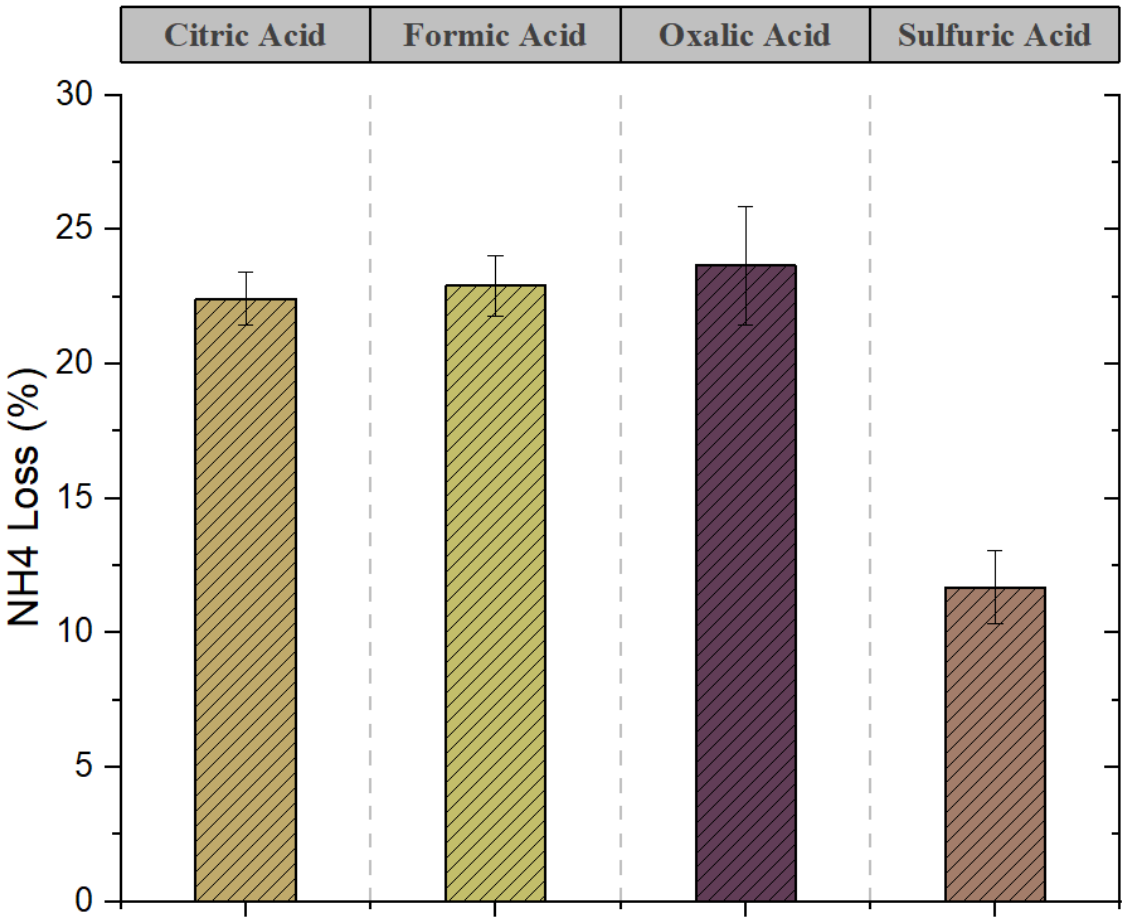

Figure 3.2 Loss of ammonia during precipitation from liquids produced during HTC with different acids. Note that loss may include loss to the gas phase by evaporation and loss to the solid phase during precipitation. Error bars represent the standard error

The variation in these results might be partly explained by the equilibrium reaction of ammonia and ammonium in aqueous solutions. The significant factors influencing ammonia's activity in aqueous solutions are pH, ionic strength, and temperature. According to Emerson *et al.*, the concentration of un-ionized ammonia (NH_3) increases with increasing pH and temperature. Conversely, there is a decrease in unionized ammonia concentration as the ionic strength increases [49]. In our experiments, precipitation

temperature was constant for all cases; thus, the effect of temperature can be ruled out. Likewise, the pH was steady at 9.5 for all precipitation experiments, so the only factor affecting the ammonia-ammonium equilibrium could be the ionic strength of the chemical species in the solution. Sulfuric acid is a strong inorganic acid that has the highest ionic strength among the four acids used for hydrothermal carbonization of cow manure, followed by oxalic acid (pKa = 1.2), citric acid (pKa = 3.13), and formic acid (pKa = 3.75), respectively. The higher ionic strength of the solution helps shift the ammonia-ammonium equilibrium toward ammonium; therefore, ammonia is less likely to be removed from the liquid phase in the gaseous form. This may help explain the reduced ammonia removal in the solutions with higher ionic strength (i.e., sulfuric acid) compared to others.

To validate this hypothesis, experiments were conducted with model solutions in the simulated precipitation condition; four solutions were prepared to contain 0.3M of each acid, and the concentration of PO_4 and NH_4 was adjusted based on the concentration of corresponding hydrothermal aqueous products. These four model solutions were similar to those prepared for precipitation but contained no dissolved organic species from HTC. The pH was then raised to 9.5, and the solutions were mixed for two hours. The goal was to emulate the precipitation reaction without obtaining any solid precipitants. Because these solutions contained no Mg, no precipitation was expected. The concentration of NH_4 in the solution was measured before and after the experiment, and the loss was calculated. The results indicate that while the ammonia loss with the sulfuric acid model solution was only around 2.3%, for formic acid, citric acid, and oxalic acid model solutions, ammonia loss was 14.3%, 14.5%, and 13.7%, respectively. From this analysis, we concluded that the

higher ammonia loss in precipitation reactions of actual hydrothermal aqueous products obtained by formic, citric, and oxalic acids is due to vaporization of dissolved unionized ammonia (NH_3) rather than precipitation of ionized ammonia cation (NH_4). Comparing the results for ammonia removal concerning different Mg:P ratios, no specific trend could be discerned based on the ANOVA analysis.

3.3.4 Characterization of obtained precipitants

To uncover more information on the chemical composition and morphology of the solids produced during precipitation experiments of hydrothermal aqueous products, X-ray diffraction (XRD), ICP-AES, and SEM/EDX analyses of the samples were conducted. Figure 3.3 presents the diffraction patterns of solid samples produced from precipitation of solutions attained from hydrothermal treatment of cow manure with different acids. The most notable feature of the patterns in this figure is that only the sample precipitated from

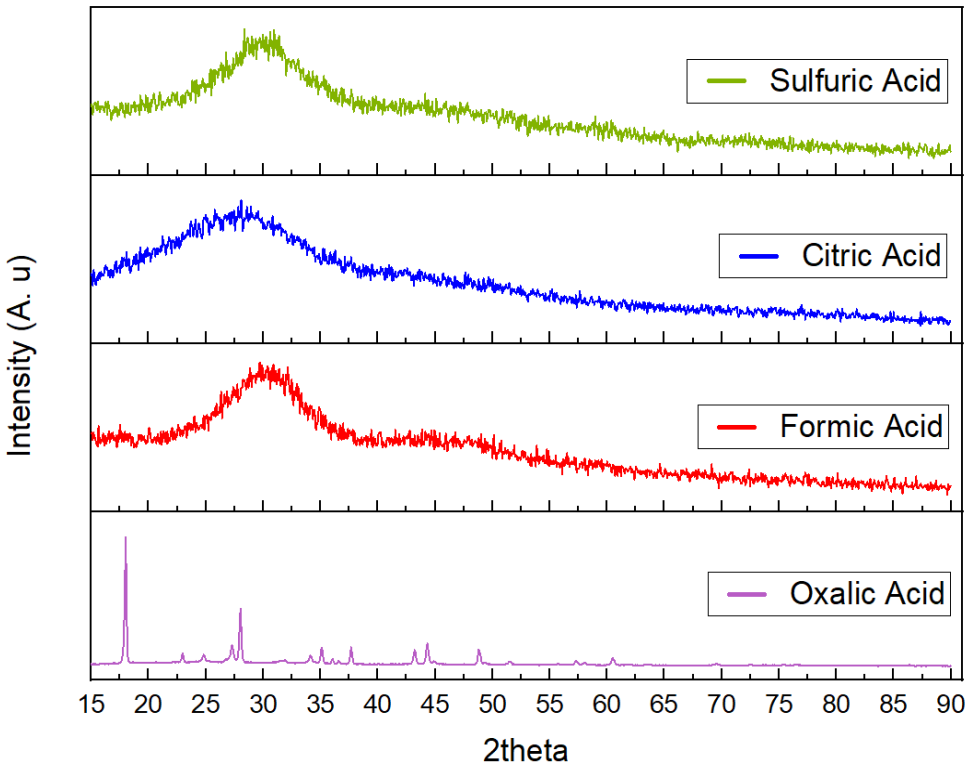

Figure 3.3 X-ray diffraction pattern of produced solids from different hydrothermal aqueous products

the solution produced by the addition of oxalic acid shows a diffraction pattern with distinctive peaks, which means the solid has a crystalline structure. However, assigning the peaks to a single substance was not possible, which likely means the precipitant was not a pure substance but a mixture of various compounds. On the other hand, samples precipitated from other hydrothermal aqueous products show broad peaks, indicating an amorphous structure. Recall that a thermodynamic analysis of the complex solution showed that several phosphorous-containing solids showed potential for precipitation, with an SI > 0. Obtaining pure crystals from such a complex solution is almost impossible without any attempt to simplify the solution before the crystallization. This can also be

seen in the literature where studies conducted with model solutions to emulate real supernatant generally yield high-purity precipitants. In contrast, studies performed using real solutions such as wastewater plant effluent indicate the opposite [50][37][39].

Table 3.3 shows the elemental composition of precipitated solids. The solid products precipitated from treatment with formic acid, and sulfuric acid reached the highest phosphorus content compared to those obtained with the other two acids. This observation complies with the phosphorus recovery efficiency results gathered from the analysis of the supernatant before and after crystallization experiments (Figure 3.1). A negligible amount of trace elements, such as Cu, Pb, Li, Mn, and Zn, were detected in the precipitated solids. Iron (Fe) and calcium (Ca) contents show the same trend as phosphorus, suggesting the co-precipitation of these two ions during the P precipitation experiments. Calcium has long been considered an inhibitor for struvite formation [51][52][53]. Consequently, the presence of Ca in the solids precipitated from sulfuric acid and formic acid added to the hydrothermal aqueous product provides evidence for the lack of any distinct struvite peak in the XRD patterns shown in Figure 3.3. The crystalline solid collected by oxalic acid hydrothermal treatment contains a relatively high fraction of Mg. The lowest Mg content was found in the solid obtained from the citric acid-added hydrothermal aqueous product. A similar concentration of Mg was measured in solids from the hydrothermal aqueous product of formic and sulfuric acids.

Table 3.3 Elemental composition of the solid precipitants from different hydrothermal aqueous products

Element [mg/g]	Citric Acid	Formic Acid	Oxalic Acid	Sulfuric Acid
P	16.20 ± 0.20	77.20 ± 0.78	3.30 ± 0.03	79.40 ± 3.6
Zn	0.40 ± 0.01	0.30 ± 0.05	0.10 ± 0.02	0.30 ± 0.01
Ca	37.90 ± 0.14	117.60 ± 0.66	1.00 ± 0.05	120.50 ± 0.49
Fe	3.30 ± 0.02	20.40 ± 0.14	4.90 ± 0.04	18.20 ± 0.10
K	10.00 ± 0.17	3.70 ± 0.02	7.70 ± 0.05	4.00 ± 0.01
Mg	8.30 ± 0.07	28.20 ± 0.09	53.70 ± 0.48	33.50 ± 0.18
Mn	0.60 ± 0.03	2.20 ± 0.01	0.50 ± 0.02	3.10 ± 0.02
Al	25.50 ± 0.21	1.30 ± 0.01	8.40 ± 0.07	2.20 ± 0.05

Figure 3.4 shows the SEM/EDX of the solid samples collected after the precipitation experiments. The SEM images revealed the similarity of the particle geometries of the solids precipitated from the solutions produced by critic acid and formic acid. In both cases, they have rigid and cubic shapes of large size. On the other hand, oxalic acid gave rise to a solid with cubic-shaped particles. However, sulfuric acid produced the finest particles among the four acids investigated in this study. EDX spectra showed variation in the intensity of P, Mg, Ca, Fe, and Al peaks among the different solid precipitants, which agrees with the results obtained by ICP-AES analysis. However, EDX also revealed large amounts of oxygen in all samples and considerable quantities of Si in some solids.

Citric Acid

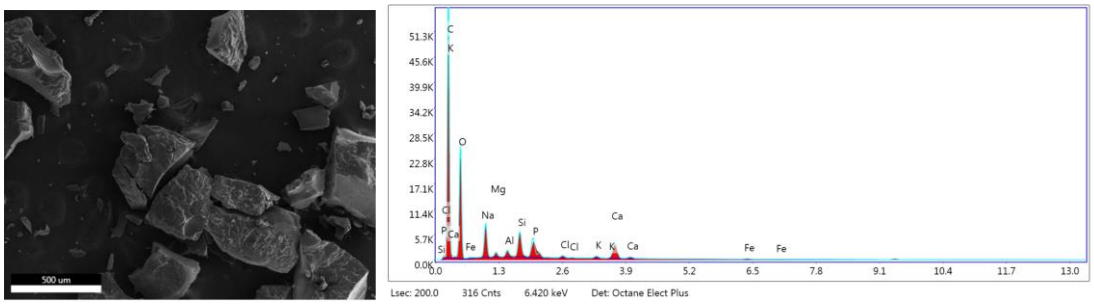

Formic Acid

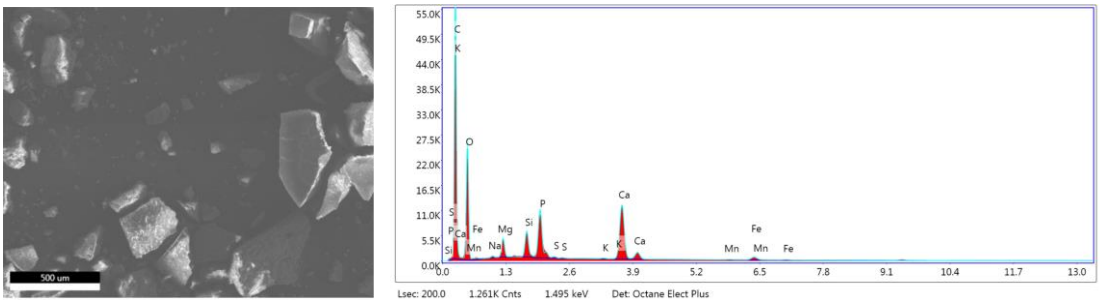

Oxalic Acid

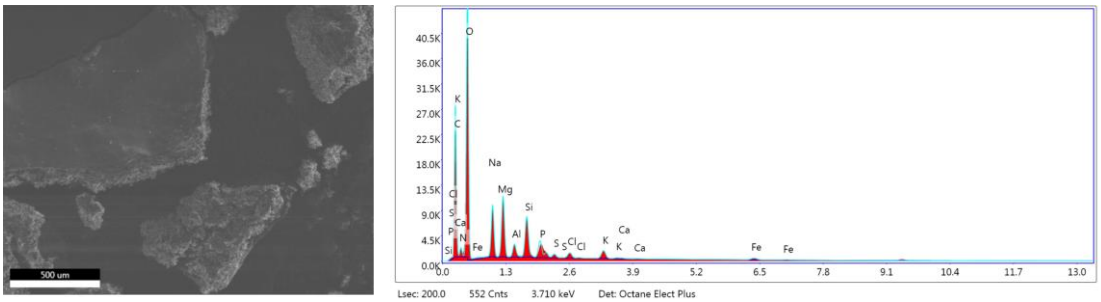

Sulfuric Acid

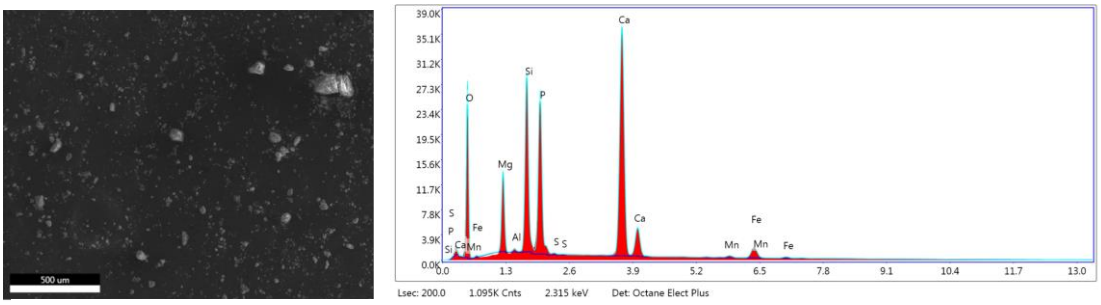

Figure 3.4 SEM/EDX image of the solids produced from different hydrothermal aqueous products

3.4 Conclusion:

In this work, a hydrothermal carbonization process was carried out at 170°C by adding four acid reagents to extract the nutrients from cow manure. Among the acids used, sulfuric acid resulted in the highest phosphate concentration and ammonia in the hydrothermal aqueous product. However, the other acids were quite effective in extracting nutrients since, in all cases, more than 90% of the phosphorus content in manure was removed. Regarding ammonia, sulfuric acid and oxalic acid had higher efficiency than citric acid and formic acid. The pH adjustment of the hydrothermal aqueous products to 9.5 and the modification of the N:P and Mg:P ratios resulted in significantly enhanced phosphorus recovery using formic acid and sulfuric acid. Nitrogen recovery in the form of ammonia showed no significant variability among the organic acids; however, there was a drop in ammonia removal from the sulfuric acid hydrothermal aqueous product. The organic ligands inserted into the solution by adding organic acids negatively affected the phosphate precipitation efficiency. This effect was amplified based on the molecular weight of the ligands. Characterization of obtained solids revealed that only solids precipitated from the oxalic acid hydrothermal aqueous product had crystalline structures, and the others were amorphous solids. Therefore, the XRD pattern of the crystalline solid could not be assigned to a pure solid phase.

3.5 References

[1] USGS, “Phosphate rock statistics and information,” 2020.

[2] D. Cordell, J. O. Drangert, and S. White, “The story of phosphorus: Global food security and food for thought,” *Glob. Environ. Chang.*, vol. 19, no. 2, pp. 292–305, May 2009.

[3] D. Cordell and S. White, “Peak phosphorus: Clarifying the key issues of a vigorous debate about long-term phosphorus security,” *Sustainability*, vol. 3, no. 10. Molecular Diversity Preservation International, pp. 2027–2049, 24-Oct-2011.

[4] USEPA, “Literature Review of Contaminants in Livestock and Poultry Manure and Implications for Water Quality,” 2013.

[5] M. Ribaudo, R. Kellogg, C. Lander, and D. Letson, “Confined Animal Production and Manure Nutrients. Noel Gollehon, Margriet Caswell, Marc Ribaudo, Robert Kellogg, Charles Lander, and David Letson; Resource Economics Division, Economic Research Service, U.S. Department of Agriculture. Agriculture Informati,” 2001.

[6] J. G. Lynam, M. T. Reza, W. Yan, V. R. Vásquez, and C. J. Coronella, “Hydrothermal carbonization of various lignocellulosic biomass,” *Biomass Convers. Biorefinery*, vol. 5, no. 2, pp. 173–181, 2015.

[7] B. Oliver-Tomas, M. Hitzl, M. Owsianiak, and M. Renz, “Evaluation of

hydrothermal carbonization in urban mining for the recovery of phosphorus from the organic fraction of municipal solid waste," *Resour. Conserv. Recycl.*, vol. 147, no. May, pp. 111–118, 2019.

[8] S. M. Heilmann, J. S. Molde, J. G. Timler, B. M. Wood, A. L. Mikula, G. V Vozhdayev, E. C. Colosky, K. A. Spokas, and K. J. Valentas, "Phosphorus reclamation through hydrothermal carbonization of animal manures," *Environ. Sci. Technol.*, vol. 48, no. 17, pp. 10323–10329, 2014.

[9] A. Sarrion, E. Diaz, M. A. de la Rubia, and A. F. Mohedano, "Fate of nutrients during hydrothermal treatment of food waste," *Bioresour. Technol.*, vol. 342, p. 125954, Dec. 2021.

[10] S. S. Dima, A. Arnob, U. Salma, K. B. Kabir, and K. Kirtania, "Fate of nutrients during hydrothermal carbonization of biogenic municipal waste," *Biomass Convers. Biorefinery 2020*, pp. 1–10, Sep. 2020.

[11] A. Funke, "Fate of Plant Available Nutrients during Hydrothermal Carbonization of Digestate," *Chemie-Ingenieur-Technik*, vol. 87, no. 12, pp. 1713–1719, 2015.

[12] I. Idowu, L. Li, J. R. V. Flora, P. J. Pellechia, S. A. Darko, K. S. Ro, and N. D. Berge, "Hydrothermal carbonization of food waste for nutrient recovery and reuse," *Waste Manag.*, vol. 69, pp. 480–491, Nov. 2017.

[13] M. J. Alhnidi, D. Wüst, A. Funke, L. Hang, and A. Kruse, "Fate of Nitrogen, Phosphate, and Potassium during Hydrothermal Carbonization and the Potential

for Nutrient Recovery," *ACS Sustain. Chem. Eng.*, vol. 8, no. 41, pp. 15507–15516, Oct. 2020.

[14] B. Motavaf, R. A. Dean, J. Nicolas, and P. E. Savage, "Hydrothermal carbonization of simulated food waste for recovery of fatty acids and nutrients," *Bioresour. Technol.*, vol. 341, p. 125872, 2021.

[15] Y. Z. Belete, V. Mau, R. Yahav Spitzer, R. Posmanik, D. Jassby, A. Iddya, N. Kassem, J. W. Tester, and A. Gross, "Hydrothermal carbonization of anaerobic digestate and manure from a dairy farm on energy recovery and the fate of nutrients," *Bioresour. Technol.*, vol. 333, p. 125164, Aug. 2021.

[16] G. C. Becker, D. Wüst, H. Köhler, A. Lautenbach, and A. Kruse, "Novel approach of phosphate-reclamation as struvite from sewage sludge by utilising hydrothermal carbonization," *J. Environ. Manage.*, vol. 238, pp. 119–125, May 2019.

[17] P. Cornel and C. Schaum, "Phosphorus recovery from wastewater: Needs, technologies and costs," *Water Sci. Technol.*, vol. 59, no. 6, pp. 1069–1076, 2009.

[18] C. Pratt, S. A. Parsons, A. Soares, and B. D. Martin, "Biologically and chemically mediated adsorption and precipitation of phosphorus from wastewater," *Current Opinion in Biotechnology*, vol. 23, no. 6. Elsevier Current Trends, pp. 890–896, 01-Dec-2012.

[19] J. T. Bunce, E. Ndam, I. D. Ofiteru, A. Moore, and D. W. Graham, "A review of phosphorus removal technologies and their applicability to small-scale domestic

wastewater treatment systems," *Frontiers in Environmental Science*, vol. 6, no. FEB. Frontiers, p. 8, 22-Feb-2018.

[20] A. L. Smith, L. B. Stadler, N. G. Love, S. J. Skerlos, and L. Raskin, "Perspectives on anaerobic membrane bioreactor treatment of domestic wastewater: A critical review," *Bioresour. Technol.*, vol. 122, pp. 149–159, Oct. 2012.

[21] W. Huang, Y. Zhang, and D. Li, "Adsorptive removal of phosphate from water using mesoporous materials: A review," *J. Environ. Manage.*, vol. 193, pp. 470–482, May 2017.

[22] N. Muisa, I. Nhapi, W. Ruziwa, and M. M. Manyuchi, "Utilization of alum sludge as adsorbent for phosphorus removal in municipal wastewater: A review," *J. Water Process Eng.*, vol. 35, p. 101187, Jun. 2020.

[23] M. M. Rahman, M. A. M. Salleh, U. Rashid, A. Ahsan, M. M. Hossain, and C. S. Ra, "Production of slow release crystal fertilizer from wastewaters through struvite crystallization - A review," *Arab. J. Chem.*, vol. 7, no. 1, pp. 139–155, Jan. 2014.

[24] L. Peng, H. Dai, Y. Wu, Y. Peng, and X. Lu, "A comprehensive review of phosphorus recovery from wastewater by crystallization processes," *Chemosphere*, vol. 197. pp. 768–781, Apr-2018.

[25] Y. J. Shih, R. R. M. Abarca, M. D. G. de Luna, Y. H. Huang, and M. C. Lu, "Recovery of phosphorus from synthetic wastewaters by struvite crystallization in a fluidized-bed reactor: Effects of pH, phosphate concentration and coexisting

ions," *Chemosphere*, vol. 173, pp. 466–473, 2017.

[26] X. Hao, C. Wang, M. C. M. Van Loosdrecht, and Y. Hu, "Looking beyond struvite for P-recovery," *Environmental Science and Technology*, vol. 47, no. 10. American Chemical Society, pp. 4965–4966, 21-May-2013.

[27] R. Liu and R. Lal, "Synthetic apatite nanoparticles as a phosphorus fertilizer for soybean (Glycine max)," *Sci. Rep.*, vol. 4, no. 1, pp. 1–6, Jul. 2014.

[28] L. Peng, H. Dai, Y. Wu, Y. Peng, and X. Lu, "A Comprehensive Review of the Available Media and Approaches for Phosphorus Recovery from Wastewater," *Water, Air, and Soil Pollution*, vol. 229, no. 4. 2018.

[29] Johnston A.E. and I. R. Richards, "Effectiveness of different precipitated phosphates as phosphorus sources for plants," *Soil Use Manag.*, vol. 19, no. 1, pp. 45–49, 2003.

[30] S. V. Qaramaleki, J. A. Villamil, A. F. Mohedano, and C. J. Coronella, "Factors Affecting Solubilization of Phosphorus and Nitrogen through Hydrothermal Carbonization of Animal Manure," *ACS Sustain. Chem. Eng.*, vol. 8, no. 33, pp. 12462–12470, 2020.

[31] A. Capdevielle, E. Sýkorová, B. Biscans, F. Béline, and M. L. Daumer, "Optimization of struvite precipitation in synthetic biologically treated swine wastewater-Determination of the optimal process parameters," *J. Hazard. Mater.*, vol. 244–245, pp. 357–369, Jan. 2013.

[32] M. I. H. Bhuiyan, D. S. Mavinic, and R. D. Beckie, “A solubility and thermodynamic study of struvite,” *Environ. Technol.*, vol. 28, no. 9, pp. 1015–1026, 2007.

[33] C. Fang, T. Zhang, R. Jiang, and H. Ohtake, “Phosphate enhance recovery from wastewater by mechanism analysis and optimization of struvite settleability in fluidized bed reactor,” *Sci. Rep.*, vol. 6, no. August, pp. 1–11, 2016.

[34] K. N. Ohlinger, T. M. Young, and E. D. Schroeder, “Predicting struvite formation in digestion,” *Water Res.*, vol. 32, no. 12, pp. 3607–3614, Dec. 1998.

[35] C. S. Sjöstedt, J. P. Gustafsson, and S. J. Köhler, “Chemical equilibrium modeling of organic acids, pH, Aluminum, and iron in Swedish surface waters,” *Environ. Sci. Technol.*, vol. 44, no. 22, pp. 8587–8593, Nov. 2010.

[36] Y. Dudal and F. Gérard, “Accounting for natural organic matter in aqueous chemical equilibrium models: A review of the theories and applications,” *Earth-Science Rev.*, vol. 66, no. 3–4, pp. 199–216, Aug. 2004.

[37] H. Huang, B. Li, J. Li, P. Zhang, W. Yu, N. Zhao, G. Guo, and B. Young, “Influence of process parameters on the heavy metal (Zn2+, Cu2+ and Cr3+) content of struvite obtained from synthetic swine wastewater,” *Environ. Pollut.*, vol. 245, pp. 658–665, Feb. 2019.

[38] B. Tansel, G. Lunn, and O. Monje, “Struvite formation and decomposition characteristics for ammonia and phosphorus recovery: A review of magnesium-

ammonia-phosphate interactions," *Chemosphere*, vol. 194, pp. 504–514, 2018.

[39] L. Vasenko and H. Qu, "Effect of NH4-N/P and Ca/P molar ratios on the reactive crystallization of calcium phosphates for phosphorus recovery from wastewater," *J. Cryst. Growth*, vol. 459, no. November 2016, pp. 61–66, 2017.

[40] A. Capdevielle, E. Sýkorová, F. Béline, and M. L. Daumer, "Effects of organic matter on crystallization of struvite in biologically treated swine wastewater," *Environ. Technol. (United Kingdom)*, vol. 37, no. 7, pp. 880–892, 2016.

[41] Y. Song, Y. Dai, Q. Hu, X. Yu, and F. Qian, "Effects of three kinds of organic acids on phosphorus recovery by magnesium ammonium phosphate (MAP) crystallization from synthetic swine wastewater," *Chemosphere*, vol. 101, pp. 41–48, Apr. 2014.

[42] J. A. M. Van Der Houwen and E. Valsami-Jones, "The application of calcium phosphate precipitation chemistry to phosphorus recovery: The influence of organic ligands," *Environ. Technol.*, vol. 22, no. 11, pp. 1325–1335, 2001.

[43] B. Li, H. M. Huang, I. Boiarkina, W. Yu, Y. F. Huang, G. Q. Wang, and B. R. Young, "Phosphorus recovery through struvite crystallisation: Recent developments in the understanding of operational factors," *Journal of Environmental Management*, vol. 248. Academic Press, p. 109254, 15-Oct-2019.

[44] M. S. Rahaman, N. Ellis, and D. S. Mavinic, "Effects of various process parameters on struvite precipitation kinetics and subsequent determination of rate

constants," *Water Sci. Technol.*, vol. 57, no. 5, pp. 647–654, 2008.

[45] A. Korchef, H. Saidou, and M. Ben Amor, "Phosphate recovery through struvite precipitation by CO2 removal: Effect of magnesium, phosphate and ammonium concentrations," *J. Hazard. Mater.*, vol. 186, no. 1, pp. 602–613, 2011.

[46] W. Li, X. Ding, M. Liu, Y. Guo, and L. Liu, "Optimization of process parameters for mature landfill leachate pretreatment using MAP precipitation," *Front. Environ. Sci. Eng. China*, vol. 6, no. 6, pp. 892–900, 2012.

[47] L. Zeng, C. Mangan, and X. Li, "Ammonia recovery from anaerobically digested cattle manure by steam stripping," in *Water Science and Technology*, 2006, vol. 54, no. 8, pp. 137–145.

[48] M. D. G. de Luna, R. R. M. Abarca, C. C. Su, Y. H. Huang, and M. C. Lu, "Multivariate optimization of phosphate removal and recovery from aqueous solution by struvite crystallization in a fluidized-bed reactor," *Desalin. Water Treat.*, vol. 55, no. 2, pp. 496–505, 2015.

[49] K. Emerson, R. C. Russo, R. E. Lund, and R. V. Thurston, "Aqueous Ammonia Equilibrium Calculations: Effect of pH and Temperature," *J. Fish. Res. Board Canada*, vol. 32, no. 12, pp. 2379–2383, 1975.

[50] N. Y. Acelas, E. Flórez, and D. López, "Phosphorus recovery through struvite precipitation from wastewater: effect of the competitive ions," *Desalin. Water Treat.*, vol. 54, no. 9, pp. 2468–2479, 2015.

[51] S. Kataki, H. West, M. Clarke, and D. C. Baruah, “Phosphorus recovery as struvite: Recent concerns for use of seed, alternative Mg source, nitrogen conservation and fertilizer potential,” *Resour. Conserv. Recycl.*, vol. 107, pp. 142–156, Feb. 2016.

[52] L. Pastor, D. Mangin, R. Barat, and A. Seco, “A pilot-scale study of struvite precipitation in a stirred tank reactor: Conditions influencing the process,” *Bioresour. Technol.*, vol. 99, no. 14, pp. 6285–6291, Sep. 2008.

[53] Y. D. Yilmazel and G. N. Demirer, “Removal and recovery of nutrients as struvite from anaerobic digestion residues of poultry manure,” *Environ. Technol.*, vol. 32, no. 7, pp. 783–794, 2011.

Chapter 4

Characterization Of Products from Catalytic Hydrothermal Carbonization of Animal Manure

4.1 Introduction

Significant environmental damage caused by livestock waste produced in large amounts is an issue of concern worldwide, especially in the United States, European Union, and China [1][2][3]. The problem stems mainly from two aspects of waste. One is the potential runoff of nutrients to nearby surface waters (eutrophication), and the other is related to the emission of greenhouse gases formed during the degradation of the animal wastes (predominantly methane) as well as ammonia which contributes to particulate matter (PM) formation in the atmosphere. As such, the research on the treatment and valorization of animal waste has recently received significant attention.

Hydrothermal carbonization (HTC) has emerged as a promising way to utilize wastes and biomass with high moisture content to produce fuels or energy materials [4]. HTC is a thermochemical process that uses water under subcritical conditions at moderate temperatures (170 – 280 °C) and autogenous pressure as the reaction medium. Therefore, unlike other thermochemical processes such as pyrolysis, torrefaction, and gasification, wet feedstocks don't need to undergo a drying step before HTC. As a result, a large body of literature on HTC of various kinds of biomass such as sewage sludge, food waste, municipal solid wastes, algae, distillery grain, and many other organic wastes has formed [5][6][7][8][9][10].

The main products of HTC treatment are hydrochar (solid), process water, and a small amount of gas. The solid product, called hydrochar, is carbonaceous, brittle, and hydrophobic, with characteristics similar to lignite. The process water contains some fraction of the carbon content in the form of various organic chemical species that may be suitable for resource recovery or recycling [11]. The chemistry and reaction pathways of HTC are pretty complex and are affected by the nature of the biomass. However, some known reactions are assumed to be involved in most HTC applications, such as hydrolysis, dehydration, decarboxylation, polymerization, and condensation [12]. In addition, there are numerous studies on operational parameters influencing the HTC process and the properties of its products. Reaction temperature, reaction time, biomass to water ratio, and catalyst are widely investigated factors. Temperature seems to have the most significant effect on HTC reactions and products [13]. Increased temperature generally reduces mass yield and raises the energy value of the hydrochar by increasing the carbon content.

Several studies have focused on the impact of catalysts on the hydrothermal treatment of biomass. Karagoz *et al.* studied the effect of K_2CO_3, RbOH, and CsOH as alkaline homogenous catalysts on the distribution of products in hydrothermal liquefaction of woody biomass at 280°C with a reaction time of 15 min and found that those catalysts reduced the production of char and favored the formation of oil products [14][15]. Mumme *et al.* used natural zeolite as a heterogeneous catalyst in HTC of digestate at different temperatures. They discovered that the catalytic effects of zeolite increased the degree of carbonization to the same extent as an increase in temperature of 9-29 K [16]. Ekpo *et al.* investigated the extraction of nitrogen and phosphorus in process water of hydrothermal

treatment of swine manure with both acidic and alkaline catalysts at different temperatures ranging from 120°C to 250°C [17]. In previous work, we investigated the influence of several organic and inorganic acids on the extraction of nutrients from cow manure [18]. One recent study focused on the impact of temperature, residence time, and acidic and alkaline conditions on the fate of nitrogen and phosphorus during the HTC of pig manure. It was found that the addition of sulfuric acid or potassium hydroxide reduced P, Ca, Mg, Cl, and heavy metal elements in hydrochars [19]. Lang *et al.* investigated the properties of the hydrochar derived from CaO-assisted HTC of swine manure and reported increased pH and yield of hydrochar. In addition, they discovered the presence of polar functional groups on the surface of the hydrochar resulting in greater hydrophilicity and well-developed porosity that improves the interaction between the hydrochar and soil when the hydrochar was used as soil amendment [20].

In this study, we aim to understand the effect of homogeneous acidic catalysts on the physicochemical properties of the hydrochar produced from HTC of both cow and swine manure. Further, we report C, N, P, and K distribution and mass balances from manures after HTC with and without acidic catalysts. An organic acid (acetic acid) and an inorganic acid (sulfuric acid) are both evaluated as HTC catalysts. The results presented in this chapter have been submitted in a manuscript to the A*CS Sustainable Chemistry & Engineering* journal on 29 June 2022.

4.2 Materials and Methods

The cow manure was acquired from the University of Nevada Reno, Main Station Farm. The dewatered swine manure sample was obtained from a 1,200-sow farrow-to-feeder and 13,00 feeder-to-finish farms in North Carolina. Both feedstocks were dried at 105 °C overnight, ground (to d_p<1mm), and stored in sealed bags until analysis or HTC experiments.

All HTC experiments were conducted at 170°C. Eighty grams of dried biomass were mixed with 1 liter of solution for every experimental run, as described below. The mixture was then placed into a glass liner and put inside a 2-liter Parr reactor that was then tightly sealed. The air inside the reactor was purged with nitrogen gas by pressurizing the reactor up to 20 bar and releasing the gas twice. After mounting the reactor to its stand, the heater was connected, and the reactor was heated at a constant rate (5°C/min) until the temperature set point (170°C) was achieved. Sulfuric and acetic acids at the concentration of 0.3M were used as homogeneous catalysts for the HTC reactions. The reactor with its contents was kept at 170°C for 10 min. Quenching was done by placing the sealed reactor in an ice-water bath. The final pressure of the reactor was recorded at 35°C to calculate the total amount of gas produced during the experiment. After cooling the reactor to room temperature, a gas sample was captured in a Tedlar bag, and all remaining gas was vented into the fume hood. Slurry from the reactor was filtered by Buchner vacuum funnel technique using Whatman® grade 6 filter papers with a pore size of 3µm. The hydrochar filter cake was rinsed with deionized water and dried in an oven at 105°C for 24 hours. Every experiment

was carried out in duplicate, and from each experiment, approximately 100mL of process water filtrate was stored at 5 ℃ for later analysis.

The ultimate analysis of all the solid samples (hydrochar and dried manure) was conducted in a Thermo Scientific FlashSmart elemental analyzer. Each sample was ground in a mortar, and three replicates were analyzed to analyze these heterogeneous solid samples best. Oxygen is measured directly with this instrument.

ICP-AES technique was employed to obtain the elemental composition of the solid samples. For this analysis, samples were first digested in a microwave digester using hydrochloric acid, nitric acid, and hydrogen peroxide.

The solid samples' proximate analysis (Ash, volatile matter, and fixed carbon) was carried out using a TA Q500 TGA instrument. The method applied for this analysis was adopted from the ASTM D7582 standard. For the analysis, nitrogen gas with a flow rate of 100 mL/min was used to purge the air. Next, the sample was heated with a ramp of 50 °C/min to 110°C and held there for 10 minutes for moisture removal. Then the temperature was increased to 950 °C with a heating rate of 40 °C/min and held there for 7 minutes for fixed carbon measurement. In the final step, the sample was cooled to 600 °C, and the gas flow was changed to air to obtain the ash content. For each solid, three samples were analyzed. The calorific values for untreated manure and hydrochar were measured in a Parr 1108 oxygen combustion bomb in a Parr 1241 calorimeter. 5-8 samples weighing in the 0.6-1gr range were used for every analysis. Results are reported on a dry-and-ash-free (daf) basis.

Total phosphorous and phosphate content in all liquid samples were measured by an ascorbic acid method equivalent to EPA 365.1 using a Hach spectrophotometer [21]. Total phosphorus was obtained following an acid and persulfate digestion aimed at the hydrolysis of all the forms of phosphorus and conversion to orthophosphates. The phosphate measurement procedure was similar, except there was no digestion involved. Total Kjeldahl nitrogen (TKN), nitrite, nitrate, and total nitrogen were measured using the Hach method 10242. In this method, inorganic and organic nitrogen is oxidized to nitrate by digestion with peroxydisulfate. The nitrate ions react with 2,6-dimethylphenol in a sulfuric and phosphoric acid solution to form a nitrophenol. Oxidized forms of nitrogen in the original sample (nitrite + nitrate) are determined in a second test vial and then subtracted, resulting in TKN [22]. Total nitrogen (TN) is the sum of TKN (ammonia and organic nitrogen) plus nitrite and nitrate. A salicylate method was used for ammonia quantification, in which free ammonia and hypochlorite are mixed to form monochloramine. Monochloramine further reacts with salicylate and nitroprusside, which produces indosalicylate with blue color. The color intensity, which is proportional to the ammonia concentration, is measured at 690 ± 5 nm with a spectrophotometer [23].

The total organic carbon of the liquid samples was done using a Shimadzu, TOC-LCSH instrument. Samples were diluted and acidified to pH 2 with phosphoric acid. The run includes sparging for 5:30 min to remove all CO and CO_2 so that the detector determines organic carbon.

The liquid samples were first extracted into dichloromethane (CH_2Cl_2) using a fourfold volume excess of solvent. This solution was analyzed using a Supelco Petrocol DH 50.2

(50 m × 0.2 mm × 0.5 µm) column in a Shimadzu QP2010 SE GC/MS. The oven program was as follows: Initial temperature was held at 50 °C for 3 min, ramped at 20 °C/min to 275 °C, with a final hold time of 2 min. The MS was operated in electron impact (EI) mode at 70 eV. Trace gas analyses were performed on a Pfeiffer Prisma Plus residual gas analyzer. For the analyses, 1.0 ml of gas was withdrawn from a Tedlar gas bag using an air-tight syringe. This gas was then injected into a stream of He flowing into the analyzer at 35 ml/min. The gas samples were analyzed in triplicate on an HP 6890 GC fitted with a thermal conductivity detector (TCD) operating at 220 °C (493 K). Gas separation was accomplished using a Poropack Q column (Restec, Bellafonte, PA, USA) with He as the carrier gas. The column was heated as follows: 40 °C (313 K) for 2 min, ramped to 180 °C (313 K) (40 °C/min), held for 5 min, ramped to 200 °C (473 K) (40 °C/min), held for 10 min, and returned to 40 °C (313 K). Gas products were quantified versus calibration of a standard gas mixture consisting of ≈3% (w/v) each of H2, CH4, CO, CO2, C2H6, and C_2H_4 in He (Linde North America Inc., Murray Hill, NJ, USA) and 5% (w/v) each C_3H_8 and C_3H_6 in He (ILMO Specialty Gasses, Jacksonville, IL, USA). Due to the TCD signal damping effect of He on H_2, a standard gas curve for H_2 was prepared from mixtures ranging from 3 to 50% (*v/v*), resulting in a calibration curve of $y = 24x^{1.5}$ ($R^2 = 0.997$).

4.3 Results and Discussion

4.3.1 Characterization of the solid products

The solid products from the hydrothermal carbonization of each manure were analyzed for their fuel properties, proximate, ultimate, and elemental compositions of the ash. The results are presented in Figure 4.1, Table 4.1, and Table 4.2. All samples are labeled using

the following system: the first two letters indicate the source (CM for cow manure and PM for pig manure.) If there is no suffix, then the sample is raw manure. A suffix of SA indicates a hydrochar processed with a sulfuric acid catalyst, a suffix of AA indicates a hydrochar processed with an acetic acid catalyst, and a suffix of DIW indicates a hydrochar processed in deionized water without any acid catalyst.

Table 4.1 summarizes the ultimate elemental composition of the feedstock (cow and pig manure) used in this study and the hydrochars. Comparing the two feedstocks reveals that there is a significant variation in pig and cow manure composition, with the most distinct difference being in their sulfur (1.16 wt. % vs. 0.31 wt. %), nitrogen (4.83 wt.% vs. 2.2 wt.%), and carbon (30.98 wt.% vs. 40.80 wt.%) contents, respectively.

The hydrochar produced from cow manure indicates minimal carbonization when done without adding acids. This is not surprising considering the low temperature (170 ˚C) applied to the hydrothermal treatment. However, by adding acids, a significant increase in the carbon content of the hydrochar can be observed. The influence of acid type in increasing the carbon content is substantial, as sulfuric acid causes more carbonization than acetic acid. The nitrogen content of the resulting hydrochar from cow manure shows slight variations among each other, although it differs remarkably from untreated manure. In contrast, the hydrothermal treatment doesn’t seem to affect hydrogen content significantly. While cow manure undergoes a modest degree of deoxygenation in deionized water (from 27.15% to 23.64%), the addition of acids seems to suppress (sulfuric acid) or even reverse (acetic acid) the deoxygenation. This is a remarkable result since deoxygenation of biomass is a typical result observed during HTC. Looking at the sulfur content of the hydrochar and

cow manure, one can notice the low percentage of this element. However, the sulfur content is increased for the hydrochar produced by applying sulfuric acid, suggesting that some of the sulfates from the acid have transferred from the solution into the hydrochar.

Unlike cow manure, hydrothermal treatment of pig manure without acid addition resulted in a noticeable increase in the carbon content of the hydrochar. This could indicate a high amount of inorganic carbon in pig manure which is not readily soluble in mild hydrothermal conditions (170 ˚C). Adding acid to the HTC reactor enhances the carbonization of pig manure. For nitrogen, there is a slight drop caused by hydrothermal treatment; however, the change is insignificant. Pig manure undergoes modest deoxygenation without acid, but deoxygenation is significantly enhanced in the presence of acetic acid.

Table 4.1 Ultimate analysis of cow manure (CM), pig manure (PM) and hydrochar

Sample Name	N [wt. %]	C [wt. %]	H [wt. %]	S [wt. %]	O [wt. %]
CM*	2.55 ± 0.32	40.80 ± 1.3	5.25 ± 0.14	0.31 ±0.02	27.15 ± 0.67
CM-DIW	1.69 ± 0.14	40.97 ± 2.22	5.09 ± 0.27	0.12 ± 0.02	23.64 ± 0.44
CM-SA	1.50 ± 0.06	49.52 ± 0.24	5.31 ± 0.11	3.53 ± 0.39	25.49 ± 0.25
CM-AA	1.86 ± 0.05	46.67 ± 0.76	5.73 ± 0.08	0.23 ± 0.01	30.55 ± 0.53
PM*	5.25 ± 0.21	30.98 ± 0.68	5.24 ± 0.15	1.16 ± 0.19	25.30 ± 0.81
PM-DIW	4.00 ± 0.28	34.90 ± 1.67	4.62 ± 0.22	0.94 ± 0.04	22.25 ± 1.26
PM-SA	3.84 ± 0.14	44.95 ± 0.40	5.32 ± 0.03	5.80 ± 0.29	24.33 ± 0.15
PM-AA	4.47 ± 0.20	38.98 ± 1.51	4.84 ± 0.18	0.93 ± 0.01	17.06 ± 0.43

* The error shown for manures represents the uncertainty associated with the ultimate analysis only. Other errors account for the experimental error for duplicate HTC tests. DIW: deionized water, SA: sulfuric acid, AA: acetic acid

Table 4.2 presents the solid yield and proximate analysis of the hydrochar produced from pig and cow manure under different scenarios. Looking at these results, it can be seen that for both types of manure, the solid yield drops as the reaction condition changes from deionized water to stronger acids. The higher heating value (HHV) of the hydrochar indicates an increased energy value relative to the feedstock for both types of manure. Comparing the heating value of cow manure versus pig manure, one can see that cow manure is slightly more energy dense. Hydrothermal treatment of both types of manure with sulfuric acid increased the heating value of final hydrochar the most, then with acetic acid, and lastly without acids. This pattern is the opposite of that of solid yield. For both CM and PM, sulfuric acid reduced the ash content to the lowest measured values for each feedstock. This may be due to the hydrolysis and leaching effect of sulfuric acid. For cow manure, hydrothermal treatment lowered the ash content for every reaction condition. However, in the case of pig manure, the ash content increased and decreased, depending on the HTC conditions, with no apparent pattern.

The fixed carbon in hydrochar produced from CM is nearly unchanged during hydrothermal treatment, except for the addition of sulfuric acid, in which case the fixed carbon increased markedly. Similarly, for the pig manure, the fixed carbon increased substantially for the sulfuric acid runs, while the fixed carbon content dropped for the case of no acid catalyst. In terms of the volatiles, one can see no specific trend among different reaction scenarios.

Table 4.2 Energy properties and proximate analysis of cow manure, pig manure, and hydrochar produced by their hydrothermal carbonization

Sample Name	Solid Yield (%, dry wt.)	Volatiles (%, dry wt.)	Ash (%, dry wt.)	Fixed Carbon (%, dry wt.)	HHV (MJ/kg)
CM	-	63.41 ± 1.17	22.88 ± 0.66	13.71 ± 0.84	16.21
CM-DIW	86.91 ± 2.41	66.14 ± 1.33	20.45 ± 1.45	13.41 ± 1.00	17.75 ± 0.10
CM-SA	58.79 ± 0.07	59.78 ± 0.69	18.62 ± 0.85	21.61 ± 0.20	20.06 ± 0.01
CM-AA	76.69 ± 0.26	63.92 ± 1.80	21.13 ± 2.23	14.95 ± 0.44	19.35 ± 0.14
PM	-	61.33 ± 0.22	26.67 ± 0.10	12.00 ± 0.13	14.96
PM-DIW	72.35 ± 1.62	53.98 ± 0.38	35.84 ± 0.42	10.19 ± 0.06	15.37 ± 0.09
PM-SA	58.52 ± 0.47	66.87 ± 0.07	18.21 ± 0.15	14.92 ± 0.20	18.66 ± 0.24
PM-AA	66.08 ± 0.07	59.07 ± 0.18	28.56 ± 0.07	12.38 ± 0.11	17.63 ± 0.21

The elemental compositions of the ash in feedstock and produced hydrochar were determined using the ICP-AES technique, and the data are presented in Figure 4.1. It can be seen that for the majority of elements, their concentration in PM surpassed the values in CM. In particular, phosphorus content in pig manure is approximately an order of magnitude larger than in cow manure. Therefore, the ash analysis coupled with the solid yield results can be used for investigating the fate of those elements by a mass balance during the hydrothermal carbonization process and will be discussed below.

Based on the solid yield, it is possible to calculate the fraction of each element present in the hydrochar as a fraction of the amount of that element in the unreacted manure. We call

this fraction the hydrochar yield of each element; these results are shown in Table 4.3. The most striking observation might be the difference between the distributions of elements when acids were added in contrast to the scenario where no acid was used. According to these results, acids significantly improved the leaching of Ca, K, Mg, and Fe elements into the process water. Moreover, sulfuric acid has shown better extraction capability for all elements and both types of manure except for potassium in cow manure, where acetic acid seemingly had better extraction performance.

Table 4.3 Hydrochar yield of selected elements.

Sample Name	Ca (%, wt.)	K (%, wt.)	Mg (%, wt.)	Fe (%, wt.)
CM-DIW	85.0	53.9	38.3	71.6
CM-SA	30.6	12.2	2.5	4.5
CM-AA	33.8	9.2	2.6	11.6
PM-DIW	98.8	53.4	65.3	69.6
PM-SA	66.8	27.8	3.2	0.6
PM-AA	74.3	31.0	15.7	19.8

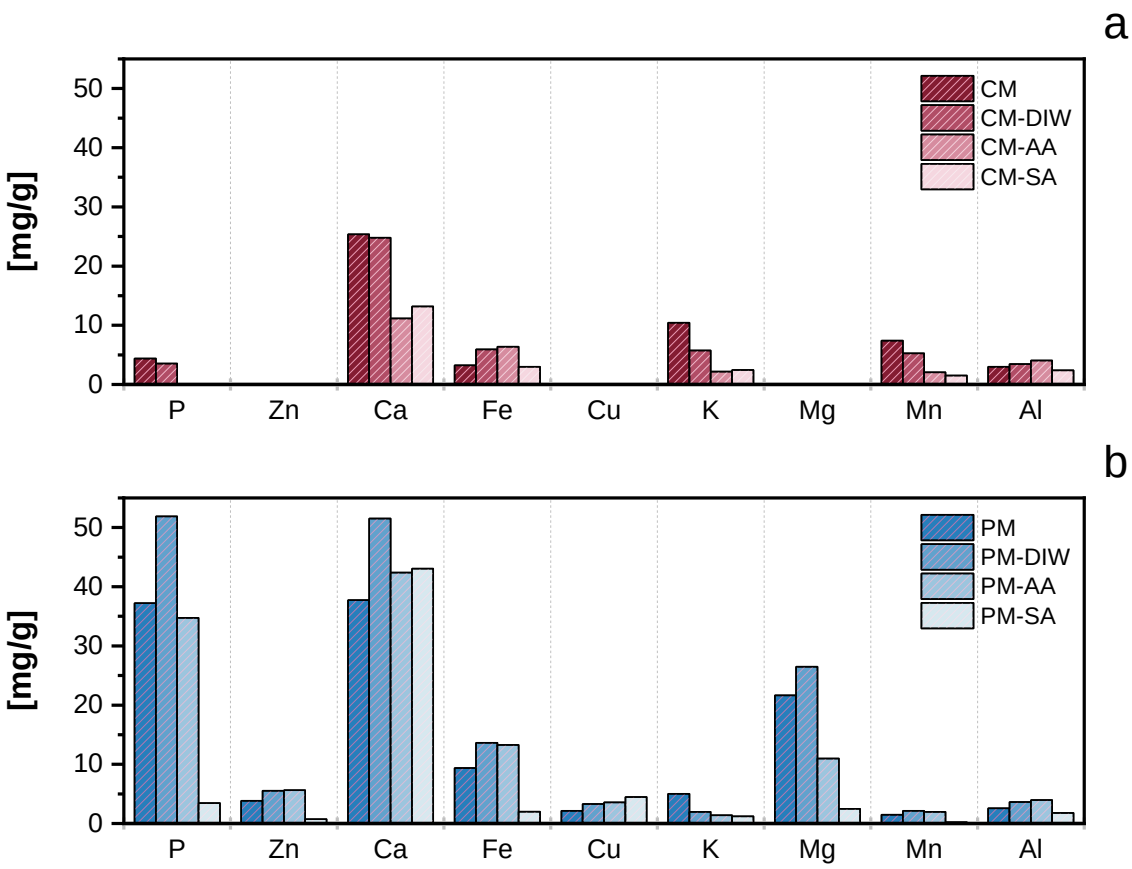

Figure ٤.1 Ash analysis of the feedstock and hydrochar from cow manure (a) and pig manure (b).

4.3.2 Characterization of the liquid products

The process water generated from the hydrothermal treatment of manure was analyzed for different chemical properties. Table 4.4 presents the pH of the reaction environment before and after the experiment. As expected, by adding acids into the process, the pH of the solution drops; however, some exciting patterns also appear. For both types of manure, whenever acids were added, the pH of the solution increased slightly at the end of the hydrothermal treatment. On the contrary, in cases where no acids were used, pH decreased during the reaction. It can be seen that the water and cow manure mixture is quite alkaline in the beginning; however, after the reaction, the pH moves towards neutral due to the formation of organic acids during the hydrothermal reaction. On the other hand, the water and pig manure mixture's pH is in the neutral range, and the mixture becomes acidic at the end. Both before and after the treatment, the pH of the solutions was identical for the cow manure and pig manure for sulfuric acid and acetic acid. The slight variation in the pH of the solutions, especially for sulfuric acid and acetic acid, hints at a potential benefit of recirculating the process water, thus improving the overall economics of the process.

Table 4.4 pH of the solution before and after hydrothermal reaction

Sample Name	Initial pH	Final pH
CM-DIW	9.3 ± 0.01	7.2 ± 0.03
CM-SA	0.9 ± 0.01	1.0 ± 0.01
CM-AA	4.4 ± 0.01	4.4 ± 0.01
PM-DIW	7.1 ± 0.03	6.4 ± 0.04
PM-SA	1.2 ± 0.02	1.4 ± 0.01
PM-AA	4.4 ± 0.01	4.5 ± 0.02

Both total phosphorus and phosphate concentrations in the process water are presented in Figure 4.2. Clearly, there is much more phosphorus in the process water produced from PM compared to that from CM, unsurprising considering the results from the ash analysis. The data presented in Figure 4.2 emphasize how readily the phosphorus contents of those two manure types are accessible. Looking at these data, one can see that phosphorus leaching improves by increasing the solution's acidity. Sulfuric acid, as a strong inorganic acid, significantly increases phosphorus extraction. Acetic acid indicates some extraction capability but is not as successful as sulfuric acid. Moreover, we can compare the total phosphorous concentration to the phosphate concentration in each process water and see that those values are pretty similar. Therefore, it would be fair to conclude that hydrothermal treatment converts a significant fraction of the total phosphorus content of feedstock into the orthophosphate form. The total phosphorus data obtained here will be used in the next section for phosphorus mass balance.

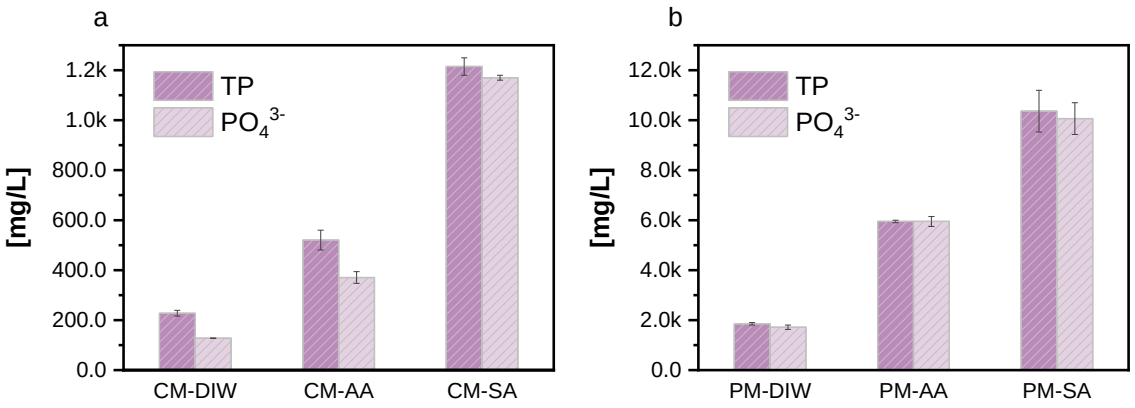

Figure 4.2 Total phosphorus and phosphate concentration in the aqueous product of hydrothermal carbonization of the cow (a) and pig (b) manure.

The nitrogen extraction that occurs during the hydrothermal carbonization of pig and cow manure is presented in Figure 4.3. The fractionation of the extracted nitrogen reveals some general trends. It can be seen that inorganic nitrogen (NH_4 and NO_2/NO_3) constitutes the tiniest fraction of the extracted nitrogen in all experimental conditions and for both types of animal manure. Therefore, it appears that nitrification reactions were quite limited. Ammonia, even though it was found at higher concentrations than nitrite/nitrate, is the second least available form of leached nitrogen. The results show total Kjeldahl nitrogen as the most abundant form of nitrogen in the aqueous product of pig and cow manure hydrothermal carbonization. However, TKN is the combination of organic and ammonia nitrogen in the solution. Thus, by subtracting ammonia from TKN, it is possible to obtain the concentration of organic nitrogen. According to this arithmetic, organic nitrogen emerges as the most dominant form in every experimental condition. Another important takeaway from Figure 4.3 is the noticeably higher extraction of nitrogen from pig manure compared to cow manure which corresponds to the higher nitrogen content of pig manure,

as was the case with phosphorus. In addition, the ratio of ammonia to the total extracted nitrogen from pig manure is relatively high concerning cow manure. Increasing the reaction media's acidity for cow manure enhances nitrogen's leaching into the solution, and this trend encompasses all forms of nitrogen. Again, sulfuric acid results in the highest proportion of nitrogen extraction, as in the case of phosphorus. Moreover, it slightly increased the share of ammonia in total extracted nitrogen. The impact of acetic acid on nitrogen leaching was relatively marginal. However, it reduced the ammonia share significantly. Distinctively, using acids led to complex outcomes with no linear trend for pig manure. Acetic acid-aided hydrothermal treatment of pig manure decreased the total nitrogen extraction even though it increased the ammonia fraction. The highest ratio of ammonia to TKN was achieved within this experimental condition. Incorporating sulfuric acid improved not only the overall nitrogen extraction but also increased TKN, ammonia, and inorganic nitrogen. In general, nitrogen extraction from cow manure appears to alter significantly with reaction conditions compared to pig manure.

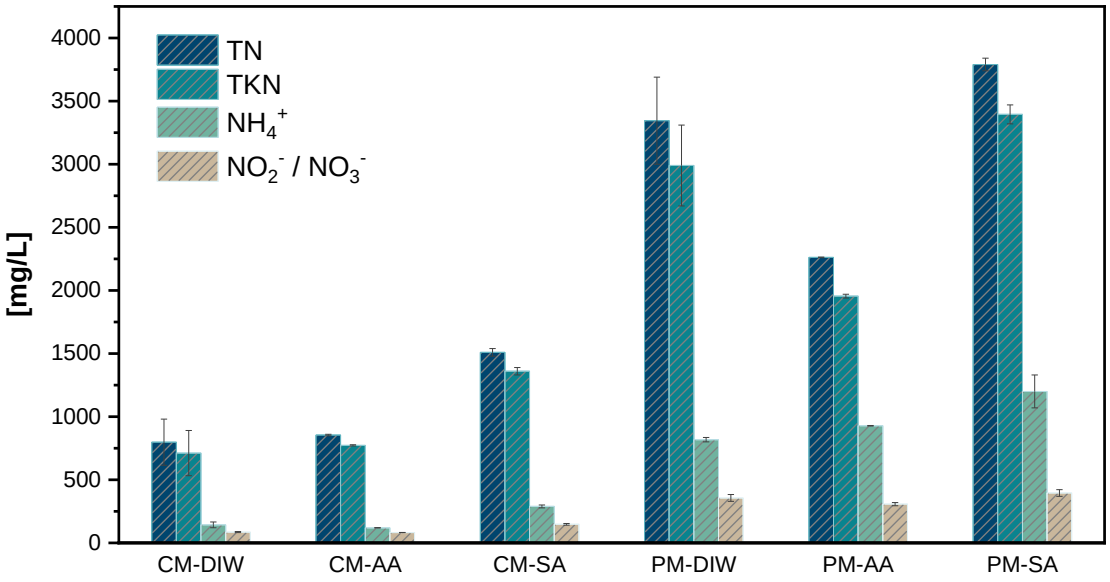

Figure 4.3 Total nitrogen, total Kjeldahl nitrogen, nitrite/nitrate, and ammonia concentration of the aqueous products of the hydrothermal carbonization of pig and cow manure.

The liquid phase GC analysis shows the enhancing effect of sulfuric acid catalyst on the formation of acetic acid, furfural, and 3-aminopyrazine 1-oxide compounds during hydrothermal treatment of cow and pig manure. A higher concentration of acetic acid was detected in the liquid produced from cow manure compared to that of pig manure. The acetic acid and furfural are likely the result of hydrolysis and dehydration reactions catalyzed by the strong acid. Acetate esters are common in the plants of cattle feed. Xylan is found both in dicotyledons and grasses and is highly acetylated. Hydrolysis of xylan would yield the acetic acid, and dehydration of the xylose monomers of xylan would produce furfural. The origin of 3-aminopyrazine 1-oxide is not apparent, but it has been reported in some pyrolysis oils [24][25].

4.3.3 Analysis of the gas products

The GC analysis of the gas samples collected at the end of each experiment showed predominantly CO_2 and N_2 for all experimental conditions. Nitrogen appeared due to the use of N_2 gas at the beginning of the experiment to purge oxygen. The average volumetric amount of CO_2 produced from pig manure was slightly higher than that of cow manure. Moreover, the variability of CO_2 production across the different experimental conditions with pig manure was relatively high compared to cow manure. The residual gas analysis of the samples by MS revealed some trace gaseous products like NO_2, SO_2, and H_2S. A qualitative comparison of the obtained results showed an interesting trend. With the only exception of sulfuric acid, in all other experimental conditions applied to both types of manure, H_2S was the most abundant compound, followed by NO_2 and SO_2, respectively. However, when sulfuric acid was used as a catalyst to treat both cow and pig manure, NO_2 gas was present at higher levels. Mass distribution of carbon, phosphorus, nitrogen, and potassium among the HTC products:

Mass balances for four key elements (C, N, P, K) are presented in Figure 4.4 – Figure 4.7. The mass balances reported in the following figures are based on normalized data. The mass balance on carbon was done by measuring the carbon content of the solids using a CHNS/O elemental analyzer and the TOC content of liquids. The amount of carbon in the gas was calculated from the ideal gas law, with the mole fraction determined by GC analysis. The average carbon mass balance for all six experimental scenarios was 99.7%, with a standard error of 2.6%. The carbon mass balance for pig manure with sulfuric acid was the most difficult to close and showed the highest divergence from 100%. The mass

balance of nitrogen was closed at an average of 113.5%, with a standard error of 6.8%. Balancing the nitrogen for the pig manure experiments was the most challenging, with quite a significant deviation from 100%. For phosphorus, the average mass balance was 102.2%, with a 0.9% standard error. In general, the mass balances for both phosphorus and potassium were quite close to 100%. In the case of potassium, the average mass balance is 110.0%, with a standard error of 5.3%. The raw data for these mass balances can be found in the supplementary material.

Carbon fractionation among the reaction products of the hydrothermal treatment of cow and pig manure, presented in Figure 4.4, suggests that for all experimental conditions, the vast majority of carbon lies in the solid hydrochar, and the smallest share of the carbon belongs to the gas phase which for all cases is below 2%. The distribution of carbon changes by introducing acids, the portion of liquid and gas carbon increases even though the increase in the fluid is more significant. The carbon partitioning among the process products was similar for cow and pig manure whenever sulfuric acid was used. This was also the case when no acid was added to the process. However, our results highlight some differences between cow and pig manure for acetic acid, where the carbon distribution is shifted more towards the liquid phase for pig manure.

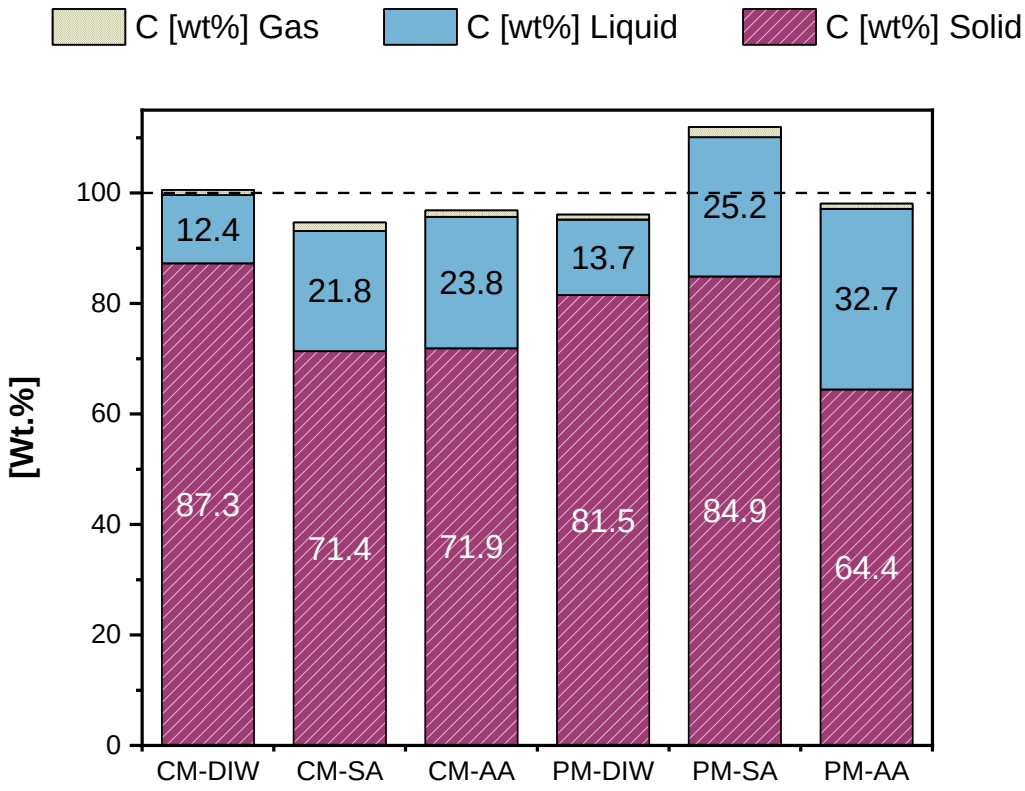

Figure 4.4 Carbon distribution among the solid, liquid, and gas products of hydrothermal carbonization of cow and pig manure.

Figure 4.5 shows nitrogen breakdown among the liquid and solid products of the hydrothermal carbonization of pig and cow manure. The different patterns that emerged for pig and cow manure for almost all experimental conditions stand out in nitrogen mass balance. For the cow manure, not using acids led to nearly 60% of the nitrogen fixation into the solid product. By applying acetic acid, a slight increase in the nitrogen portion in the liquid can be seen. The data in this figure shows that the highest nitrogen extraction into the liquid phase could be achieved by sulfuric acid. For almost every experimental scenario involving pig manure, hydrothermal treatment resulted in more nitrogen in the

liquid phase than cow manure. Moreover, unlike cow manure adding acetic acid reduced the nitrogen extraction from pig manure. Like cow manure, sulfuric acid resulted in the highest amount of nitrogen transferred into the liquid product.

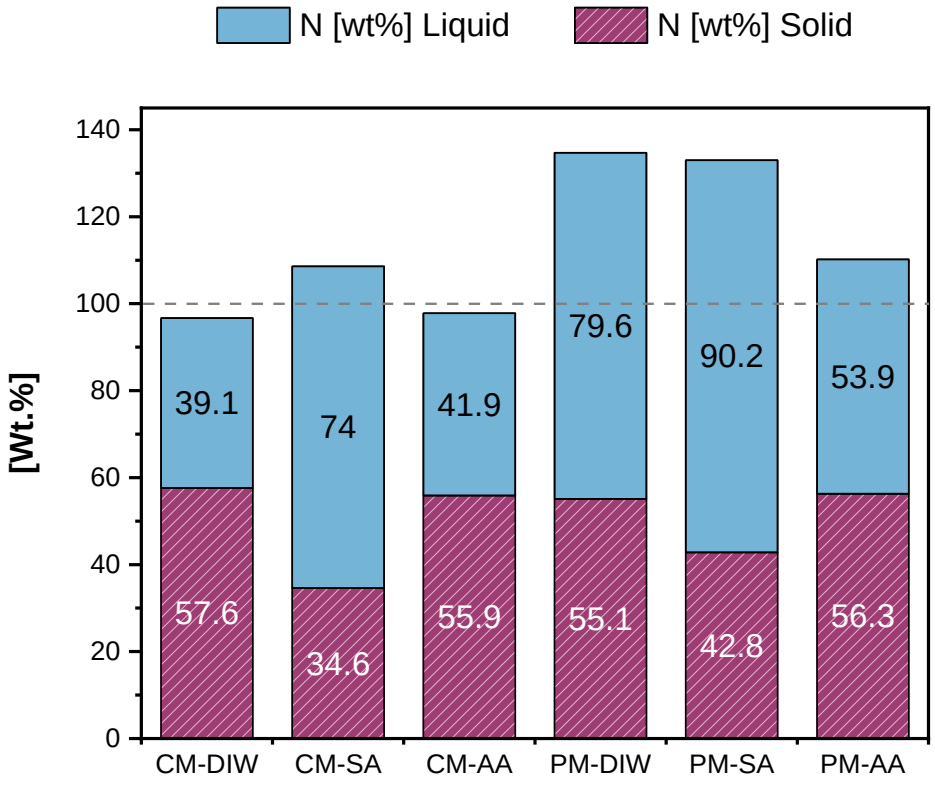

Figure 4.5 Nitrogen distribution among the solid and liquid products of hydrothermal carbonization of cow and pig manure.

Phosphorus mass balance is summarized in Figure 4.6. The data reveal an interesting pattern in phosphorus distribution during hydrothermal processing of pig and cow manure. For both types of feedstocks, increasing the solution's acidity enhanced the transformation of phosphorus from the solid into the liquid phase. However, this transition is slightly more

prominent in pig manure than in cow manure. Similar to carbon and nitrogen, our data show that sulfuric acid was the most effective additive in solubilizing phosphorus.

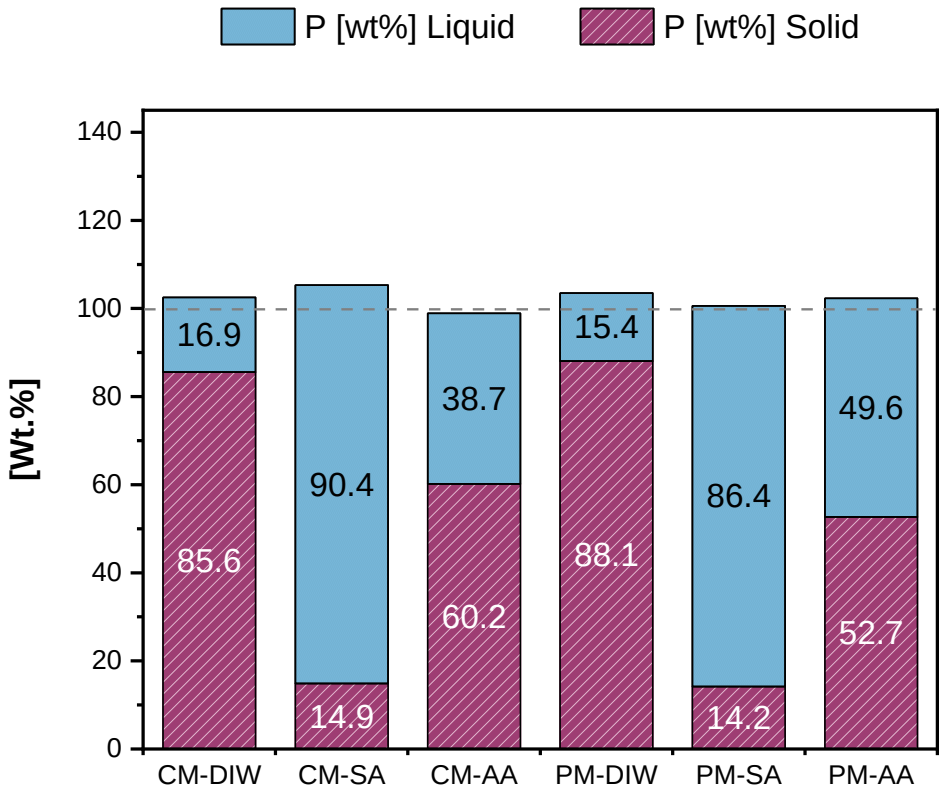

Figure 4.6 Phosphorus distribution among the solid and liquid products of hydrothermal carbonization of cow and pig manure.

The potassium mass balances presented in Figure 4.7 show that in all cases, most of the potassium is partitioned to the aqueous phase for both types of manure, with and without acid catalysts. That being said, applying acid catalysts further increased the solubilization

of potassium, with sulfuric acid emerging as the most influential catalyst for both types of manure.

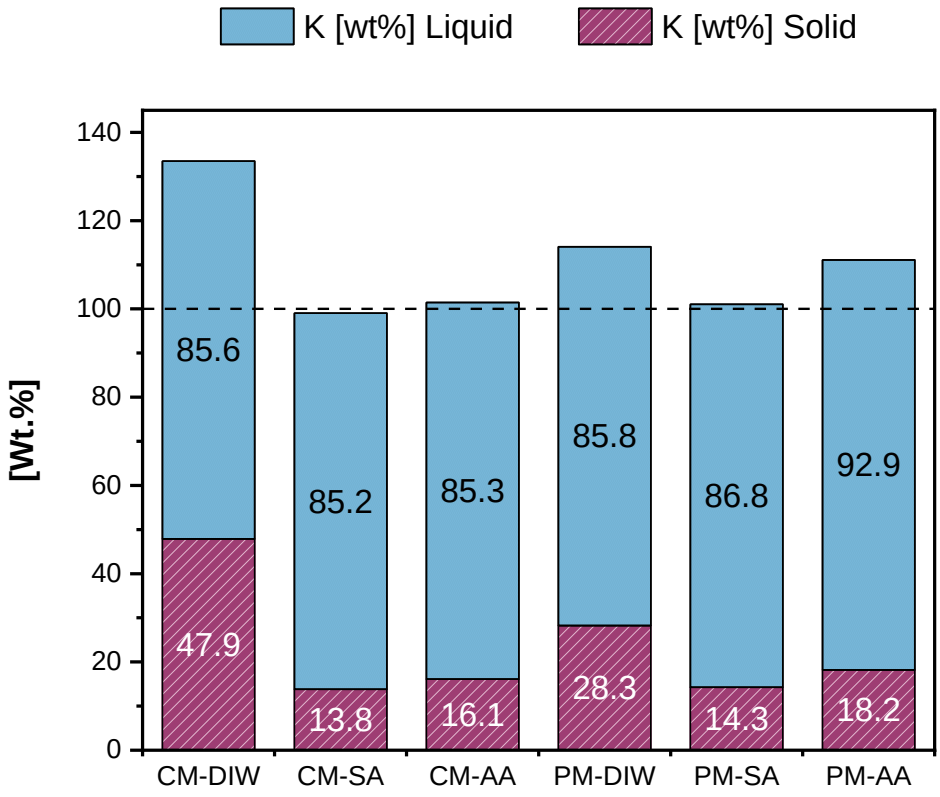

Figure 4.7 Potassium distribution among the solid and liquid products of hydrothermal carbonization of cow and pig manure.

Previous studies on animal manure treatment with HTC suggest an increase in the C content of hydrochar [26][27], similar to that observed in this work. Also, similar results were reported by Ro *et al.* on the enhancing effect of hydrothermal treatment on the fixed carbon content of the hydrochar produced through the sub and near-critical HTC of hen and swine manure [28]. On the other hand, CaO-assisted HTC of swine manure conducted by Lang *et al.* reported higher hydrochar yield and near 100% P enrichment in the

hydrochar, which contrasts with the results shown in Figure 4.2 and Figure 4.6. Because in that study, the reaction temperature (180 °C) was relatively close to our reaction temperature of 170 °C, the remarkably different result emphasizes the role of the acid catalysts in transferring P into the liquid phase during HTC [20].

However, in terms of hydrochar ash content, a striking divergence between the results of this study and other studies emerges. Previous studies reported increased ash content due to HTC treatment when no acidic catalyst was applied [29][30][31][32]. As shown in Table 4.2, hydrochar produced in water shows increased ash in the case of pig manure but slightly decreased ash in the case of cow manure. The reduced ash may be due to the low reaction temperature and relatively mild reaction conditions, with hydrochar having very similar characteristics to the untreated manure but without readily dissolved species. The results from Table 4.2 demonstrate that a strong impact of acidic catalysis during HTC is a reduced ash content in the resulting hydrochar. Other studies reported similar conclusions with sulfuric and acetic acid, where lower pH was hypothesized to catalyze flocculation and polymerization [33][34].

Regarding nitrogen and phosphorus extraction, our results presented overlapping implications of sulfuric acid application, as reported by Ekpo et al. [17]. That is, the phosphorus extraction was strongly dependent on the presence of an acidic catalyst. In contrast, even though the extraction was improved for nitrogen, the impact of an acidic catalyst was not as remarkable. This can be attributed to the increased solubility of phosphate salts in acidic solutions, which is less of a factor with nitrogen salts.

4.4 Conclusion

This study investigated the catalytic hydrothermal carbonization of pig and cow manure with sulfuric and acetic acids at 170 °C. Our findings indicate that using acids as homogenous catalysts enhanced carbonization, improved the energy values of the produced hydrochar, and reduced the solid yield. These effects can be achieved with increased reaction temperature and corresponding reaction pressure. However, the acid functions as a catalyst, allowing similar reaction results at a lower temperature. Moreover, we have shown that employing acids increases the hydrothermal leaching of phosphorus, while a modest increase in nitrogen solubilization was observed for sulfuric acid. Overall, our results demonstrate a strong effect of an inorganic acid such as sulfuric acid on the fractionation of the extracted nitrogen in the hydrothermal aqueous product. Therefore, the hydrochar product may be better suited as a fuel with reduced ash and nitrogen content than that produced without an acid catalyst. In addition, these findings provide future information about the partitioning of minerals such as Ca, K, Mg, and Fe across different products during hydrothermal treatment of pig and cow manure.

4.5 References

[1] USEPA, “Literature Review of Contaminants in Livestock and Poultry Manure and Implications for Water Quality,” 2013.

[2] J. Xiong, Z. Pan, X. Xiao, H. Huang, F. Lai, J. Wang, and S. Chen, “Study on the hydrothermal carbonization of swine manure: The effect of process parameters on the yield/properties of hydrochar and process water,” *J. Anal. Appl. Pyrolysis*, p. 104692, Sep. 2019.

[3] H. L. Foged, X. Flotats, A. B. Blasi, J. Palatsi, A. Magri, and K. M. Schelde, “Inventory of manure processing activities in Europe,” 2011.

[4] M. Hitzl, A. Corma, F. Pomares, and M. Renz, “The hydrothermal carbonization (HTC) plant as a decentral biorefinery for wet biomass,” *Catal. Today*, vol. 257, no. Part 2, pp. 154–159, 2015.

[5] V. Gunarathne, A. Ashiq, S. Ramanayaka, P. Wijekoon, and M. Vithanage, “Biochar from municipal solid waste for resource recovery and pollution remediation,” *Environ. Chem. Lett.*, vol. 17, no. 3, pp. 1225–1235, Sep. 2019.

[6] V. Karthik, P. S. Kumar, D. V. N. Vo, J. Sindhu, D. Sneka, B. Subhashini, K. Saravanan, and J. Jeyanthi, “Hydrothermal production of algal biochar for environmental and fertilizer applications: a review,” *Environ. Chem. Lett. 2020 192*, vol. 19, no. 2, pp. 1025–1042, Nov. 2020.

[7] S. Nizamuddin, N. M. Mubarak, M. Tiripathi, N. S. Jayakumar, J. N. Sahu, and P.

Ganesan, “Chemical, dielectric and structural characterization of optimized hydrochar produced from hydrothermal carbonization of palm shell,” *Fuel*, vol. 163, pp. 88–97, Jan. 2016.

[8] S. Román, B. Ledesma, A. Álvarez, C. Coronella, and S. V. Qaramaleki, “Suitability of hydrothermal carbonization to convert water hyacinth to added-value products,” *Renew. Energy*, vol. 146, pp. 1649–1658, Feb. 2020.

[9] S. M. Heilmann, L. R. Jader, M. J. Sadowsky, F. J. Schendel, M. G. von Keitz, and K. J. Valentas, “Hydrothermal carbonization of distiller’s grains,” *Biomass and Bioenergy*, vol. 35, no. 7, pp. 2526–2533, Jul. 2011.

[10] S. M. Heilmann, L. R. Jader, L. A. Harned, M. J. Sadowsky, F. J. Schendel, P. A. Lefebvre, M. G. von Keitz, and K. J. Valentas, “Hydrothermal carbonization of microalgae II. Fatty acid, char, and algal nutrient products,” *Appl. Energy*, vol. 88, no. 10, pp. 3286–3290, 2011.

[11] J. A. Libra, K. S. Ro, C. Kammann, A. Funke, N. D. Berge, Y. Neubauer, M. M. Titirici, C. Fühner, O. Bens, J. Kern, and K. H. Emmerich, “Hydrothermal carbonization of biomass residuals: a comparative review of the chemistry, processes and applications of wet and dry pyrolysis,” *http://dx.doi.org/10.4155/bfs.10.81*, vol. 2, no. 1, pp. 71–106, Jan. 2014.

[12] A. Funke and F. Ziegler, “Hydrothermal carbonization of biomass: A summary and discussion of chemical mechanisms for process engineering,” *Biofuels, Bioprod. Biorefining*, vol. 4, no. 2, pp. 160–177, Mar. 2010.

[13] M. Möller, P. Nilges, F. Harnisch, and U. Schröder, “Subcritical water as reaction environment: Fundamentals of hydrothermal biomass transformation,” *ChemSusChem*, vol. 4, no. 5, pp. 566–579, May 2011.

[14] S. Karagöz, T. Bhaskar, A. Muto, and Y. Sakata, “Hydrothermal upgrading of biomass: Effect of K2CO3 concentration and biomass/water ratio on products distribution,” *Bioresour. Technol.*, vol. 97, no. 1, pp. 90–98, Jan. 2006.

[15] S. Karagöz, T. Bhaskar, A. Muto, and Y. Sakata, “Catalytic hydrothermal treatment of pine wood biomass: Effect of RbOH and CsOH on product distribution,” *J. Chem. Technol. Biotechnol.*, vol. 80, no. 10, pp. 1097–1102, Oct. 2005.

[16] J. Mumme, M. M. Titirici, A. Pfeiffer, U. Lüder, M. T. Reza, and O. Mašek, “Hydrothermal Carbonization of Digestate in the Presence of Zeolite: Process Efficiency and Composite Properties,” *ACS Sustain. Chem. Eng.*, vol. 3, no. 11, pp. 2967–2974, Oct. 2015.

[17] U. Ekpo, A. B. Ross, M. A. Camargo-Valero, and L. A. Fletcher, “Influence of pH on hydrothermal treatment of swine manure: Impact on extraction of nitrogen and phosphorus in process water,” *Bioresour. Technol.*, vol. 214, pp. 637–644, 2016.

[18] S. V. Qaramaleki, J. A. Villamil, A. F. Mohedano, and C. J. Coronella, “Factors Affecting Solubilization of Phosphorus and Nitrogen through Hydrothermal Carbonization of Animal Manure,” *ACS Sustain. Chem. Eng.*, vol. 8, no. 33, pp. 12462–12470, 2020.

[19] C. Song, W. Yuan, S. Shan, Q. Ma, H. Zhang, X. Wang, N. K. Niazi, and H. Wang, “Changes of nutrients and potentially toxic elements during hydrothermal carbonization of pig manure,” *Chemosphere*, vol. 243, 2020.

[20] Q. Lang, B. Zhang, Z. Liu, W. Jiao, Y. Xia, Z. Chen, D. Li, J. Ma, and C. Gai, “Properties of hydrochars derived from swine manure by CaO assisted hydrothermal carbonization,” *J. Environ. Manage.*, vol. 233, pp. 440–446, Mar. 2019.

[21] EPA, “Method 365.1, Revision 2.0: Determination of Phosphorus by Semi-Automated Colorimetry,” 1993.

[22] EPA, “Determination of Nitrate-Nitrite Nitrogen By Automated Office of Research and Development,” 1993.

[23] M. J. Fishman, “Methods of analysis by the U.S. Geological Survey National Water Quality Laboratory--Determination of inorganic and organic constituents in water and fluvial sediments: U.S. Geological Survey Open-File Report,” 1993.

[24] J. Tao, C. Li, J. Li, B. Yan, G. Chen, Z. Cheng, W. Li, F. Lin, and L. Hou, “Multi-step separation of different chemical groups from the heavy fraction in biomass fast pyrolysis oil,” *Fuel Process. Technol.*, vol. 202, p. 106366, Jun. 2020.

[25] C. Mattos, M. C. C. Veloso, G. A. Romeiro, and E. Folly, “Biocidal applications trends of bio-oils from pyrolysis: Characterization of several conditions and biomass, a review,” *J. Anal. Appl. Pyrolysis*, vol. 139, pp. 1–12, May 2019.

[26] L. Dai, F. Tan, B. Wu, M. He, W. Wang, X. Tang, Q. Hu, and M. Zhang, "Immobilization of phosphorus in cow manure during hydrothermal carbonization," *J. Environ. Manage.*, vol. 157, pp. 49–53, Jul. 2015.

[27] K. Wu, Y. Gao, G. Zhu, J. Zhu, Q. Yuan, Y. Chen, M. Cai, and L. Feng, "Characterization of dairy manure hydrochar and aqueous phase products generated by hydrothermal carbonization at different temperatures," *J. Anal. Appl. Pyrolysis*, vol. 127, no. May, pp. 335–342, 2017.

[28] K. S. Ro, M. A. Jackson, A. A. Szogi, D. L. Compton, B. R. Moser, and N. D. Berge, "Sub- and Near-Critical Hydrothermal Carbonization of Animal Manures," *Sustainability*, vol. 14, no. 9, p. 5052, Apr. 2022.

[29] Q. Lang, Z. Liu, Y. Li, J. Xu, J. Li, B. Liu, and Q. Sun, "Combustion characteristics, kinetic and thermodynamic analyses of hydrochars derived from hydrothermal carbonization of cattle manure," *J. Environ. Chem. Eng.*, vol. 10, no. 1, p. 106938, 2022.

[30] J. D. Marin-Batista, J. A. Villamil, S. V. Qaramaleki, C. J. Coronella, A. F. Mohedano, and M. A. d. la Rubia, "Energy valorization of cow manure by hydrothermal carbonization and anaerobic digestion," *Renew. Energy*, vol. 160, pp. 623–632, Nov. 2020.

[31] S. Zhou, H. Liang, L. Han, G. Huang, and Z. Yang, "The influence of manure feedstock, slow pyrolysis, and hydrothermal temperature on manure thermochemical and combustion properties," *Waste Manag.*, vol. 88, pp. 85–95,

Apr. 2019.

[32] M. Toufiq Reza, A. Freitas, X. Yang, S. Hiibel, H. Lin, and C. J. Coronella, "Hydrothermal carbonization (HTC) of cow manure: Carbon and nitrogen distributions in HTC products," *Environ. Prog. Sustain. Energy*, vol. 35, no. 4, pp. 1002–1011, Jul. 2016.

[33] A. M. Smith, U. Ekpo, and A. B. Ross, "The influence of pH on the combustion properties of bio-coal following hydrothermal treatment of swine manure," *Energies*, vol. 13, no. 2, 2020.

[34] B. M. Ghanim, W. Kwapinski, and J. J. Leahy, "Hydrothermal carbonisation of poultry litter: Effects of initial pH on yields and chemical properties of hydrochars," *Bioresour. Technol.*, vol. 238, pp. 78–85, 2017.

Chapter 5

Conclusions and Recommendations for Future Research

5.1 Conclusions

This chapter will summarize the key findings concerning the overall progress towards achieving the goals to remedy the problems associated with manure management in CAFOs. It will also review the study's limitations and propose opportunities for future research.

5.1.1 Hydrothermal carbonization

As a thermochemical conversion technology, hydrothermal carbonization shows great potential for processing feedstocks with high amounts of moisture, such as animal waste and other agricultural waste biomass. Generally, solid products out of the HTC process exhibit higher energy density and carbon content than untreated biomass. The ability of the HTC process to take advantage of the water content of the biomass feedstock is significant potential. The role of water is determined mainly by temperature. At Low temperatures, water facilitates ionic reactions leading to a more predictable product array. On the other hand, high-temperature HTC typically results in free radical reactions, producing more unpredictable and complex molecules.

5.1.2 Nutrient leaching/extraction

Animal waste is very rich in nutrients, especially phosphorus and nitrogen. The HTC process was applied to solubilize the nutrients into the process water. Several process variables were studied to understand the impact of each factor. The results indicate that

reaction temperature was highly influential in phosphorus extraction, while the effect was minimal for nitrogen. Furthermore, adding citric acid and HCl acids led to a higher degree of nutrient extraction. The concentration of the acids used had significant importance as well. However, this factor became less impactful at concentrations above 0.3M for all acid types. The effect of reaction time was not pronounced, considering how experiments were conducted.

5.1.3 Precipitation of nutrients from the hydrothermal aqueous product

Reactive crystallization was applied to precipitate out the nutrients extracted into the HTC process water. The acids used during the HTC process showed relatively similar leaching capability. However, there was significant divergence among them during the precipitation process. Three organic acids and sulfuric acid were added as a leaching agent into the HTC process. Phosphorus recovery was selected as a measure for successful nutrient recovery. The results showed higher P-contained solid precipitation from sulfuric acid solution than other acids. And among the organic acids, formic acid indicates better P recovery performance. The complexity of the solution composition prevented the formation of struvite which was deemed a more desirable product.

5.1.4 Characteristics of the products in acid-catalyzed HTC

The catalytic effects of sulfuric and acetic acid on the properties of solid, liquid, and gas products of the hydrothermal carbonization of cow and pig manure were quite remarkable. The results indicate that the application of acids significantly impacted the distribution of inorganics among different HTC products. In general, acids reduced the share of inorganics in solid hydrochar and increased them in liquid products; thus, better quality fuel hydrochar

was produced with low ash content. The degree of carbonization also increased due to acid addition, even at low temperatures. The fractionation of phosphorus was not impacted markedly, where above 90% of P was detected as being in phosphate form. On the other hand, with sulfuric acid added as a catalyst, nitrogen fractionation slightly moved towards more ammonia-type nitrogen.

This research showed that hydrothermal carbonization successfully separated the nutrinets from the energy aspect of manure management in CAFOs. Primarily it was demonstrated that the combination of acid-catalyzed HTC and reactive crystallization (precipitation) recovered and recycled above 90% of the phosphorus from the animal waste generated by CAFOs. Moreover, it was possible to produce solid biofuels at low temperatures using an acidic HTC process which could be utilized to offset some of the energy input to the farm. This dissertation also helped to understand the fractionation of other inorganics present in animal waste during hydrothermal treatment.

5.2 Recommendations for future research

Even though this work showed near total recovery and recycling of the manure phosphorus, the same can not be said about nitrogen. While the fate of nitrogen was of interest and was investigated, nitrogen recovery remains a challenge to be addressed. Especially the fact that nitrogen is better extracted at higher temperatures goes against the low solubility of P under those conditions. On the other hand, the extracted nitrogen was mainly in the organic form, which further complicated the use of a chemical technique such as crystallization. Therefore other separation techniques or a combination of them could be more helpful.

Also, since solubilization of phosphorous and nitrogen was oppositely affected by temperature, the investigation of a two-step HTC process is necessary. Studying the temperature ramp's effect on nutrient extraction would be interesting. For example, the biomass slurry could heat up to higher temperatures for a specific time to maximize nitrogen extraction. Then the temperature could be reduced for phosphorus or vice versa. Another scenario could involve changing the aqueous reaction media between the two steps.

Moreover, the crystallization of nutrient-rich solids from HTC process water needs a more in-depth investigation, considering the complexity of the chemistry, presence, and interactions of organic matter and plethora of inorganic ions. In addition, the application of produced solids as fertilizers should be investigated for their impact on the plants and other characteristics, such as release rate and toxicity.

Finally, the industrial deployment of the manure management process introduced in this dissertation requires a continuous flow HTC reactor with high enough throughput. Unfortunately, the short residence time continuous flow reactor constructed and commissioned as part of this work could not provide a sufficient reaction time for biomass such as animal manure with high cellulosic and other complex molecules. Therefore, further investigation of the potential reactors is needed. For example, oscillatory flow reactors could be a good candidate for high-residence time reactions.

Appendix A

Supplementary material for Chapter 2

Factors Affecting Solubilization of Phosphorus and Nitrogen Through Hydrothermal Carbonization of Animal Manure

Saeed V. Qaramaleki [a], Charles J. Coronella [a], John A. Villamil [b], A.F. Mohedano [b]

[a] University of Nevada, Reno, Reno, Nevada, United States
[b] Universidad Autónoma de Madrid, Madrid, Spain

This appendix includes liquid and solid analyses found for all experiments which were used to produce figures 1 – 6 of the primary manuscript.

Table A1. Phosphate and nitrogen analysis of the liquid HTC products. All data reported in this table were measured by spectrophotometry.

Time	Temperature (°C)	Additive	Additive Concentration (M)	PO_4 (mg/L)	TKN (mg/L)	NO_2/NO_3 (mg/L)
5min	170	Water	*	234	937	132
5min	170	HCl	0.1	158	859	73.1
5min	170	HCl	0.5	1370	1060	184
5min	170	CA	0.1	1260	627	101
5min	170	CA	0.5	1450	746	136
5min	200	HCl	0.3	929	797	234
5min	200	HCl	0.3	1060	875	245
5min	200	CA	0.3	1400	260	246
5min	200	CA	0.3	1350	242	258
5min	200	Water	*	312	989	180
5min	200	Water	*	105	918	86.2
5min	230	HCl	0.1	51.2	314	164
5min	230	HCl	0.5	1220	1190	98

5min	230	CA	0.1	76.7	893	228
5min	230	CA	0.5	794	623	364.5
5min	230	Water	*	67.4	657	129
30min	170	Water	*	98	878	142
30min	170	HCl	0.1	207	606	107
30min	170	HCl	0.5	1380	1130	184
30min	170	CA	0.1	1020	570	149
30min	170	CA	0.5	1500	778	223
30min	200	HCl	0.3	809	932	198
30min	200	HCl	0.3	758	804	183
30min	200	CA	0.3	1410	873	285
30min	200	CA	0.3	1390	920	323
30min	200	Water	*	90.8	823	155
30min	200	Water	*	50.1	855	172
30min	230	HCl	0.1	38.6	553	150
30min	230	HCl	0.5	1080	1260	98.1
30min	230	CA	0.1	56.8	833	238
30min	230	CA	0.5	299	782.5	341.5
30min	230	Water	*	58.7	665	125
120min	170	Water	*	62.1	684	194
120min	170	HCl	0.1	72.9	386	134
120min	170	HCl	0.5	1470	1140	138
120min	170	CA	0.1	1050	869	165
120min	170	CA	0.5	1370	304	235
120min	200	HCl	0.3	755	1040	174
120min	200	HCl	0.3	848	1190	153
120min	200	CA	0.3	782	1120	237
120min	200	CA	0.3	730	1218	280
120min	200	Water	*	53.1	869	169
120min	200	Water	*	32.7	697	114
120min	230	HCl	0.1	37.2	739	99.1
120min	230	HCl	0.5	1110	1250	86.5
120min	230	CA	0.1	34.2	820	156
120min	230	CA	0.5	141.5	791.5	249.5
120min	230	Water	*	46.2	638	140

Table A2. Mass balances.

Time	Temperature	Additive	Additive Concentration	P % in liq	P %in Hchar	TN% in liq	TN %in Hchar
120min	170	HCl	0.1	6.4	93.0	36.9	65.1
120min	170	HCl	0.5	98.5	0.8	72.7	29.4
120min	170	CA	0.1	78.2	21.2	54.2	47.9
120min	170	CA	0.5	94.7	4.7	43.9	58.2
120min	170	Water	*	5.7	93.6	55.7	46.4
120min	200	HCl	0.3	80.1	19.3	69.1	33.0
120min	200	HCl	0.3	83.3	16.1	70.2	31.9
120min	200	CA	0.3	95.0	4.4	66.9	35.2
120min	200	CA	0.3	93.8	5.5	64.7	37.3
120min	200	Water	*	5.6	93.8	59.6	42.5
120min	200	Water	*	2.7	96.7	51.2	50.9
120min	230	HCl	0.1	3.3	96.1	52.0	50.1
120min	230	HCl	0.5	93.8	5.6	78.7	23.4
120min	230	CA	0.1	3.3	96.1	58.7	43.4
120min	230	CA	0.5	15.4	84.0	60.2	41.9
120min	230	Water	*	4.6	94.8	51.9	50.2

Table A3. Elemental analysis of the solid samples.

Time	Temperature	Additive	Additive Concentration	Al (mg/Kg)	Ca (mg/Kg)	K (mg/Kg)	Mg (mg/Kg)	Na (mg/Kg)	P (mg/Kg)
120min	170	HCl	0.1	3197.6	17665	343.3	3500.7	631.8	6536.9
120min	170	HCl	0.5	1071.3	475.5	40.3	232.1	260.6	111.3
120min	170	CA	0.1	2587.2	20428.6	214.8	1497	614.6	1663.4
120min	170	CA	0.5	1057.8	3057.9	385.9	511.2	752.4	422.2
120min	170	Water	*	1923.7	18664.4	1244.4	5873.3	4893.2	5809.5
120min	200	HCl	0.3	3136.1	587.1	5.9	264.7	265.9	1570.8
120min	200	CA	0.3	2097.6	3699.3	41.7	349	456.2	260.3
120min	200	Water	*	2751.4	20539.3	841.1	6392.2	1379.4	6689.9
120min	230	HCl	0.1	3604.9	19175.6	96.4	4016.6	292.4	8444.8
120min	230	HCl	0.5	1533.8	593	53	204.2	292.2	697.6
120min	230	CA	0.1	4271.8	18551.5	379	6128.1	764.8	7291.3
120min	230	CA	0.5	3977	7824.3	54.7	986.1	393.6	4820.2
120min	230	Water	*	4104.7	23050.4	96.2	8669.6	443.3	7886.8
Raw manure				1635.9	14374.5	4092.9	4306	6906.5	3814

Table A4. Elemental analysis of the solid samples. (CHNS analysis)

Time	Temperature	Additive	Additive Concentration	Solid Yield	C (Wt.%)	H (Wt.%)	N (Wt.%)	S (Wt.%)
120min	170	HCl	0.1	57.4	40.7	5	1.7	0.2
120min	170	HCl	0.5	38.9	53.8	5.1	1.4	0.5
120min	170	CA	0.1	59.9	45.8	5.4	1.6	0.1
120min	170	CA	0.5	56.4	47.5	5.3	1.4	0.2
120min	170	Water	*	60.4	40.3	5.2	1.6	0.4
120min	200	HCl	0.3	38.5	61.1	5.6	1.7	0.4
120min	200	CA	0.3	48	51	5.9	1.6	0.2
120min	200	Water	*	54.9	41.9	5	1.6	0.3
120min	230	HCl	0.1	45.5	46	4.7	1.9	0.4
120min	230	HCl	0.5	33.6	60	5.2	1.3	0.4
120min	230	CA	0.1	47.3	40.6	4.2	1.6	0.3
120min	230	CA	0.5	46.3	55.6	5.3	1.7	0.2
120min	230	Water	*	43.5	48.7	5.3	1.9	0.4
Raw manure				*	37.4	5	1.8	0.5

Appendix B

Supplementary material for Chapter 3

Phosphorus Recovery from Aqueous Product of Hydrothermal Carbonization of Cow Manure

Saeed V. Qaramaleki [a], A.F. Mohedano [b], Charles J. Coronella [a]

[a] 1664 N. Virginia St., Chemical and Materials Engineering Dept., University of Nevada, Reno, Nevada, United States

[b] Departamento de Ingeniería Química, Universidad Autónoma de Madrid, Madrid, Spain

Table B1 List of solid phases and reactions involved:

		K_{sp}	SI
Struvite	$Mg^{2+} + NH_4^+ + PO_4^{3-} + 6H_2O \leftrightarrow MgNH_4PO_4 \cdot 6H_2O$	13.26	2.19
Newberyite	$Mg^{2+} + HPO_4^{2-} + 3H_2O \leftrightarrow MgHPO_4 \cdot 3H_2O$	5.8	0.03
Bobierrite	$3Mg^{2+} + 2PO_4^{3-} + 8H_2O \leftrightarrow Mg_3(PO_4)_2 \cdot 8H_2O$	25.2	4.97
Amorphous calcium phosphate	$3Ca^{2+} + 2PO_4^{3-} + xH_2O \leftrightarrow Ca_3(PO_4)_2 \cdot xH_2O$	25.46	5.83
Hydroxyapatite	$10Ca^{2+} + 6PO_4^{3-} + 2OH^- \leftrightarrow Ca_{10}(PO_4)_6(OH)_2$	44.3	19.11
Monetite	$Ca^{2+} + HPO_4^{2-} \leftrightarrow CaHPO_4$	6.81	1.24
-	$Fe^{3+} + 3\,H_2O \leftrightarrow Fe(OH)_3 + 3\,H^+$	4.89	3.82
Gibbsite	$Al^{3+} + 3\,H_2O \leftrightarrow Al(OH)_3 + 3\,H^+$	8.11	2.10
Goethite	$Fe^{3+} + 2\,H_2O \leftrightarrow FeO(OH) + 3H^+$	42.97	9.71
Hausmannite	$3Mn^{2+} + 4\,H_2O \leftrightarrow Mn_3O_4 + 8\,H^+ + 2\,e^-$	54.15	9.78
Hematite	$2Fe^{3+} + 3H_2O \leftrightarrow Fe_2O_3 + 6H^+$	87.95	21.42
Manganite	$Mn^{2+} + 2\,H_2O \leftrightarrow MnO(OH) + 3H^+ + e^-$	18.26	2.76
-	$3Zn^{2+} + 2PO_4^{3-} + 4\,H_2O \leftrightarrow Zn_3(PO_4).4H_2O$	32.04	2.70

In order to determine the supersaturation of the precipitate phase in the solution using, the following equation for saturation index can be used:

$$\text{SI} = \frac{IAP}{K_{sp}} \qquad \text{(B1)}$$

Where IAP is the free ionic activity product, and K_{sp} is the thermodynamic solubility product constant.

$$IAP = \prod C_i . \gamma_i \qquad \text{(B2)}$$

Where C_i and γ_i are the concentration and ion activity coefficient of ion i in the solution. The ionic activity coefficient (γ_i) can be calculated by the Davies equation, which is the modification of the Debye–Hückel equation.

$$\log \gamma_i = -10^6 \frac{\sqrt{2}}{(\varepsilon T)^{\frac{3}{2}}} Z_i^2 \left(\frac{\sqrt{I}}{1+\sqrt{I}} - 0.3I\right) \quad \text{(B3)}$$

where ε is the dielectric constant; Z_i is the number of the oxidation state of the ion; and I is the ionic strength of the solution, mol/L, which can be determined by:

$$I = \frac{1}{2} \sum C_i Z_i^2 \quad \text{(S4)}$$

Appendix C

Supplementary material for Chapter 4

Characterization of products from catalytic hydrothermal carbonization of animal manure

Saeed V. Qaramaleki[a], Jose Cardenas[a], Michael A. Jackson[b], David L. Compton[b], Ariel A. Szogi[c], Kyoung Ro[c], Charles J. Coronella[a]

[a] 1664 N. Virginia St., Chemical and Materials Engineering Dept., University of Nevada, Reno,

Nevada, United States

[b] 1815 N. University St., USDA-ARS Renewable Products Technology Research, National Center for Agricultural Utilization Research, Peoria, Illinois, United States 61604

[c] 2611 West Lucas St., USDA–ARS Coastal Plains Soil, Water & Plant Research Center, Florence, South Carolina, United States

Figures C1-C6 show the residual gas analysis results from the hydrothermal treatments of the cow and pig manures. The inset in each plot shows the gases that are also part of the larger peak but are at much lower levels. For example, in Figure C1, the inset shows H_2S as the predominant gas, but it is present at only about 0.1% of the volume of the N_2 and CO_2 shown in the main plot. These levels are very low, but due to the toxic nature of these

gases, they need to be considered. Despite the fact that these results are only semiquantitative and only collected on a limited number of samples, the impact of the acid catalysis is evident. In each manure, hydrothermal treatment in water gave H_2S the largest minor gas. Strong acid treatment reduced the amount of this gas formed, but this increased the amount of NO_2 formed. This same change is observed with the pig manure, but more minor gases were formed in these runs.

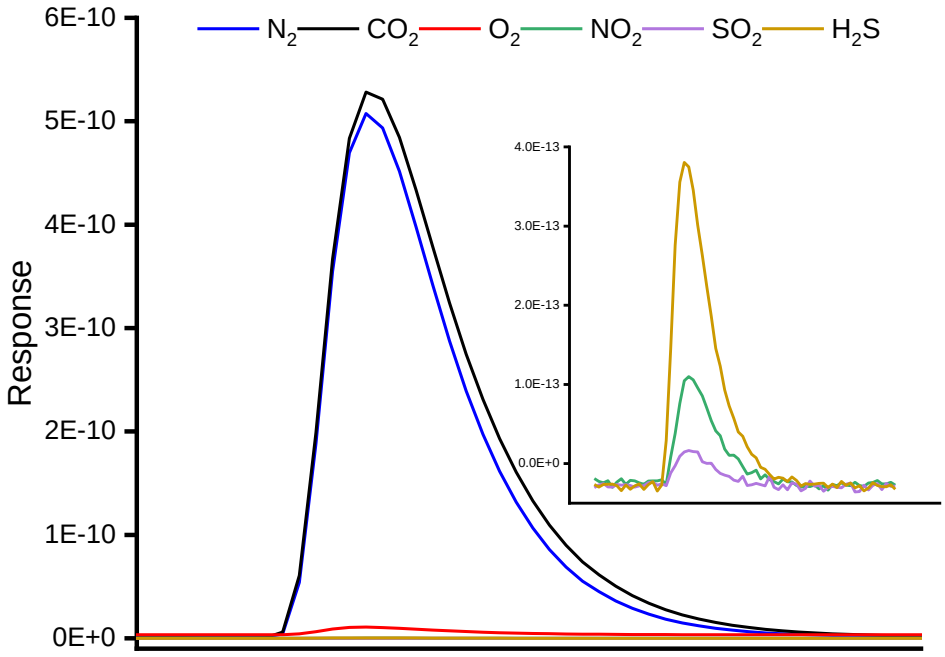

Figure C1. Residual gas analysis of CM-DIW

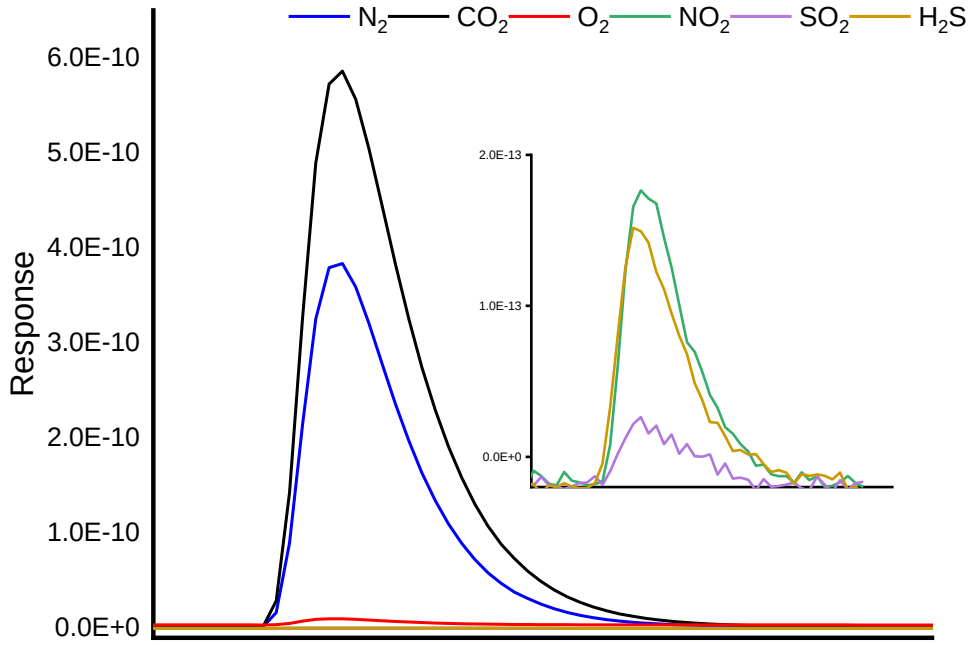

Figure C2. Residual gas analysis of CM-SA.

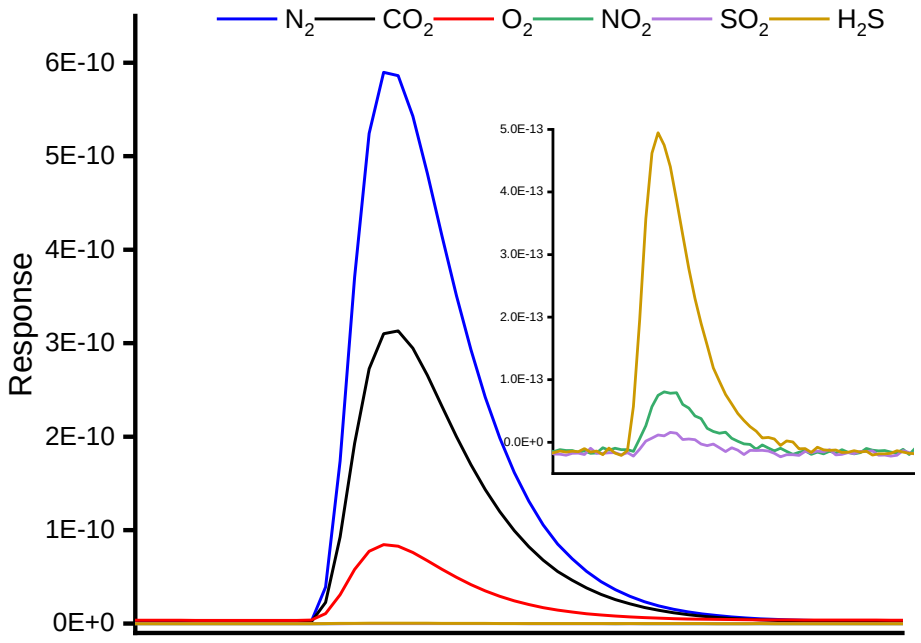

Figure C3. Residual gas analysis of CM-AA.

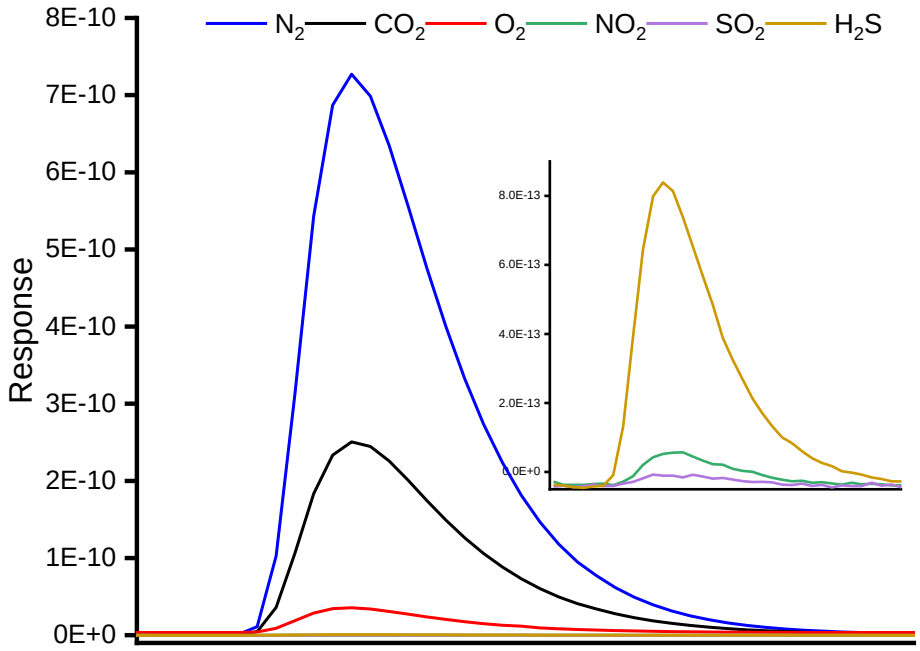

Figure C4. Residual gas analysis for PM-DIW.

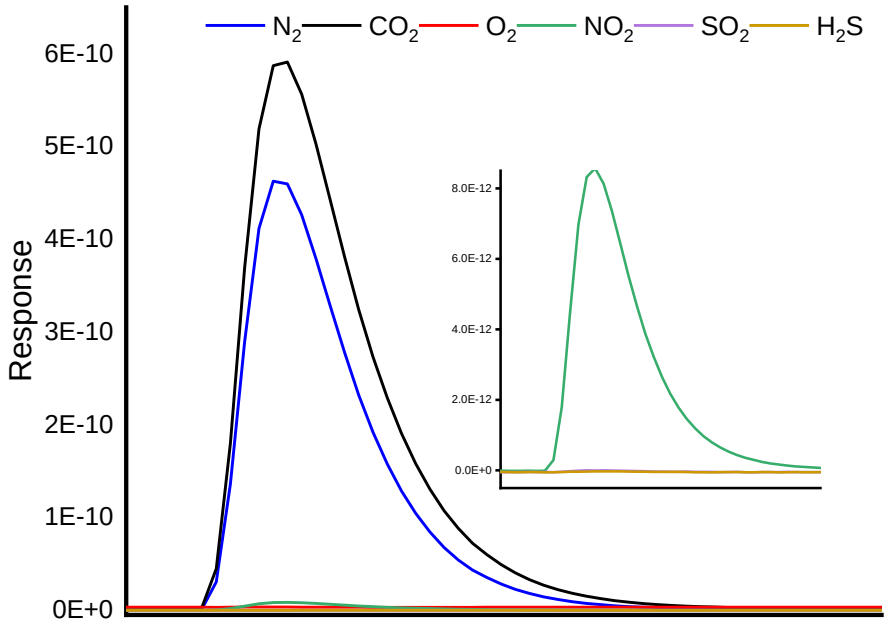

Figure C5. Residual gas analysis for PM-SA

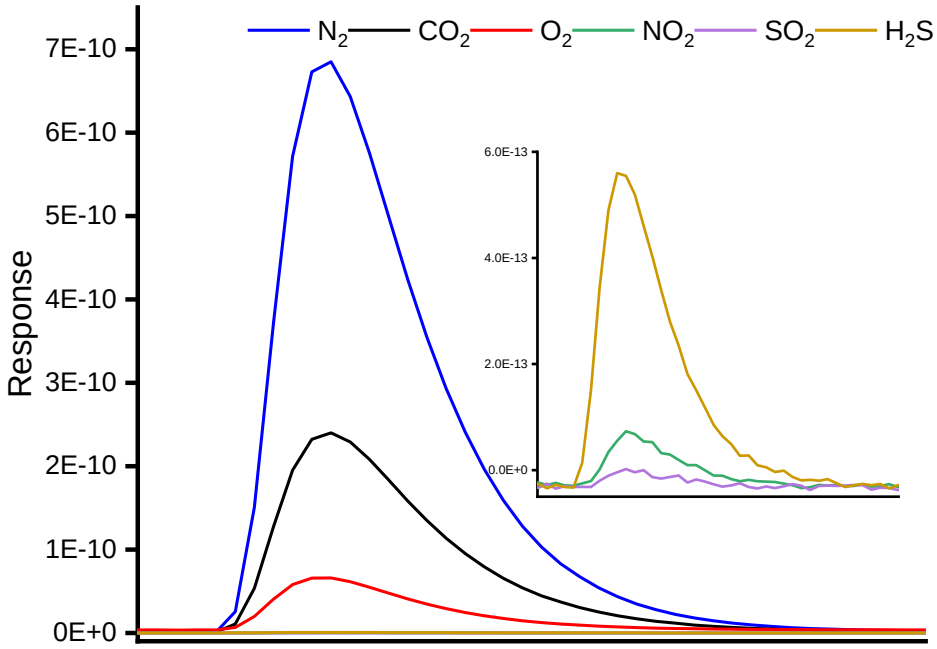

Figure C6. Residual gas analysis for PM-AA

Appendix D

Commissioning, testing, and Operation of Continuous HTC reactor

The preliminary research on the HTC process has been mainly done in batch reactors. The simplicity of batch operation was an important factor in its selection; however, limitations primarily related to smaller throughput prevent further process development. In continuous operation, on the other hand, more extensive amounts of feedstock can be processed and achieve a smaller process footprint and better energy integration and recovery. Moreover, piloting before scaleup is essential, as most of what works in the laboratory environment doesn't work as well in large-scale industrial plants. Finally, it allows benchmarking and discovery of variances between different stages of process development, which starts on the laboratory bench and ends at the commercialized process plant.

A continuous process unit was designed and constructed as the next step in the HTC process development. The unit comprises three main segments: biomass feeding and flow control, continuous flow hydrothermal reactor, and energy recovery and depressurizing.

The feeding system comprises a 15-gallon cone bottom inductor tank connected to a diaphragm pump (Hydrocell pump) rated for 70 bar pressure with stainless steel gauge and connection. The pump can deliver a flow rate of 0.05 gal/min at the pressure required to sustain the flow rate. In addition, a pulsation dampener and surge suppressor is connected to the pump discharge to remove system shocks and enhance performance, reliability, and safety in pumping application. The pump's flow rate can be controlled by a variable frequency drive (VFD) unit by adjusting the speed of the inverter-duty motor driving the

pump. The flow rate is measured by a Coriolis mass flow meter and transmitted to the computer's data aquation unit (LabJack) to be utilized in a virtual instrument (VI) programmed in LabVIEW. A check valve is installed on the feeding line to prevent the reverse flow of the slurry.

The reactor is built with a 120-inch long schedule 80 carbon steel pipe with an inner diameter of 2 inches. The reactor can be divided into three different sections. At the bottom of the reactor is the heating zone, where a heavy-duty (15 KW) immersion heater made with passivated stainless steel is installed, which is compatible with mild acid or alkaline conditions. Slurry flows upward through this zone and is heated to reaction temperature. Above the heating is the reaction zone where the HTC reaction occurs temperature of the fluid is measured at the beginning and end of this zone to ensure a steady and uniform temperature regime along the reactor. The slurry containing the solid and liquid products of the HTC process exits the reactor at this end of the reaction zone. Finally, the uppermost zone of the reactor is a headspace for gas collection and instrumentation for level and pressure measurements. A back pressure valve is installed to release the gas out of the reactor if the reactor pressure exceeds a preset value. In addition, a rupture disc is installed as a safety measure to prevent accidents due to over-pressuring.

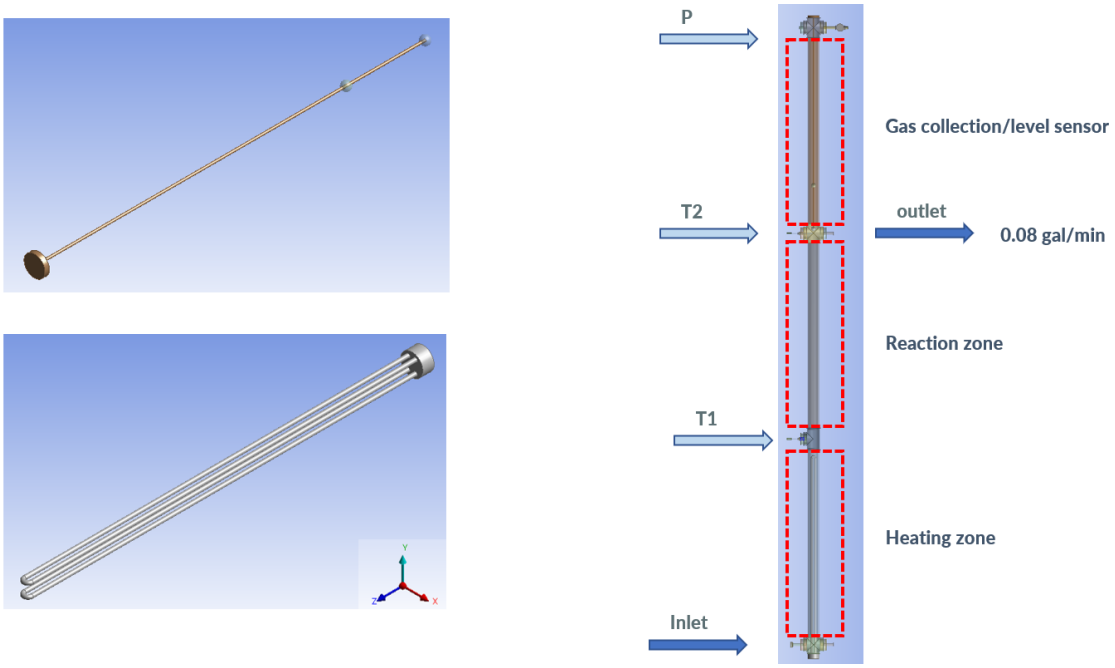

Figure D1 Continuous reactor configuration.

The flow from the reactor enters a shell and tube heat exchanger designed and built to cool down the reactor effluent below 30 °C and is connected to depressurizing segment made of a slightly wider pipe and two solenoid valves. The solenoid valves are operated automatically to control the fluid level in the reactor.

As mentioned earlier, a virtual instrument (VI) programmed in LabVIEW monitors and controlled the operation. For the most part, PID controllers adjust the heater power based on the temperature input from two thermocouples installed at the beginning and end of the reaction zone. A PID controller uses the flow meter data to set the VFD frequency that adjusts the pump output flow. A pressure transducer installed at the headspace zone monitors and records the reactor's pressure. The temperature of the stream coming out of the heat exchanger is also monitored and recorded. The level sensor is made of a magnet

float that activates a Reed switch inside a rod. It is installed from the top of the reactor. This sensor's on-off signal is used to automatically open and close the solenoid valves after a preset waiting time (2 mS).

Manure test:

The reactor was first cold-tested with water multiple times to check for leaks and examine the instrumentation by increasing the reactor's pressure above typical operational conditions. Next, hot tests with water were performed. The reactor was heated to 230-250 °C manually, and the functioning of the pump and heater was monitored. In addition cooling performance of the heat exchanger and the chiller used to provide the cooling water for the heat exchanger were evaluated. Finally, all the PID parameters were tuned for accurate and robust control of the related process variables, most importantly reaction temperature and flow rate.

The rector was then ready for the actual biomass slurry tests. First, cow manure was ground in a ball mill until the particle size was below 74 micrometers. This was done to avoid two critical issues: clogging the check valve installed on the feeding stream and settling the solid particles while moving upwards inside the reactor by decreasing the terminal velocity of single particles.

The test run was done with a 3% slurry of fine manure (≤75μm) in water. The temperature was 230 °C, and the slurry's flow rate was set to 0.08 gpm. A mixer stirred the feeding tank to homogenize the slurry and avoid settling or floatation of manure particles. During the

test run, sampling was carried out from the slurry feeding stream and the reactor product stream after the heat exchanger.

Table D1 Characterization of samples from continuous HTC of cow manure

Sample #	Solid	Water	Solid/Water%	Ash %	Solid yield
Feed 1	2.7	105.9	2.55	27.5	-
Feed 2	2.9	109.1	2.66	27.08	-
Feed 3	3	108.5	2.76	27.19	-
Feed 4	2.9	106.7	2.72	26.93	-
Average	-	-	-	**27.18**	-
Product 1	5.4	262.2	2.06	28.74	80.78
Product 2	5.7	253.1	2.25	28.63	84.72
Product 3	5.8	255.9	2.27	26.91	81.97
Product 4	6.6	269.9	2.45	29.17	89.97
Average	-	-	-	**28.36**	**84.36**

The entire test run lasted around 40 minutes, and sampling started at 17 from the feeding stream. Four samples were collected from each feed and product stream every 5 minutes. The samples were weighed and dried inside the oven (105 °C) overnight to calculate the mass of each sample's solid and fluid components. The ash content of the samples was also measured by heating the samples in the furnace for 24 hr at 650 °C.

The results are reported in Table D1. Comparing these results with the batch tests reveals significant variability in solid yield and ash content of the generated solid product. Generally, the treatment of biomass in the HTC process causes an increase in the ash content of the final solid product or hydrochar. The ash percentage reported in Table D1 shows an increased ash content of the solid products; however, the rate of increase is way

below previously reported values in the literature, in addition to our observations in the lab. For example, Goldfarb *et al.,* in a study focused on the valorization of cow manure via HTC, reported the ash content change from 24.9% to 29.2% due to HTC treatment of cow manure at 230 °C.

Another difference between batch and continuous HTC reactor results was the solid yield of the generated solid product. As seen from the above Table D1, the average solid yield of the continuous flow reactor was 84.36% which is substantially high compared to the 47.16 % solid yield obtained from the batch test at the same experimental condition (3% slurry, 230 °C, and 5 min reaction time). These results highlight that the manure slurry entering the continuous reactor does not undergo the complete HTC process by the time it leaves the reactor.

At this point, two scenarios were proposed as the most likely reason for the different results observed in the continuous flow reactor. First, it could be the lack of good mixing due to the laminar fluid flow field in the reactor that prevented effective heat transfer in the heating zone at the bottom of the reactor. Second, there might be a problem with the residence time distribution for different manure slurry elements across the reactor's reaction zone. This issue could also be due to the lack of turbulence in the flow field. The fluid flow is in a laminar regime even with the elevated temperature of the reactor, which causes reduced density and viscosity of water.

To address the heat transfer issue, the heating zone of the reactor was treated as a shell-and-tube heat exchanger, and it was decided to install baffles. Generally, baffles are placed on the shell side space for the heat exchangers, which provides the cross-flow direction of

the shell side fluid, so the more intensive heat exchanger between fluids could be realized. A segmental baffle made by cutting a disk segment was selected initially. The baffle cut of 50% was proposed, meaning the depth of the cut was 50% of the baffle diameter. The baffle was designed to have a 1 mm clearance from the reactor wall and the heater rods.

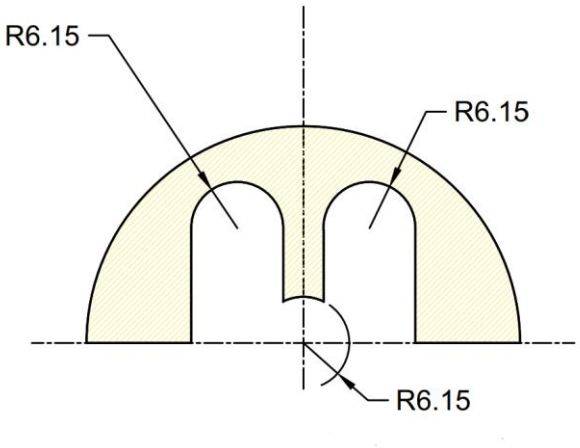

Figure D2 Baffle design for the heating zone

To figure out an effective spacing scheme of the baffles along the heating zone of the reactor, computational fluid dynamics (CFD) of the flow inside the reactor was carried out in COMSOL Multiphysics. The CFD was based on the single-phase κ-ε model, and the fluid properties were constant across the modeling domain. Since the goal was to obtain a qualitative flow field, the fluid's temperature was not considered. The software's default settings were used for meshing without further mesh refinement or grid convergence study.

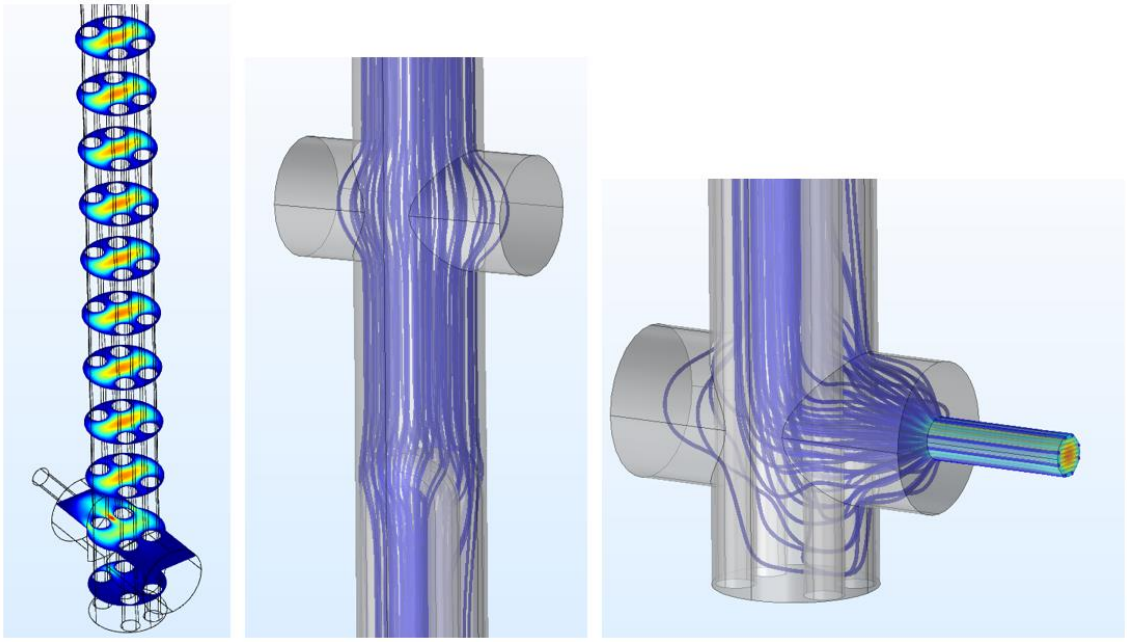

Figure D3 streamline and velocity profile in the heating zone

The sliced plot of velocity profile and streamlines across the heating zone of the reactor are presented here. As seen, the bulk of fluid flows through the middle of the reactor. This was valuable insight provided by CFD because it showed that the baffle design was not done correctly. The purpose of installing baffles is to block and redirect the flow from high-velocity regions to low-velocity ones. However, the initial baffle design was not serving this goal. Therefore, a new baffle shape was introduced according to Figure D4.

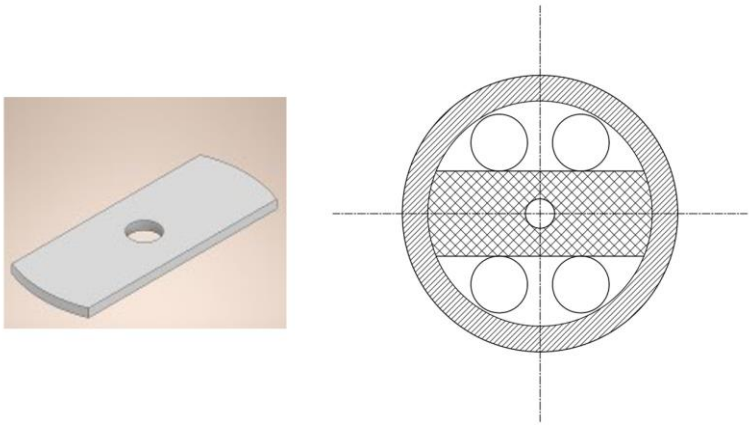

Figure D4 Modified baffle design for the heating zone

The baffle was designed to block the area between the heating rods and redirect the fluid toward the heating elements. First, using a Torchmate CNC plasma table, the pieces were cut out of a corrosion-resistant 316 stainless steel 316 sheet with a thickness of 0.0075 inches. To install the baffles, we removed the thermowell in the base of the heater by a grinder. Then, the baffles were mounted on a super-corrosion-resistant 316 stainless steel threaded rod using hex nuts and put between the heater elements, as shown in the picture below. This technique would allow altering the spacing among the baffles if needed.

Finally, sealed the hole at the heater base using stainless steel washer, nuts, and ultra-high-temperature chemical-resistant vermiculite gasket material. In addition to handling temperatures up to 1800° F, these vermiculite gasket sheets resist acids (except hydrofluoric), alkalies, and detergents. In addition, they have a stainless steel insert that provides strength under pressure. They are typically used when a strong seal is required

in boilers and furnaces. In total, 20 baffles were installed with a 2-inch space between two baffles.

Figure D5 Baffle installation

Mixing problems in the reaction zone were addressed by inserting a static mixer right after the heater. Static mixers redistribute the fluid in radial and tangential directions resulting in a homogenous solution. In addition, laminar flow causes temporal non- homogeneity because molecules leaving at a given instant have spent different times inside the reactor. Fluid redistribution induced by the static mixer provides both spatial and temporal mixing. In the ideal case, entering segregated fluid elements would be uniformly redistributed by the time they leave the mixer, and all the molecules left would have entered together. The

extent to which real static mixers approach the ideal plug flow can be assessed using the residence time distribution (RTD).

Residence time distribution:

One of the most effective approaches for characterizing non-ideal flow is investigating fluid elements' RTD, accomplished by tracer experiments and population-based modeling and analysis. The simplicity and adequate accuracy of resulting RTD models give them an advantage in reactor modeling, optimization, and control. Different models have been proposed to fit the data from tracer experiments and predict the non-ideal flow behavior, such as the axial dispersion model, tank in series, pure convection, etc.

Tracer experiments were carried out to determine the flow pattern of slurry in the reactor. Two different sets of experiments were performed to obtain the reactor's RTD for the liquid and solids. Because of its high optical density at low concentrations, methylene blue was a good fit as a tracer for the liquid phase RTD. The absorption wavelength of this methylene blue is 664 nm. In all experiments, the reactor was at atmospheric pressure and temperature. Ground manure ($\leq$75μm) was used as a tracer for the solid phase, and mixing cup sampling at the reactor exit was done every 30 seconds. The tracer was introduced as a step function into the system at $t \geq 0$ with an unchanged flow rate of 0.08 gal/min. For the liquid phase RTD, the samples collected at the reactor effluent were measured for their methylene blue concentration (C_t), and the data was plotted against time. For the solid particles RTD, the samples collected were dried, and the amount of the solid was measured by weighting.

Step inputs are less helpful for RTD modeling but can be used to produce an E curve. After obtaining the tracer experiment data from the continuous HTC reactor, the E curve was created by differentiating the Boltzmann function used to fit the original C_t-t or F curve. Then, the E curve was fitted with the dispersion model. This model uses a dimensionless number to characterize the flow spread in the system called the dispersion number. The resulting E curves are presented in Figure D6.

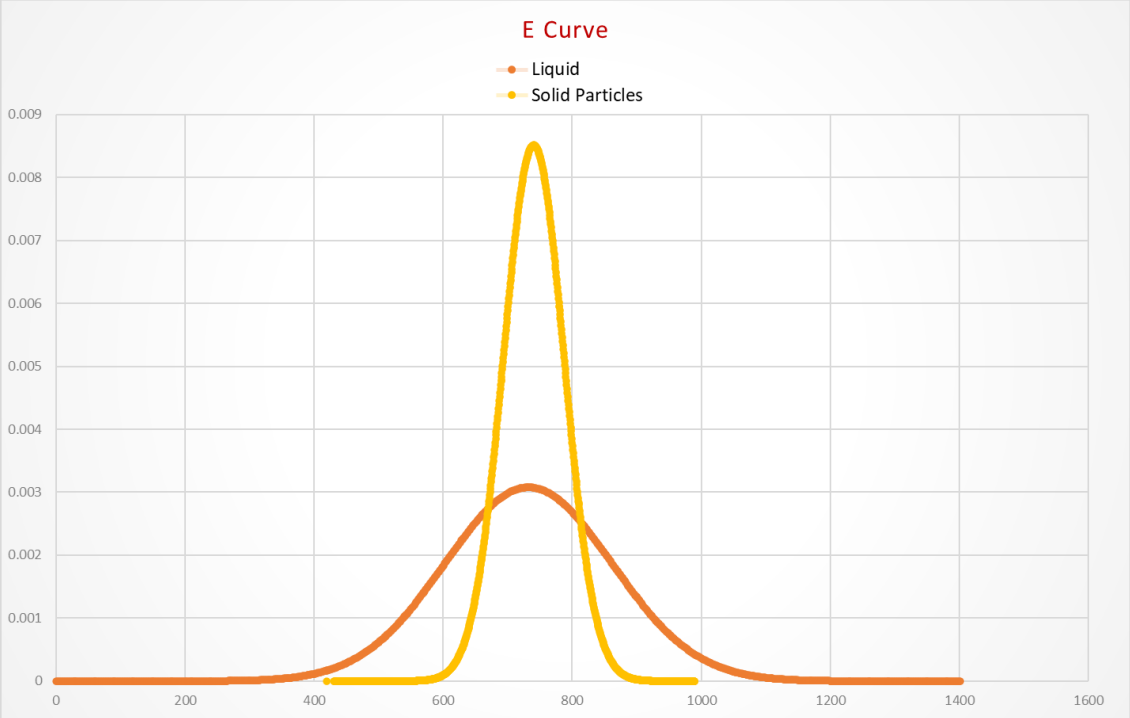

Figure D6 Residence time distribution for the liquid and solid particles in the continuous reactor

It was interesting to see that the dispersion number of the liquid phase (0.0219) was higher than that of solid particles (0.0029). The dispersion number of the solid particles indicates a small deviation from the plug flow, while for the liquid phase, the dispersion

number was in the range that shows a large variation from the ideal case, which is the plug flow.

Fast heating – fast cooling HTC:

In a typical operating procedure for HTC experiments, the mixture of biomass and water at a specific ratio goes into the sealed batch reactor at room temperature. Then the heating starts until the desired temperature for the experiment is achieved. This heating process lasts approximately 40-50 minutes. When the temperature reaches the preset value, the reaction time starts. Finally, at the end of the experiment, the reactor is immersed in an ice water bath for cooling, which takes about 50-60 minutes until the reactor cools to room temperature. Then the reactor can be opened to retrieve the products. Unfortunately, the time spent during the heating and cooling imposes significant errors and difficulties in controlling reaction time precisely. Solving this problem required substantial changes to the technique used for the short-time HTC reactions.

In the new method, the reactor was charged with only water and preheated to a certain temperature. This temperature was usually above the intended HTC temperature. The mixture of biomass and water was then injected into the preheated reactor instantly at time t = 0. Then, after the reaction time was finished, a sample was withdrawn from the rector using a sampling pipet installed in the reactor. This technique allowed a more accurate HTC time control for the biomass mixture. However, some trial and error were inevitable to achieve a reasonable temperature control since the whole procedure was done manually.

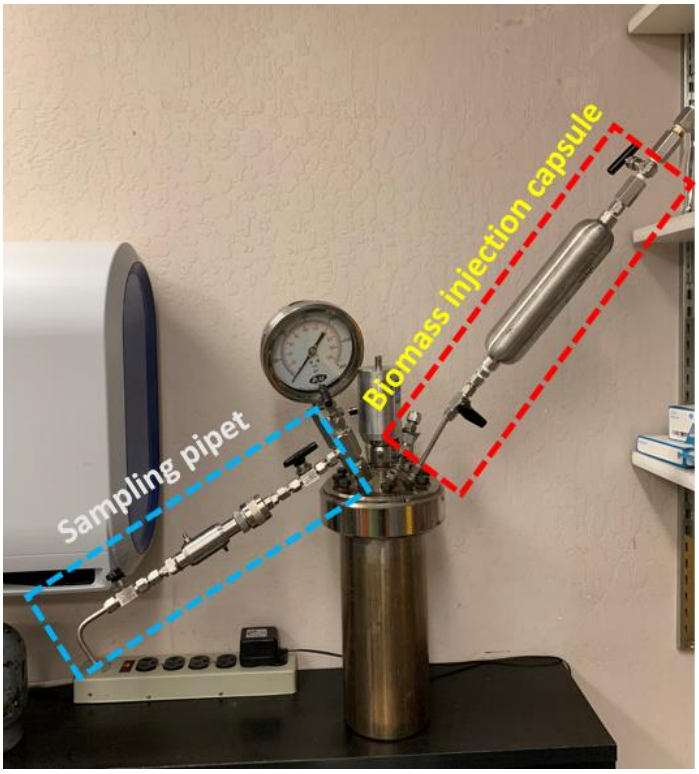

Figure D7 Fast injection and sample withdrawing setup for the batch reactor

The experiments were started with 800 ml of water being preheated in the reactor to 257°C. Then 200 ml of water and 30 gr of ground cow manure were mixed and put into the injection capsule. The other end of the injection capsule was connected to a high-pressure nitrogen tank, pressurized up to 20psi above the pressure of preheated reactor. At the right time, the ball valve between the reactor and the injection capsule opened to push the biomass into the reactor. The results of the HTC experiments with the new technique and their comparison with continuous HTC reactor data provided insightful conclusions. Table D2 presents the ultimate analysis of the solid samples for different reaction times. In addition, it includes data for new and old batch HTC tests.

Table D2 Elemental analysis of the solids from fast heating – fast injection experiments

Sample	Nitrogen %wt.	Carbon %wt.	Hydrogen %wt.	Sulphur %wt.	Oxygen %wt.
Cow manure	2.30	38.87	5.11	0.21	27.59
Continuous @ 230°C(5min)	2.02	42.40	5.08	0.2	26.42
Batch @ 230°C(5min) fast heating & cooling	1.17	42.19	5.09	0.10	26.56
Batch @ 230°C(10min) fast heating & cooling	1.13	42.46	5.24	0.07	25.14
Batch @ 230°C(30min) fast heating & cooling	1.13	43.76	5.30	0.14	24.86
Batch @ 230°C(60min) fast heating & cooling	1.28	45.16	5.35	0.14	24.78
Batch @ 230°C(5min) Old technique	1.37	45.27	5.40	0.12	24.94

The carbon content of the produced solids was used to measure carbonization in the experiments. As seen from the data, the carbon content of solids from the continuous flow reactor falls between the batch tests with reaction times of 5 and 10 minutes. On the other hand, comparing the batch tests conducted the old way (i.e., prolonged heating and cooling) versus the new technique (i.e., instant biomass injection and sample withdrawal) signifies the similarity in the carbon content of the solids from the new technique at 60 minutes with that of the old technique at 5 minutes. An important conclusion that could be drawn from these results is that the actual reaction time for the batch test carried out with the old method was way higher than what was intended (i.e., 5 minutes). Another conclusion is that 5 minutes of reaction time is insufficient for hydrothermal carbonization of cow manure.

Batch vs. continuous hydrothermal carbonization of glucose:

To increase the residence time in the continuous flow reactor, either the flow rate must be reduced or an extra length should be added to the reactor. However, the study only aimed to compare the performance of the continuous flow reactor with that of the batch reactor. Therefore, any biomass that is reactive enough to be carbonized in a short time would serve the purpose. Glucose is a simple sugar and the most abundant monosaccharide. Due to its simple molecular structure, it is highly reactive in hydrothermal conditions. In addition, much literature is available on the HTC study of glucose.

The continuous HTC of glucose was first attempted with a 3% concentration in water; however, the heat exchanger got clogged due to tar formation. As a result, some components got damaged due to pressure build-up, and a complex washing procedure had to be applied to unclog the system. Therefore, the glucose concentration was reduced to 1% in the subsequent trial. The overall run time for the continuous experiment was around 70 minutes, during which reaction parameters such as temperature, flow rate, heater power, and reactor pressure were measured and recorded. In addition, six samples were collected with a 10-minute time interval between each sampling, and the pH of the samples was measured immediately. The samples were then dried in the oven to measure the water in each sample. Since the dried samples contained unreacted glucose and HTC solid product (hydrochar), they were washed in warm water multiple times to dissolve the unreacted glucose. The hydrochar was then separated by centrifuge. This method allowed the calculation of the solid yield and glucose conversion in the continuous HTC reactor. The results are presented in Table D3. As can be noticed, the conversion of glucose varied

between 70% and 81%, with an average conversion of 76%. In addition, the conversion data showed s an increasing trend over time of the test run. The pH of the samples dropped from 3.19 to 2.99, indicating increased acidity, which is in line with the increased conversion of glucose. Because according to previous studies, the hydrothermal treatment of glucose produces organic acid in the reaction media. The hydrochar yield is defined as the percentage of hydrochar in the product stream compared to glucose in the feed stream. The results indicated an increasing pattern in the hydorchar yield along with increased glucose conversion. The average hydrochar yield for the whole test run was around 27%.

Comparing the continuous and batch reactor results shows that the batch test had a relatively low pH, higher conversion, and higher hydrochar yield. Nonetheless, these results indicate comparable products between the batch and continuous reactor.

Table D3 Solid yield and conversion of continuous HTC of glucose

Sample	pH	Glucose conversion(%)	Hydrochar yield
Cnt. sample #1	3.19	70.50	22.06
Cnt. sample #2	3.06	71.85	25.37
Cnt. sample #3	3	75.23	28.46
Cnt. sample #4	3.02	79.09	30.02
Cnt. sample #5	3	78.96	29.52
Cnt. sample #6	2.99	80.60	29.14
Batch	2.65	79.26	28.12

Further characterization of the products obtained from batch and continuous reactors helped to understand the differences between the two. Table D4 presents the elemental composition of the hydrochar generated from the continuous reactor and the batch reactor

test run. The samples' carbon, hydrogen, nitrogen, and sulfur content were measured using an elemental analyzer. As seen from the results, no sulfur and nitrogen were detected in all samples. The carbon content of the samples from the continuous reactor varied as time passed. It started with 55% for the first sample and went up to 58% with an average of 57%. For comparison, the carbon content of the samples was measured as 57%. The average hydrogen content of the solid samples obtained from the continuous reactor was 4.6% versus 4.8% for the batch reactor. For all the samples from both the continuous and batch reactors, the carbon content improved markedly. On the other hand, the hydrogen content dropped for all samples. The significant change in the carbon and hydrogen content of the collected samples implied a high degree of carbonization of the original glucose entering the reactor.

Table D4 Elemental analysis of the solids from batch and continuous HTC of glucose

Sample	Nitrogen wt.%	Carbon wt.%	Hydrogen wt.%	Sulfur wt.%
Glucose	0	40.00	6.70	0
Cnt. sample #1	0.05	55.34	4.47	0
Cnt. sample #2	0	56.29	4.55	0
Cnt. sample #3	0	56.55	4.6	0
Cnt. sample #4	0	57.16	4.64	0
Cnt. sample #5	0	57.08	4.62	0
Cnt. sample #6	0	57.81	4.62	0
Batch	0	56.55	4.78	0

The IR spectroscopy of the solids produced by glucose hydrothermal treatment in the batch and continuous reactors is shown in the following figure. The vibrational spectra of glucose indicated in Figure D8 can be arranged into two main groups of ranges. First, the region

from 600 to 1500 cm^{-1} where C-O and C-C groups vibration modes are present and the carbohydrates commonly show their indicative absorption bands. On the other hand, the range from 2900 to 3500 cm^{-1} was assigned to CH and OH vibrations groups. The FTIR spectra of the solids produced by batch and continuous reactors altered dramatically from that of glucose. It can be noticed that the band from 2900 to 3500 cm^{-1} was diminished radically, suggesting oxygen and hydrogen removal as a result of hydrothermal treatment. The C-O and C-C absorption range (600-1500 cm^{-1}) was also affected significantly, which meant higher oxygen removal from the glucose.

Furthermore, a new band (1600-1800 cm^{-1}) appeared in the spectra of the solids from HTC of glucose. The carbonyl group, C=O, has an intense stretching vibration whose peak generally seems from 1900 to 1600. The similarity of the IR spectra among the solid samples from both reactor types was worth mentioning.

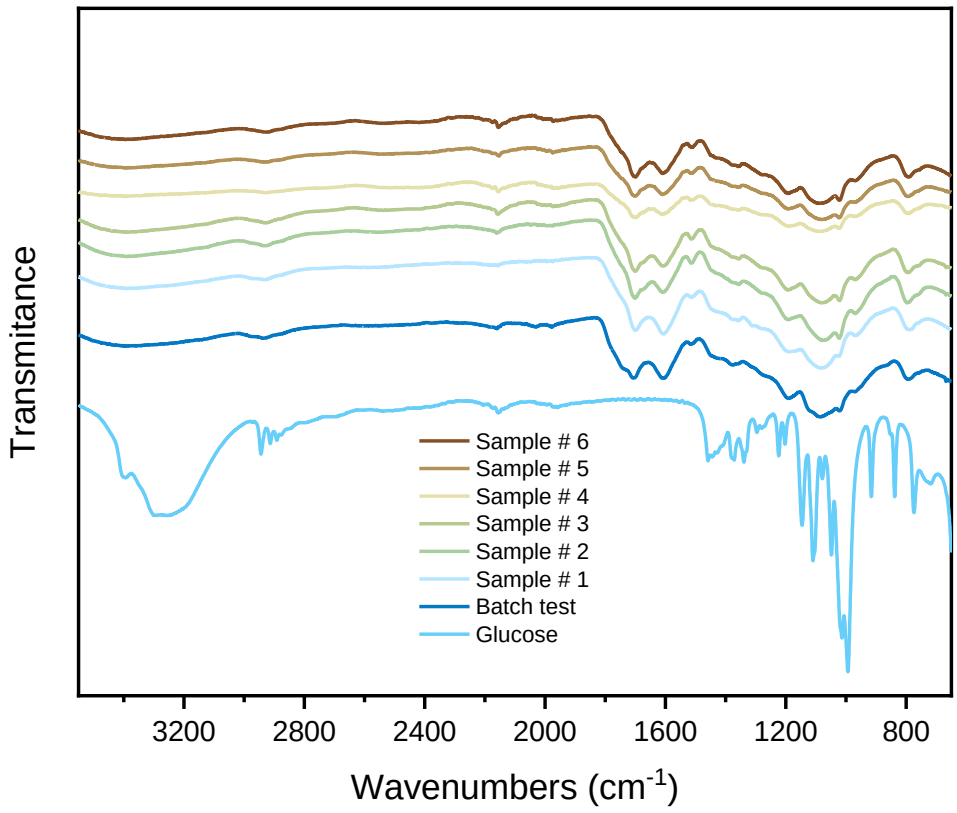

Figure D8 IR spectra of solids from continuous and batch reactors with glucose